UNIVERSITAT POLITÈCNICA DE VALÈNCIA

ETSI Aeroespacial y Diseño Industrial

UNIVERSITAT POLITÈCNICA DE VALÈNCIA

School of Aerospace Engineering and Industrial Design

Conceptual design of a hydrogen-powered UAV with LiDAR functionality.

End of Degree Project

Bachelor's Degree in Aerospace Engineering

AUTHOR: García Miñarro, Jorge

Tutor: García-Cuevas González, Luis Miguel

ACADEMIC YEAR: 2023/2024

Bachelor's Thesis

Conceptual design of a hydrogen-powered UAV with LiDAR functionality

Universitat Politècnica de València

Escuela Técnica Superior de Ingeniería Aeroespacial y Diseño Industrial

July 23, 2024

Author
Jorge García Miñarro

Tutor
Luis Miguel García-Cuevas González

My deepest gratitude to my family for their support over the years and for making this possible, for everything they have given to me, all those sacrifices count.

To my old friends, thank you for always being there for me and sharing so many unforgettable moments, eternal. To the friends made along the way, with whom I have shared many experiences and laughs.

Special mention to my girlfriend, whose unconditional support encourages me to be a better person every day, for all those happy moments and for those that remain, thank you.

I also extend my sincere thanks to all the professors at the university who have guided and taught me throughout my academic journey.

Thank you all for being an integral part of this journey.

"Sic Parvis Magna"

Abstract

The main objective of this study is to conceptually develop an Unmanned Aerial Vehicle (UAV) which uses a Hydrogen Fuel Cell (HFC) as the main propulsion system, under the pretext of performing a mission based on Light Detection and Ranging (LiDAR) functionality.

The purpose is to achieve the essential objectives of a ground surface measurement mission by briefly showing what is the LiDAR capable of, and establish the environmental benefits of the HFCs by the time its worthiness is verified.

The study begins with the designation of the flight conditions and the consideration of the constraints which are relevant to the performance of the LiDAR device. Geometry, weight, propulsion and aerodynamics are established through a sizing methodology, followed by the optimization of the model developed. The study consists of a comparison of different models with different performance, weights and geometries for the justification of the final designated model, based on iterations, focusing in the results analysis.

To conclude, an analysis of the environmental impact of the conceptual design is performed, overviewing the current stage of hydrogen energy and future goals of this technology.

This work aims to show a state-of-the-art UAV application, giving visibility to LiDAR among other functionalities, establishing the new carbon-free technology as a potential replacement for internal combustion engines in UAV applications.

Contents

List of Figures

List of Tables

Nomenclature

Symbol	Description	SI
WL	Wing Loading	[N/m^2]
PL	Power Loading	[N/W]
DL	Disk Loading	[N/m^2]
AR	Aspect Ratio	[-]
TW	Thust-to-Weight ratio	[-]
RoC	Rate of Climb	[m/s]
FoM	Figures of Merit	[-]
CoG	Centre of Gravity	[m]
NP	Neutral Point	[m]
MAC	Mean Aerodynamic Chord	[m]
e	Oswald's efficiency factor	[-]
V	Speed	[m/s]
η	Efficiency	[-]
q	Dynamic pressure	[kg/$m \cdot s^2$]
C_D	Drag coefficient	[-]
C_L	Lift coefficient	[-]
α	Angle of attack	[°]
k	Induced drag factor	[-]
ρ	Density	[kg/m^3]
g	Gravity constant	[m/s^2]
T	Thrust	[N]
W	Weight	[N]
D	Drag	[N]
L	Lift	[N]
S	Surface	[m^2]
n	Number of something	[-]
π	Pi number	[-]
R	Radius	[m]
c	Chord	[m]
RPM	Revolution per minute	[rev/min]
U_{rated}	Rated voltage	[V]
P	Power	[W]
Kv	RPM per 1 volt	[-]
D	Diameter	[m]
M	Mass	[kg]
f_{install}	Factor for the weight of electric components	[-]

Symbol	Description	SI
d	Lift sharing	[%]
f_{usable}	Factor to prevent voltage drop	[-]
F	Faraday constant of 96,485.4	[C/mol]
ΔH	Chemical reaction energy of 284,000	[J/mol]
LHV	Low heating value	[Wh/g]
HC	Hydrogen consumption	[g/h]
t	Time	[s]
V_{tank}	Volume of the tank	$[m^3]$
m_{H_2}	Mass of hydrogen	[kg]
AE	Aerodynamic efficiency	[-]
b	Span	[m]
V_{t}	Volume of the tail	$[m^3]$
SM	Static Margin	[%]
x	Referred to distance	[m]

Index	Description
max	Maximum
ceiling	at ceiling altitude
VTOL	referred VTOL mode
FW	referred FW mode
cruise	at cruise segment
0	initial value
prop	propeller
LE	Leading edge
stall	at stall
w	referred to wing
t	referred to tail
root	at root section
mid	at middle section
tip	at tip section
ratio	it is a ratio
hover	referred to hover segment
proj	projected
take-off	referred to take-off segment
blade	referred to blade
i	used as a counter
seg	referred to segment

Index	Description
batt	referred to battery
mot	referred to motor
req	required
HFC	referred to HFC
avionics	referred to avionics
subsys	subsystem
sys	system
propulsion	referred to propulsion
payload	referred to payload
frame	referred to the frame
CoG	referred to CoG
NP	referred to NP

Acronym	Description
UAV	Unmanned Aerial Vehicle
HFC	Hydrogen Fuel Cell
LiDAR	Light Detection and Ranging
RPAS	Remotely Piloted Aircraft System
eVTOL	electric Vertical Take-Off and Landing
GPS	Global Positioning System
DGPS	Differential Global Positioning System
IMU	Inertial Measurement Unit
PNOA	“Plan Nacional de Ortofotografía Aérea”
MCA	Multi-mode Constraint Analysis
FOV	Field of View
RMSE	Root Mean Square Error
FW	Fixed Wing
VTOL	Vertical Take-Off and Landing
PMFC	Proton Exchange Membrane Fuel Cell
DMFC	Direct Methanol Fuel Cell
BoP	Balance of Plants
DFAFC	Direct Formic Acid Fuel Cell
PAFC	Phosphoric Acid Fuel Cell
SOFC	Solid Oxide Fuel Cell
AFC	Alkaline Fuel Cell
MCFC	Molten Carbonate Fuel Cell
DBFC	Direct Borohybride Fuel Cell
FCV	Fuel Cell Vehicle
EPS	Electric Propulsion System
ESC	Electronic Speed Controller
FCC	Flight Control Computer
CFD	Computational Fluid Dynamics

Acronym	Description
3D	Three Dimensional
BIM	Building Information Modeling
AGL	Above Ground Level
CNIG	"Centro Nacional de Información Geográfica"
STOL	Short Take-Off and Landing
ICE	Internal Combustion Engine
VLM2	Vortex Lattice Method
LLT	Lifting Line Theory
RANS	Reynolds-Averaged Navier-Stokes
GHG	Greenhouse Gas
SMR	Steam Methane Reforming
CCS	Carbon Capture and Storage
HFCV	Hydrogen Fuel Cell Vehicle
BEV	Battery Electric Vehicle
SDGs	Sustainable Development Goals
IVA	"Impuesto de Valor Añadido"

Part I

Memory

Chapter 1

Introduction

The worthiness of the Unmanned Aerial Vehicles has undoubtedly increased due to their ability to perform a wide range of tasks. The use of this type of aircraft, known also as drones or correctly called Remotely Piloted Aircraft System (RPAS), is continuously expanding in many sectors, including both military and civil applications.

As the use of UAVs has grown, so too have the innovations within the field. Initially driven by the need to improve fuel efficiency, but later on, these advancements are also influenced by environmental concerns such as greenhouse gas emissions.

Electrification is already a reality for UAVs, but the current technology level is limited, and the drones have a reduce endurance of a couple of hours. Even though this should be enough to carry out the mission, there is a continual push to enhance efficiency and broaden the scope of possible missions. Hydrogen Fuel Cells represent the new technology which is required and selected for overcome the current limitations. By combining both energy sources, UAVs can achieve better efficiency and pave the way for further technological improvements.

1.1 Historical background

In this section, the UAVs field is briefly described by exposing its roots and most noteworthy applications. The primary driving factor, as for many things in the aeronautical sector, has been its military use.

UAV concept date back to ancient Greece and China, around 2,500 years ago. Archytas of Tarantas, Italy, is consider the inventor of the first autonomous flying machine, around 425 BC, called 'the pigeon' which is shown in *Figure 1.1a*. Whereas, in China, there were experiments included kites, hot air balloons, rockets and simple toys like the 'top', which is inspired by the flight of sycamore and maple tree seeds.

In the 15th century, Leonardo Da Vinci designed the aerial screw, an aircraft capable of hovering, *Figure 1.1b*. It is considered as the precursor of the modern helicopter, although the idea was never brought to reality due to the rudimentary propulsion methods of the time.

(a)

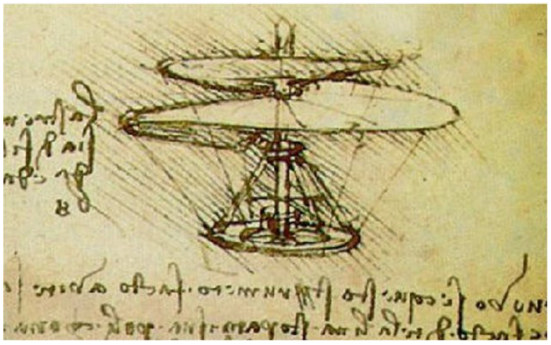

(b)

Figure 1.1: First autonomous flying machines: (a) The depiction of 'the pigeon', the first documented UAV in history. (b) The air screw of Leonardo Da Vinci. [1]

In 1917, some years after the first manned flight of the Wright's 'flyer', Dr. Cooper and Elmer Sperry invented the automatic gyroscopic stabilizer, leading to the first radio-controlled UAV. It was derived from the U.S Navy Curtiss N-9 trainer aircraft, the 'Hewitt-Sperry Automatic Airplane', used for delivering explosives during World War I.

In the first half of the 20th century, some experiments were carried out in Britain with UAVs like the Queen Bee, shown in *Figure 1.2a*, mainly to serve as targets for gunnery practice.

Post-World War II saw the development of reconnaissance drones such as the SD-1 in *Figure 1.2b*. This aircraft was remotely piloted, carried a camera on board and returned to the base after 30 minutes of flight, from which it was recovered with a parachute. Also, the TBR1 and DBR-1 in the Soviet Union can be highlighted.

(a)

(b)

Figure 1.2: After war drones: (a) The DH.82B Queen Bee drone. (b) The SD-1, also known as the MQM-57 Falconer [1].

Modern military systems such as the RQ-4 Global Hawk or the MQ-9 Reaper, which is

shown in *Figure 1.3*, have considerably improved the size, endurance and overall capabilities of their predecessors.

Figure 1.3: The MQ-9 Reaper is an updated version of the Predator UAV [1, 2].

In recent years, a growing interest has emerged for high-endurance UAVs. In 1998, the Laima aerosonde, in *Figure 1.4a*, became the first UAV to cross the Atlantic ocean. Also, the Helios Prototype, in *Figure 1.4b*, was a highly-flexible lightweight solar UAV developed under a NASA program to eventually serve as a communications platform and to be used for Earth science missions.

(a)

(b)

Figure 1.4: High endurance UAVs: (a) The Aerosonde Laima which makes a transatlantic crossing. (b) The Helios UAV developed by NASA and AeroVironment [1, 3].

In addition, the field of small UAVs is rapidly developing, with versatile models like the Skylark and Puma being used for various missions on a smaller scale. These aircraft are now widely used in various civil sectors.

Certainly, flying UAVs has become a popular hobby, using them for amateur photography, drone racing and recreational flights. They can be used for capturing images and videos for commercial purposes, including filming.

Furthermore, in the agriculture sector, they are used for crop spraying and monitoring with sensors which inform on crop health. Landscape images are also used to plan for terrain expansions. In the same way, they are used to create high-resolution aerial and terrain maps, 360-degrees virtual tours and measure cattle pickets volume, enhancing accuracy and reducing costs.

In addition, drones aid in locating lost people, conducting rescue missions after natural catastrophes and assessing damage. So, one of its facets is monitoring. It is used for aerial surveillance and law enforcement, evaluating traffic and detect law infractions. In relation to natural resources, it is able to track wild life, prevent illegal deforestation, dumping and hunting. Drones can inspect dangerous locations such as roofs, wind turbines, power lines at the time it reduces risk, time and costs.

On a day-to-day, new concepts of product delivery are reached with UAVs. They help to reduce shipping costs and delivery times. Companies are also exploring UAVs for short-range passenger transport, although this is still in its early stages.

In summary, UAVs have evolved from ancient concepts to sophisticated modern tools, driven initially by military needs and now expanding into numerous civil applications. This evolution is supported by advancements in propulsion, aerodynamics, flight mechanics, and control systems.

1.2 Motivation and state of the art

The UAV field has experienced rapid growth and has garnered the attention of researchers globally. Its diverse subdomains and expansive scope have turn it into a dynamic and active area of study, attracting significant investments.

Technological advancements are opening new possibilities in the UAV market. Studies are currently dealing with the endurance and efficiency of these aircraft, which are becoming more accessible as their capabilities continue to evolve.

The rising importance of hydrogen and other sustainable fuels is a critical factor to consider. As a result of population growth and industrial expansion, global energy consumption is expected to surge in the next years. In this case, there will be a larger need to develop alternative and sustainable energy sources to meet the increasing demand without harming the environment.

Additionally, the adverse environmental effects of traditional fossil fuels are becoming more evident. The use of fossil fuels has been linked to climate change, air pollution, and other environmental issues, which can have serious consequences for human health and well-being. Transitioning to more sustainable energy sources is essential for mitigating these negative impacts and ensuring a healthier future for the environment.

The applicability of UAVs today is outstanding. Looking at its sensor-carrying capacity, LiDAR is worth highlighting as it allows a wide range of options for data processing and in-

formation gathering in different areas such as mountainous terrain, coastal areas among others. Knowing that 3D mapping is considered a very useful tool for several functions, which makes it a UAV functionality worthy of study.

Then, the essence of this thesis lies in the fusion of ongoing innovations around UAV field and the exponential growth of their applications.

1.3 Objectives and structure

There are several initiatives for changing the fact that the aerospace sector hardly depends on fossil fuels, and becoming a cleaner one. In UAV market, the use of electric batteries is widely considered, but for this thesis, the objective of designing a hydrogen-powered eVTOL (electric Vertical Take-Off and Landing) UAV is chosen. This is because the wide range of advantages considering environmental impact and sustainability, as well as efficiency.

Among the several fields where the use of drones has augmented, the hydrology, geomorphology, spatial planning and ecosystem planning are the highlighted ones, among others. For this designations, the LiDAR sensor is the selected one to be incorporated due to the interest in introducing this particular application of the UAV and the different options it provides.

Mixing these objectives and studying the conditions required to be in the current market will give the key for this thesis.

To accomplish this, a conceptual model of a hydrogen-powered eVTOL UAV will be designed, with the incorporation of a LiDAR sensor and considering, qualitatively and approximately, the limitations of this sensor while modeling the UAV.

The model will be obtained by following some iterative sizing methodologies, defining the propulsive and power systems in accordance with the designated flight limitations and desired flight characteristics. Finally, an aerodynamic optimization of the design is done. From the conceptual design result, the economical factor will be considered by selecting market products and pretending to plan a potential future model.

A comprehensive analysis of the environmental impact will be performed, considering the aimed design and compare it to its predecessor, establishing the option of hydrogen technology as an alternative energy source fully capable of substituting the current energy sources used in order to achieve a reduction of the carbon footprint, while improving efficiency and performance. This will offer a potential pathway for improvement through ongoing research, enabling the extraction of its full potential.

The project is structured into various sections, each addressing different aspects. Initially, there will be an exploration of LiDAR and UAV concepts to gain a deeper understanding, followed by an analysis of market opportunities. This will be complemented by an examination of the theoretical principles of hydrogen-powered propulsion. Subsequently, a detailed explanation of the iterative process and proposed optimization for the case study will be provided, followed by the presentation and analysis of the results.

The environmental analysis will be developed by outlining its considerations and future

impact. Ending with a summary of the main conclusions, ensuring the paper concludes with a review of the initial goals and key takeaways, and determining future steps to be taken.

Chapter 2

Theoretical research

2.1 Fundamental principle of LiDAR

LiDAR, which stands for Light Detection and Ranging, is a powerful technology with several applications in different fields. It is considered an active sensor for emitting its own energy source. By using laser beams, the sensor enables highly accurate distance measurements and the creation of detailed three-dimensional models of the surrounding environment.

The fundamental principle of LiDAR involves emitting laser pulses, rather than sound or radar, and measuring the time it takes for these pulses to return after hitting objects in the environment. By accurately calculating the time-of-flight, LiDAR sensors can determine distances to objects with remarkable precision [4, 5].

Using the time measured, the distance between the sensor and objects can be determined using the formula $R = C\ (t/2)$, being R the distance and C the speed of light.

Additionally, since the system includes a Global Positioning System (GPS) and an Inertial Measurement Unit (IMU), the exact coordinates of all reflections produced by each laser pulse can be calculated. This allows the recorded data to be converted into points with (x, y, z) coordinates, enabling the analysis of height distribution to obtain information about topographic surfaces, in example.

Remember that an inertial measurement unit (IMU) is an electronic device that measures and reports the velocity, orientation, and gravitational forces of an apparatus by using a combination of accelerometers and gyroscopes. The IMU is the main component of inertial navigation systems used in aircraft, ships, and other vehicles. The data collected by the IMU allow a computer to track the position of the device accurately.

Differential GPS (DGPS) is a receiver that processes satellite information simultaneously with additional information from a terrestrial station located at a known position. This complementary information corrects positioning errors in the signals received from satellites. Based on this measurement principle, the LiDAR sensor can precisely generate a dense, georeferenced point cloud.

An example of the concepts is seen in *Figure 2.1*.

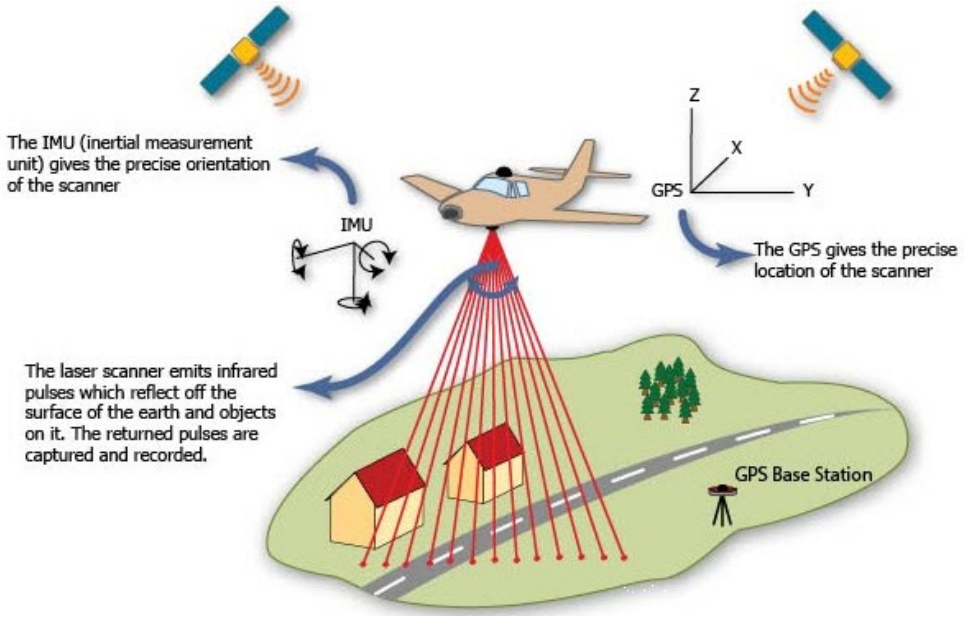

Figure 2.1: Briefly description of LiDAR concepts [6].

Current LiDAR basic components are:

- **A laser emitter**
- **Electro-optical receiver**
- **Scanner**
- **High-precision chronometer**
- **GPS + IMU**
- **Computational system for data processing**

The laser emitter emits energy at a wavelength near-infrared (1064 nm) and is directional, meaning the energy is concentrated at a single point with high intensity. The receiver captures the return of the laser, sharing the same electro-optical path as the laser to ensure the detected object is within the field of view. The scanner distributes the laser in various patterns. The chronometer synchronizes all sensors. Finally, the computational system processes and stores all collected information, calculates coordinate triplets, and records intensity values, supported by the inertial navigation system and GPS [5].

Additionally, the system may include cameras that perform simultaneous photogrammetric flights, which subsequently facilitate the classification and coloring of LiDAR points, such as those conducted by the "Plan Nacional de Ortofotografía Aérea" (PNOA) which will be introduced later on [7].

In summary, the basic principle of LiDAR operation involves emitting laser pulses, measuring their time-of-flight to determine distances, capturing the reflected pulses, and generating three-dimensional (3D) maps. This enables LiDAR sensors to provide precise spatial information for various applications in fields such as mapping, navigation, and object detection.

2.1.1 Functionality

The behavior of LiDAR pulses is highly related to the characteristics of the objects they encounter. This relationship depends on the spectral response, of each object, to received radiation, which distributes energy among absorption, transmission, and reflection processes.

LiDAR systems can be divided into two broad categories according to the method of recording the return signal, in example, discrete-return system and full-waveform system as illustrated in *Figure 2.2*.

Discrete-return systems identify returns from a pulse, with the collection criterion based on the energy received by the laser receiver. The received energy is positively related to the energy emitted by the laser, the effective area and reflectivity of the target, and the diameter of the laser receiver. It is negatively related to the emission angle, scattering angle, and ranging distance. Various echoes arrive at the receiver with different energy levels. If the received energy surpasses a certain threshold, the echo signal is recorded as a discrete point.

During laser transmission, due to the specific diameter of a laser pulse, it is possible that only a part of the pulse encounters an object. Hence, one emitted laser pulse may return to the laser receiver as one or multiple returns. For instance, flat ground typically corresponds to only one return, whereas complex forests may result in more than three returns. These returns provide the elevation and distribution information of different reflective surfaces within the laser spot. In general, the energy threshold prevents the discrete-return system from receiving unnecessary information, thereby reducing data storage and processing requirements. However, the system may miss subtle details of complex surfaces, which affects the accuracy of 3D reconstruction.

In contrast, full-waveform systems can record the complete waveform of backscattered signal echoes. This capability allows full-waveform systems to obtain the detailed 3D structural features of targets and provide additional physical attributes, such as intensity and amplitude, through a wave profile analysis. However, the amount of waveform data is usually large, and the corresponding data processing is complex and difficult.

According to the size of the laser spot, full-waveform systems can be divided into small-footprint systems (0.2-3 m) and large-footprint systems (8-70 m). Small-footprint full-waveform systems can produce a high-density point cloud with precision but are expensive and have relatively poor penetration due to low pulse energy, making them more suitable for small-scale surveys. Large-footprint full-waveform systems, with higher pulse energy, are better suited for wide-coverage surveys despite slightly lower data accuracy and spatial discontinuities [5].

Currently, discrete point clouds are the mainstream data format for recording and storing LiDAR data. The first step of processing full-waveform data typically involves converting the waveform data into discrete point cloud data before further analysis.

Then, surfaces like the ground or building roofs only absorb or reflect radiation, without transmission, resulting in a single return when directly hit by LiDAR pulses.

Nevertheless, it's important to note that not all pulses will penetrate through the entire canopy to reach the shrub layer or ground. This depends on the forest density and technical flight properties. Hence, adjusting pulse density according to specific objectives becomes crucial. Commercial systems typically store up to five returns. For instance, low-density flights from PNOA show that most pulses correspond to first returns, with a small percentage of second returns, and practically none or very few third, fourth, or fifth returns [7].

In addition to height distribution data from returns, LiDAR sensors also capture intensity

data for each return. Intensity can be defined as the amount of energy reflected by the object struck by the laser. This energy varies depending on laser characteristics, material properties, health status, and environmental conditions, leading to intensity fluctuations across different flights and even within the same flight line. These variations often discourage their use in quantitative forest inventories, according to some authors. However, intensity data from LiDAR returns remains valuable for generating useful images when updated orthophotos of the study area are lacking.

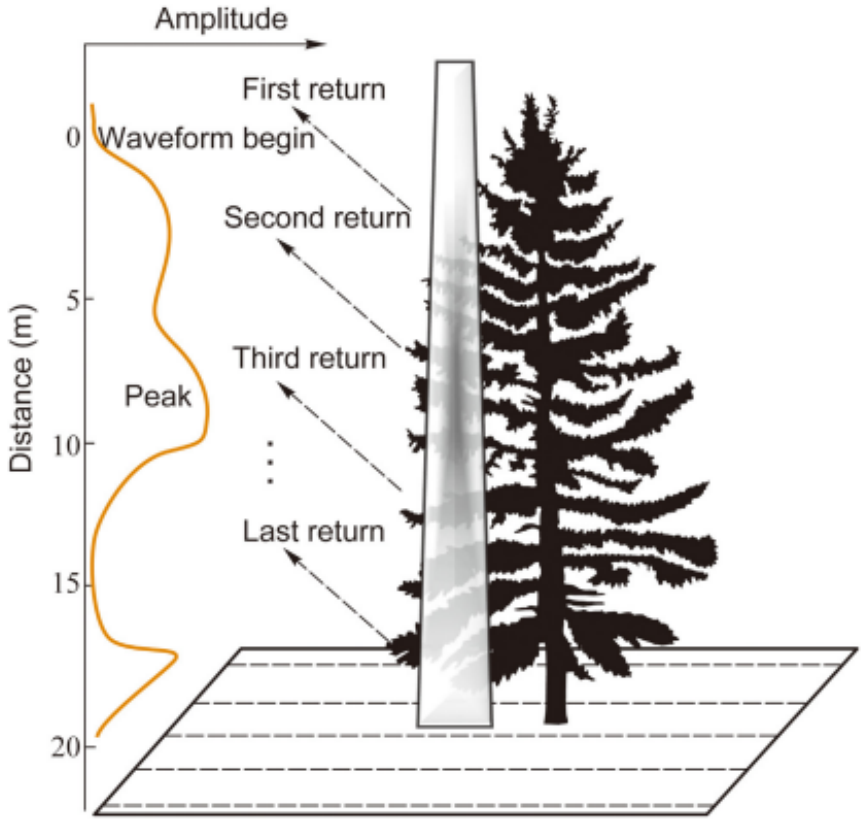

Figure 2.2: Comparison of the discrete-return and full-waveform LiDAR systems [5].

LiDAR data, along with field data, constitute the foundational information necessary for a project. Generally, some attributes of LiDAR data include flight altitude, pulse density per unit area, scanning frequency, scanning angle referred to the Field of View (FOV), the number of returns the sensor can record, and swath width, among others. When planning a LiDAR flight, it is advisable to follow the recommendations of the provider, ensuring data reliability and quality.

When discussing LiDAR information, special attention is given to pulse density per square meter, as this attribute is the most crucial for the study. Pulse density in a LiDAR flight typically refers to the average density of first returns.

Overall, the pulse density obtained in a LiDAR flight depends on several factors:

- **Flight altitude and speed**: Airborne LiDAR sensors (airplanes, drones, etc.) can capture point densities exceeding 40 points/m^2. These LiDAR flights are used, for instance, to characterize power lines and detect hazardous elements or trees that may pose a risk to the lines in the future.
- **Pulse frequency**: This frequency can reach around 200,000 Hz, meaning 200,000 light pulses emitted per second.

- **Scanning angle, typically referred to as FOV**: Larger scanning angles result in lower point densities. The scanning angle affects data quality and the laser's ability to penetrate vegetation; as the scanning angle increases, LiDAR penetration into vegetation decreases.

Combining low point density with a large scanning angle can have adverse effects.

LiDAR is extensively used in robotics and drones. In these fields, LiDAR sensors facilitate obstacle avoidance, path planning, and navigation, enabling robots and drones to operate autonomously in complex environments. Additionally, LiDAR's capability to generate detailed 3D maps supports applications such as environmental monitoring, terrain analysis, and infrastructure inspection.

Beyond transportation and robotics, LiDAR is valuable in environmental monitoring, including forestry management, floodplain mapping, and ecosystem analysis. It assists archaeologists and cultural heritage experts in site mapping, documentation, and preservation efforts. Furthermore, LiDAR supports urban planning and infrastructure development by providing accurate data for Building Information Modeling (BIM), city modeling, and intelligent transportation systems [4].

In the forestry sector, LiDAR is a highly versatile tool for evaluating and describing forest ecosystems from both qualitative and quantitative perspectives. It provides a large volume of data that is invaluable for the planning and management of our forests.

2.1.2 Conditions and limitations

LiDAR sensors provide highly accurate distance measurements, allowing for precise mapping and object detection. The time-of-flight principle enables sub-centimeter level accuracy, making LiDAR suitable for applications that require precise spatial information.

Also, they generate detailed 3D maps of the environment, capturing fine-grained information about the shape, structure, and elevation of objects and surfaces.

LiDAR sensors operate using active illumination, emitting their own laser pulses. This makes them less susceptible to varying lighting conditions compared to passive sensors like cameras. LiDAR can function effectively even in low-light or nighttime scenarios, ensuring reliable data acquisition.

These sensors enable accurate detection and classification of objects in the environment. By analyzing the reflected laser pulses, LiDAR can distinguish between various objects, such as pedestrians, vehicles, and obstacles.

LiDAR sensors have a relatively long detection range, allowing them to capture data over large distances. Their wide field of view and ability to scan in multiple directions enable comprehensive coverage of the environment, facilitating efficient mapping and monitoring tasks.

Among the limitations of LiDAR Sensors:

- **Cost**: LiDAR sensors can be expensive compared to other sensing technologies, which can limit their widespread adoption in certain applications. However, advancements in technology and mass production are gradually reducing the cost of LiDAR systems.

- **Limited Penetration Capability**: LiDAR sensors have difficulty penetrating certain materials, such as dense vegetation, fog, or rain. In such cases, the laser pulses may be scattered or absorbed, resulting in reduced performance or incomplete data acquisition. This limitation can affect applications like forest analysis or remote sensing in adverse weather conditions.

- **Data Processing Requirements**: LiDAR sensors generate large volumes of point cloud data that require substantial computational resources for processing and analysis. Efficient algorithms and powerful computing systems are necessary to handle the data and extract meaningful insights, which can increase the complexity and cost of implementing LiDAR-based systems.
- **Limited Color and Texture Information**: While LiDAR sensors provide accurate geometric information, they do not capture color or texture details of objects or surfaces. This can be a limitation in certain applications where color or texture information is crucial, such as in visual recognition tasks or detailed material analysis.
- **Physical Size and Weight**: Traditional LiDAR sensors can be bulky and heavy, making them challenging to integrate into compact or weight-sensitive devices like drones or handheld devices. However, advancements in solid-state LiDAR technology have led to the development of smaller, lighter sensors that are more suitable for such applications.

PNOA-LiDAR

Knowledge of terrain elevation is essential to help determine suitable locations for human activities and developments, for mapping, generating 3D models, defining watersheds, mapping flood zones, forest inventories, predicting the spread of physical phenomena (pollution, landslides, etc.), studying ecosystems or studying climate change. In fact, terrain elevations are considered a fundamental global geospatial data by the United Nations, the INSPIRE directive and the National Cartographic System.

The technology that allows the most accurate capture of elevation information is LiDAR. Its development and consolidation throughout the 20th century has made it possible to obtain high quality orographic information.

Then, the PNOA, developed by the Ministry of Transport and Sustainable Mobility of Spain, is introduced.

In 2009, after carrying out a series of pilot tests, and in response to the need of some of the project partners for more accurate digital terrain models, the opportunity arose to incorporate LiDAR technology into the PNOA project, thus giving rise to the PNOA-LiDAR project.

The aim of the project is to capture three-dimensional information by means of airborne LiDAR sensors of the whole territory of Spain, generating a series of products from this capture (point cloud with coordinates, Digital Terrain Models, etc).

The project cycles are the following ones:

- **1st coverage**: flights carried out between 2009 and 2015.
- **2nd coverage**: flights carried out between 2015 and 2021.
- **3rd coverage**: flights planned between 2022 and 2025.

The density at which the coverages were captured has evolved, starting at 0.5 points/m^2 for the first coverage and reaching 5 points/m^2 for the 3rd coverage. The altimetric accuracy has also evolved, starting with a RMSE (Root Measurement Square Error), in Z direction, of 40 cm in the 1st coverage and reaching 10 cm in the 3rd coverage.

The point clouds and derived products are distributed through the CNIG ("Centro Nacional de Información Geográfica") which is the spanish national centre for geographic information .

Having defined the PNOA, the mission for the eVTOL UAV is to be part of this project and perform flights for the 3rd coverage.

Assuming that the mentioned coverage is done in the "Comunidad Valenciana" (denotated as VAL), which is actually being processed by the PNOA. The 3rd coverage started in agost of 2023 and it is still on going. In *Figure 2.3*, it can be seen the state of the PNOA along Spain.

Figure 2.3: Years for flights of the PNOA [7].

Then, the limitations and conditions for the mission designated to the eVTOL UAV developed are an adaptation from some of the PNOA technical specifications [8].

Ending up in the following ones:

- **Frequency of data analysis**: greater or equal to 200 Hz.
- **Precision**: lower or equal to 2 cm.
- **Accuracy**: lower or equal to 2 cm.
- **Altitude**: from 100 to 440 AGL (Above Ground Level).
- **FOV**: the maximum FOV will not be set, it can go from 0 to 360 degrees.
- **Flight speed**: The speed shall be set according to the data capture specifications such as maximum allowed FOV, sweep and pulse frequency. Also, in function of the final point density to be obtained.
- **Weight**: the weight of the sensor should be lower or equal to 3.5 kg (without considering de battery).
- **Distance**: Instead of determining a certain distance, as a specific flight plan is not going to be developed, the autonomy is set to be the critical parameter. It is aimed to obtain an autonomy of 4 hours considering the flight consumption and the LiDAR battery duration.

- **Weather conditions**: in general, flight shall not be possible in clouds, fog, haze, seasonal snow, smoke, dust, flooded areas, or environmental factors that hinder or degrade the accuracy of the sensor.

It must be mentioned that PNOA consideration, as the specifications determined for the project, are just an approximation for developing the conceptual design. So, there is no study behind the specifications which are just set for optimizing the autonomy of the flight with an altitude and speed fixed. With this, it is introduced the different constraints that a project like this could have.

In addition, further restricted parameters to consider will be stated in order to obtain the best performance, being possible to adapt this characteristics to the conditions designated to perform the PNOA flights. This conditions will be shown in the UAV Sizing Methodology, as the mission profile.

2.1.3 Market overview and selection

For the PNOA project designated, the LiDAR sensor selected is ATLM Galaxy T2000 of Optech, from the hand of UTE Geofit - Heligràfics [9, 10].

However, due to the UAV selection as airborne, instead of an airplane, the payload it can carries out is limited. So, the market is studied for selecting the best option while fulfilling the requirements for the project.

In *Table 2.1*, it is shown the different models of LiDAR sensors considered and its specifications.

Table 2.1: Market comparison of different LiDAR sensors models [11, 12].

	Mapper+	***Explorer***	***Voyager***	***Surveyor Ultra***	***JoLiDAR-LR22***
Precision [cm]	3.5	2	0.5	3	2
Accuracy [cm]	4	2	1	2.5	1.5
Flight Speed [m/s]	10	10	30	10	-
Maximum AGL altitude [m]	100	200	440	140	500
Point density [points/m^2 @ m AGL- m/s]	170@100-10	50@100-10	24@300-30	60@100-10	70@150-30
FOV	70.4° x 4.5°	360°	100° x 20°	360° x 40.3°	360°
Frequency of analysis [Hz]	to 10	to 165	to 400	to 20	to 600
Weight [kg]	1.1	1.8	3.5	0.98	5.4
Size [LxWxH in mm]	150x104x132	270x118x135	369x117x183	153x113x117	323x209x129
Autonomy [h]	1	1	1	1.2	-
Electric consumption [W]	35	55	55	20	65
Working temperature [°C]	-10 to +40	-10 to +40	-10 to +40	-10 to +40	-
Echoes by shoot	to 3	to 5	to 32	to 3	to 15
Shoots per second	to 240,000	to 500,000	to 2,400,000	to 640,000	to 1,500,000
Laser range [m]	230	300	1250	300	1845
Laser wave longitude [nm]	905	1550	1556	905	905

After exploring several options and checking the common factor in the LiDAR sensors used in UAVs, the selected devise is the Mapper+, seen in *Figure 2.4*.

This is due to the searched optimization of the model and the comparison with the UAV market over view, done in next chapter.

Figure 2.4: LiDAR sensor selected [11].

The selected sensor fulfills the requirements and it is extremely light. In the case that other requirements were searched, the sensor could be changed to the Voyager in example, which seems to be also suitable as well, with better characteristics but heavier.

2.2 Unmanned Aerial Vehicles (UAVs)

2.2.1 Previous considerations

The main objective is to propose a conceptual design for an UAV with hydrogen propulsion system, but it must deal with the market competitors, so a study of similar UAVs and LiDAR sensors used by them is done.

2.2.2 Multi-Mode eVTOL UAV concept

Multicopter-type UAV systems have become extremely popular in recent years and are widely used due to their high maneuverability, ease of control, and VTOL capabilities. However, the main disadvantage of multicopters is their high power consumption, which results in relatively short operational time, typically less than half an hour. On the other hand, Fixed Wing (FW) aircraft provide greater power efficiency for the cruising flight, resulting in longer endurance and/or higher payload capability. The development of multicopter systems leads to the introduction of a new type of VTOL aircraft that has a conventional FW configuration with an additional multicopter style VTOL propulsion system.

This configuration inherits the advantages of both schemes. It is able to replace UAV systems that are currently used for aerial mapping and surveillance and to enter the developing market of personal delivery aircraft.

In *Table 2.2* the features of all three aircraft schemes are summarized.

Table 2.2: Comparison of multicopters, fixed wing and FW-VTOL aircraft schemes [13].

	Multicopter	**Fixed wing aircraft**	**FW-VTOL aircraft**
Takeoff/landing	VTOL	Runway, catapult	VTOL/STOL
Hovering	Yes	No	Yes
Maneuvering	Very agile	Medium	Medium
Stability	Unstable	Stable in forward flight	Stable in forward flight
Range, endurance	Low	High	Medium
Forward speed	Low	High	High
Payload	Low	High	Medium
Control system	Propeller RPM change	Control surface deflection	Both

Considering the situations in which the UAV with LiDAR functionality could be encountered while performing its mission, the UAV is set to be a Multi-Mode eVTOL. The geographic characteristics and the short distances to take-off, in the terrain designed to be measure, can lead to the necessity of VTOL mode.

Nevertheless, with the distances, time invested in the measurements and in consequence the speed of the UAV on mind, a fixed wing mode is incorporated, matching with the efficiency optimization purposes as well.

Multi-mode eVTOL UAVs have separated FW and VTOL propulsion systems that operate independently in function of the flight mode. During the transition mode, both systems work simultaneously since the VTOL system does not provide enough lift until the UAV gains sufficient forward speed. Despite this, the functions of the two systems are not shared, allowing for independent sizing of each propulsion system.

Furthermore, the energy supply systems and propulsion systems are categorized based on flight modes. The VTOL mode demands more power but has a shorter mission time, resulting in lower energy requirements compared to the FW mode. Conversely, the FW mode consumes lower power compared to the VTOL mode, however, it demands more energy due to the extended mission duration. Hence, it is essential to implement a suitable energy supply system for the flight modes of the UAV. *Table 2.3* shows a recommended energy supply system based on power and energy needs.

Table 2.3: Operation concept of a multi-mode UAV [14].

Mission	**Required Power**	**Required Energy**	**Energy Supply System**
Hovering	High	Low	Battery
VTOL	High	Medium	Battery
Transition	High	Low	Battery
Steady level flight	Low	High	HFC
Climb	Medium	High	HFC
Descent	Low	Low	HFC

2.2.3 Market overview and selection

Bearing in mind the energy supply requirements, an investigation of the current market is done. The considered aircraft have similar characteristics and are being used for missions with

the same aim as the one selected for this thesis. Also, the LiDAR sensors that usually are integrated in the studied models are checked out [15].

Moreover, on the basis that there have been several attempts to hydrogen-powered UAVs since the last decade, some of them are named in order to compare with the current market of UAVs with LiDAR functionality.

Now, a brief description of the model is done, accompanied by an illustration of each one to verify their common aspects, available in *Figure 2.5*.

After that, *Table 2.4* shows some of the characteristic data of the models considered. In this way, an order of magnitude of their geometry and weights, for certain flight conditions and performance, are shown.

- **JOUAV CW-25H (DJ25)**: CW-25H hydrogen-powered VTOL fixed-wing UAV system is a co-production by JOUAV and Doosan Mobility Innovation.

  CW-25H deploys the new generation of DM15 lightweight fuel cell system [16], which adopts the integrated design of fuel cell power system, hydrogen tanks, and power management system all in one to achieve high stability and reliability.

  This UAV has VTOL capability. The endurance almost reaches the 5 hours. The geometry form can be seen in *Figure 2.5a*.

- **Sparkle Tech Eagle plus VTOL**: For this UAV, the configuration of the propeller allows a VTOL capability as well. It is powered by a HFC and battery (in order to help during the peak power). The payload it can carry out is quite important and the endurance almost reaches the 5 hours. The geometry form can be seen in *Figure 2.5b*.

Apart from the Hydrogen-powered UAVs which already exists, the electric-powered UAVs are exposed due to the necessity of competing with them for a place in the current market. In this way, even though the hydrogen has the potential to take the innovation to other levels, it must demonstrate the capacity to compete with the current characteristics of the UAVs which lead the market.

- **JOUAV CW-25E (Voyager)**: CW-25E is a battery-operated UAV designed to efficiently and safely collect data, it can support various payloads to suit every job, and can work virtually every type of site. From the same company as the first JOUAV model, having similar characteristics despite the fact that the electric one has almost half of the endurance of the hydrogen-powered. It also has lower cruise speed but it can carry out a slightly greater weight.

  Highlighting the fact that for this model, the Voyager LiDAR sensor can be incorporated.

  The model appearance is shown in *Figure 2.5c*, with the sensor incorporated.

- **Carbonix Volanti (Mapper+)**: Volanti is an advanced all-electric fixed-wing RPAS developed by Carbonix. It is capable of rapid aerial surveys across vast and difficult terrain with high accuracy and high confidence. With VTOL capability, in common with previous models. It is shown in *Figure 2.5d*.

  The Mapper+ sensor can be incorporated to this design.

- **Germandrones Songbird VTOL (Surveyor Ultra/Mapper+ OEM)**: The Songbird is an analysed UAV with the V-Tail form. Its parameters turns out to be similar than the ones for the pre-selected models, having a high speed and range. Its geometry can be seen in *Figure 2.5e*.

  For this model, the Surveyor Ultra, as the Mapper+, can be incorporated.

- **StriekAir CarryAir VTOL (Explorer)**: Being the first UAV with delta wing to be analysed. The parameters obtained from the investigation of this aircraft shows a similar behaviour and data to the other UAVs. In *Figure 2.5f*, the dimensions of this UAV can be seen as the sensor Explorer incorporated which is the commonly used.

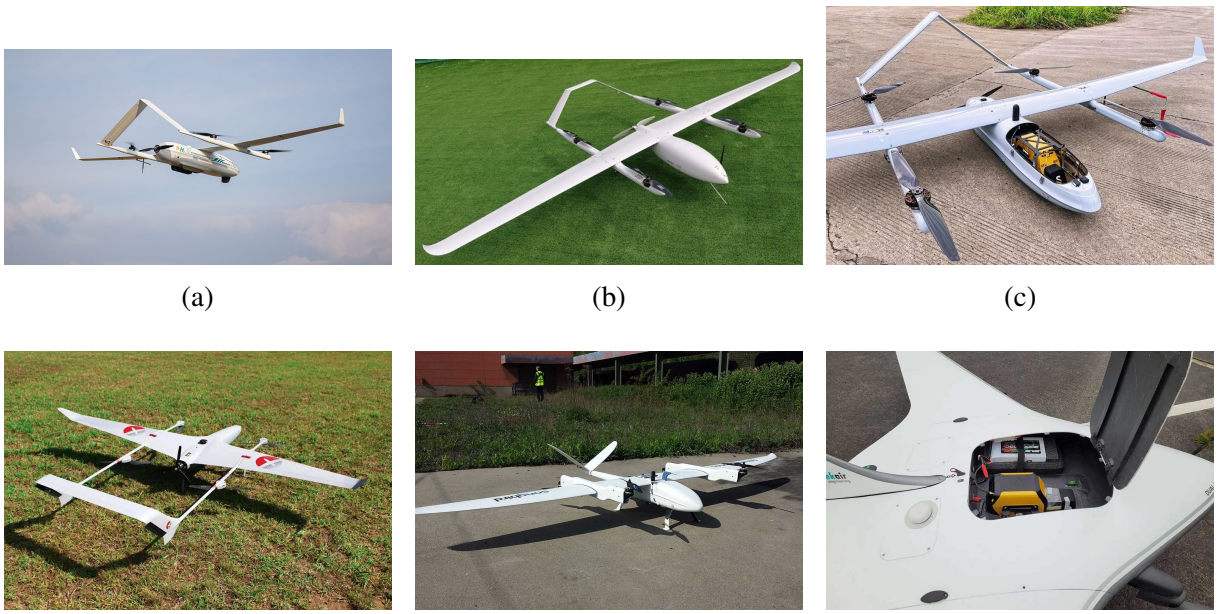

(a) (b) (c)

(d) (e) (f)

Figure 2.5: UAVs pre-selected from the current market: (a) CW 25H hydrogen-powered VTOL fixed-wing UAV [17]. (b) Eagle plus drone [18]. (c) JOUAV CW 25E [19]. (d) Carbonix [20]. (e) German Drones Songbird [21]. (f) StriekAir [22].

Table 2.4: Characteristics for similar aircraft.

	CW 25H	**Eagle plus**	**CW 25E**	**Volanti**	**Songbird**	**CarryAir**
b_w $[m]$	4.40	3.50	4.35	3.6	3	2.99
S_w $[m^2]$	1.23	0.70	-	-	-	-
AR	15.74	17.50	-	-	-	-
l_f $[m]$	2.10	2.00	2.18	2.040	-	-
d_f (max) $[m]$	0.40	0.30	-	-	-	-
W_{empty} $[kg]$	25	12.50	-	-	-	17.50
$MTOW$ $[kg]$	31	22	31.58	16	14	25
W_{PL} $[kg]$	4.00	10.00	6	2	4.4	7
W_{fuel} $[kg]$	2.00	1.50	-	-	-	-
V_{max} $[m/s]$	27	33	-	28	32	28
V_{cruise} $[km/h]$	22.20	26	19.50	24	24.5	19.50
E_{max} $[h]$	6	5	3.5	2	1.3	7.5
z_{max} $[m]$	3500	4000	6000	2000	5000	2000

The models are very similar, with the first three having a similar geometry and identical tail shape. For the rest of the models, Π and V-shaped tails can be seen.

From this data, although there is a lack of information on the characteristics of some models, a general idea of the parameters sought can be conceived. Restricting, in this way, the characteristics of the conceptual design to be developed in a range according to the data presented. This constraints are exposed in the optimization chapter.

2.3 Fundamentals of Hydrogen-powered propulsion

Hereafter, the systems of hydrogen-powered vehicles are introduced, giving a brief description and analysing the different elements involved. Also, giving some of the advantages provided by these systems, as well as future challenges.

The electric-powered systems are placed as the alternative to the fossil fuels for a cleaner energy consumption. However, the substitution of the fossil fuels, currently used in so many fields, seems to be far away by the moment. This is due to the fact that the current battery technology does not catch up the requirements of the vehicles technology of today. The energy density stored by lithium batteries is very small (0.2 Kwh/kg) compared to petrol (1.4 Kwh/kg).

Fuel cells powered by hydrogen (H_2) appears as a game changer, with an energy density of 1 Kwh/kg. By the hand of this technology, it is possible to increase the autonomy with an electric motor and battery.

In the UAVs field, pressurised bottle of H_2 gas have recently arrived on the market. The autonomy of a drone is increased in four times, reaching 2 hours or more without any problem.

Drones up to 30 kg, even heavier, can be found being supplemented by batteries for power peaks. In addition, the use of H_2 as fuel has the advantage, over petrol, that the emission of polluting gases is zero, as the only waste from the cell is water. With this, the environment goals, towards a greener world, are satisfied.

In terms of suppliers of HFC for UAVs, the US company H^3 Dynamics and the Korean firm DOOSAN Mobility stands out [16, 23].

The price of H_2 cells ranges from 9,200 € for low-power cells to 36,800 € for higher-power cells, including the cost of the H_2 cylinder and pressure regulator. These are high prices, but they are expected to fall in the medium term due to competition between companies and increased production.

As for the supply of H_2, it is marketed in hydrogenerators or in steel bottles at a pressure of 200 bar. The average price in hydrogenerators is 10 €/kg (with a minimum cost per supply of around 50 €) and 100 €/kg in 50-litre bottles. As a reference, a 25 kg drone can be considered to consume 200 g/h if it is of the multicopter type and 100 g/h if it is fixed-wing.

2.3.1 Fuel Cells working principle and architecture

A concise summary of the systems utilized in hydrogen-powered vehicles is presented, offering a detailed explanation and assessment of the various components, along with an examination of the advantages and obstacles encountered by these systems. Additionally, an examination of a Balance of Plant (BoP), a term commonly used to refer to the supplementary components necessary in a fuel cell system, will be conducted.

Fuel cells utilize "REDOX" reactions to generate electrical energy from fuels such as hydrogen, without the need for combustion. The reaction is divided into two parts, resulting in the production of electricity rather than heat.

Fuel cells operate by utilizing two distinct chemical processes: oxidation and reduction. During these processes, the fuel undergoes oxidation, releasing electrons that are then acquired by the oxidizer, leading to its reduction.

A diverse range of fuel cells have been created to suit different applications, yet they all adhere to a common design pattern as depicted in *Figure 2.6*.

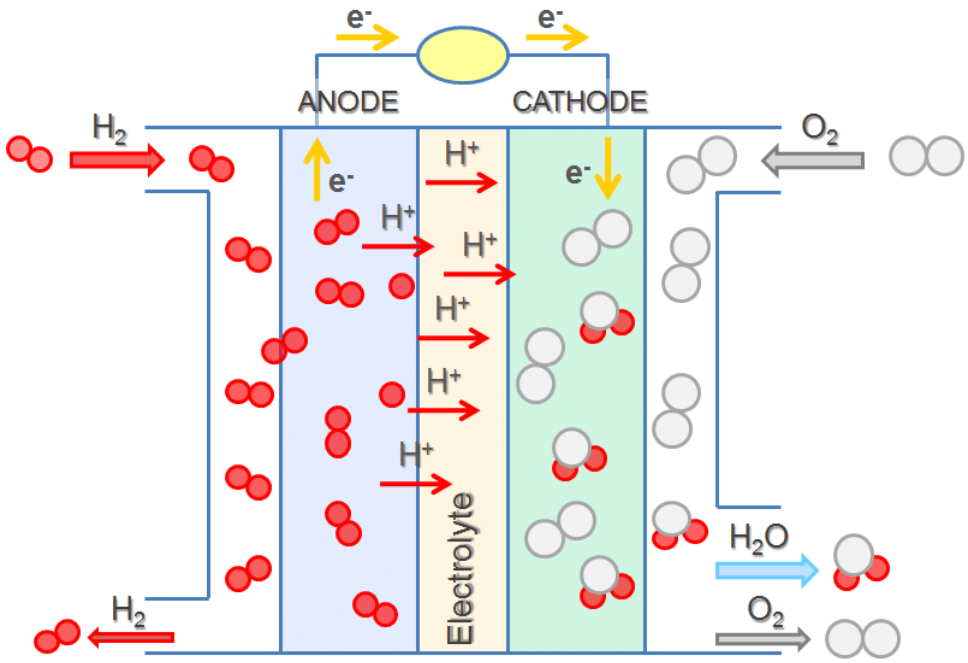

Figure 2.6: Hydrogen-oxygen fuel cell scheme [24].

The fuel is divided into a positively charged ion and electrons at the "Anode" in the presence

of a catalyst. The electrolyte membrane permits only ions to pass through, so the electrons are compelled to travel through the electric circuit, generating the current that powers the loads. Upon exiting the circuit and reaching the cathode, the electrons combine with the oxidizer, producing an electric current.

The reactions differ according to the specific fuel cell utilized, depending on its design and particularly the electrolyte component. To simplify matters, a chemical equation pertaining to solid oxide fuel cells is selected to illustrate the reactions:

$$\begin{aligned} \text{ANODE:} \quad & H_2 \longrightarrow 2\,H^+ + 2\,e^- \\ \text{CATHODE:} \quad & O_2 + 4\,e^- + 4\,H^+ \longrightarrow 2\,H_2O \\ \text{OVERALL:} \quad & 2\,H_2 + O_2 \longrightarrow 2\,H_2O \end{aligned}$$

In many cases, a single anode and cathode pair is not adequate for generating sufficient electrical power. Instead, a "stack" system, formed by arranging single cells in layers and connecting them through a bipolar plate, is used to increase the overall power output of the system.

There is a wide range of fuel cell technologies available. Distinguishing them by their electrolyte material and operating temperatures [25], appart from the fuels used.

For example, a Direct Methanol Fuel Cell (DMFC) directly uses the fuel without reforming processes. Also, some fuel cells allow a wider range of fuels to be used in the system as a result of their operating temperature and hence internal reforming capability.

With "reforming processes", it means the chemical reactions used to convert a hydrocarbon fuel into hydrogen gas before it is used in the fuel cell. Reforming typically involves processes like steam reforming, partial oxidation, or autothermal reforming, which break down the hydrocarbon fuel into hydrogen and other byproducts.

The main fuel cell systems are shown in *Figure 2.7*, but not necessarily limited to the types registered there. Other differences between the fuel cell types are the BoP components needed to create a full system, efficiencies, typical system power range and application type.

The fuel type is limited for fuel cells such as the Proton Exchange Membrane Fuel Cell (PEMFC), where only hydrogen can be used. Variations of the PEMFC are DMFC and DFAFCs (Direct Formic Acid Fuel Cells), which directly use methanol (CH_3OH) and formic acid (HCOOH) as fuels respectively.

The fact that some fuel cells, such as PEMFC, are limited to hydrogen only with very low or no carbon monoxide (CO) allowed, does not mean that no other hydrocarbon fuels can be used. Another option that is considered in the literature study is the option for reforming hydrocarbon fuels into hydrogen (and CO) which can then be fed into the fuel cell system directly. Methane and methanol are popular fuels for this specific purpose, but other options could even be formic acid or fuels normally used in the combustion engine. An important consideration would be the cleaning of the fuel, added BoP components, and complexity. This means that instead of using DMFC or DFAFC, PEMFC could still be used with the same fuels, but adding a reformer. However, reforming options will not be discussed because of the lack of necessity regarding the scope of this thesis [26].

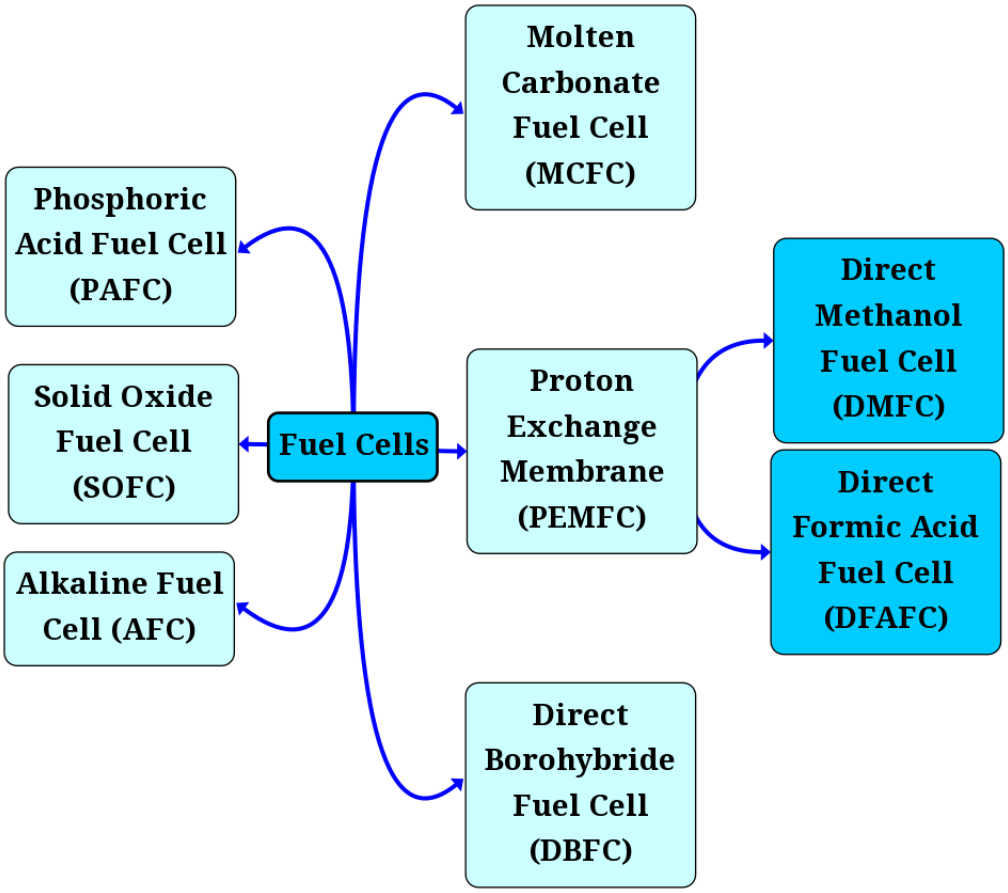

Figure 2.7: Overview of Fuel Cell types.

Even though the fuel cell serves as the core of the power generation system, various other components are necessary to maintain optimal operating conditions and ensure proper exhaust of reaction byproducts. The integration of the fuel cell stack for a propulsive application is illustrated in *Figure 2.8*. In this configuration, hydrogen is supplied to the fuel cell through the anode with wet air. The water vapor produced at the cathode outlet is utilized in the humidifier, where the incoming air is humidified before being discharged into the surroundings. The fuel cell stack is responsible for powering the entire propulsive system.

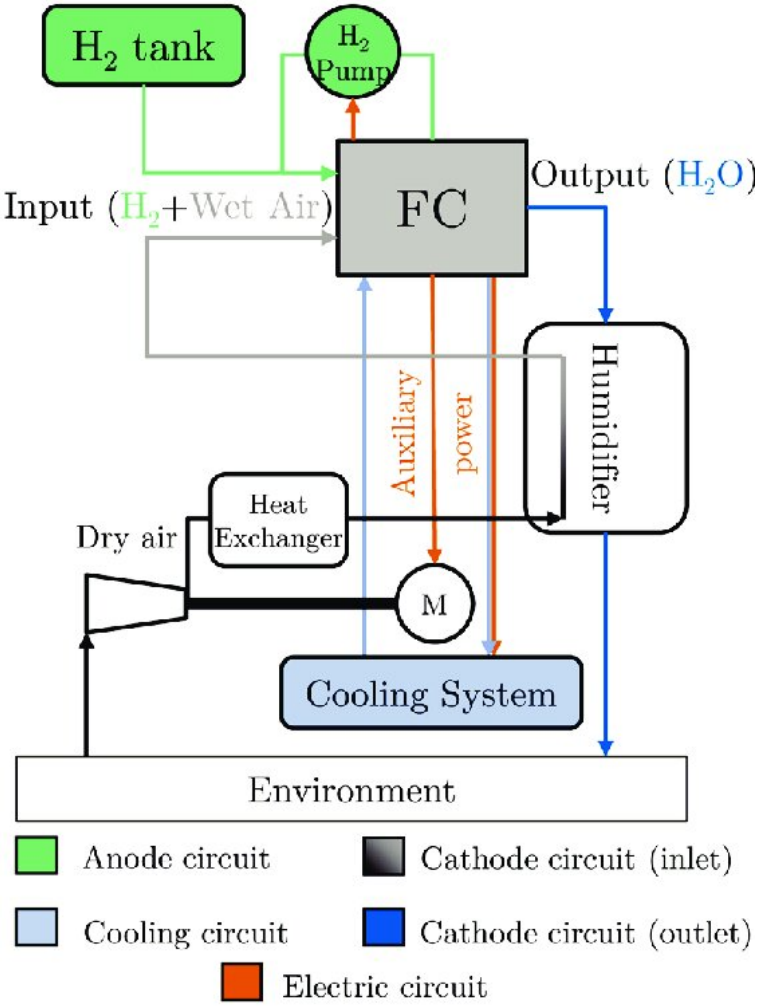

Figure 2.8: Overview of Fuel Cell System [27].

BoP is used as terminology for the fuel cell system hardware required on top of the hydrogen storage and the fuel cell stack itself. It consists of multiple elements which either increase system mass or the power requirements, reducing efficiency, energy density and power density.

BoP is needed for smooth and proper operation of the fuel cell and hence consists of systems that support the fuel cell stack. The pressure of the reactant gases for example influences the fuel cell performance and hence an air compressor is often included to improve the performance. Some of the larger components are humidifiers, compressors and the cooling system. However, other components seen are, but not limited to, pumps, blowers, pressure regulators and reformers. The fuel storage tank, often for gaseous hydrogen, can also be included in the BoP. It is important to understand the system requirements, although some fuel cell stacks in industry include cooling and self-humidification [26].

The complexity of a fuel cell design is enough itself. Such as, it is out of the scope of this thesis but, at least, a brief introduction to this topic is done.

2.3.2 Hydrogen storage system

Efficiently storing a significant amount of hydrogen as a lightweight gas requires the enhancement of its density. In standard atmospheric conditions, pure hydrogen is 11 times less

dense than air.

Approximately 11 m^3, equivalent to the size of the trunk of a large utility vehicle, are required to store 1 kg of hydrogen at atmospheric pressure. This amount would only allow for driving approximately 100 km in current hydrogen-powered cars. There are two primary methods to enhance the density of hydrogen: storing it as a pressurized gas or as a liquid under cryogenic conditions.

Gaseous storage is an effective method for storing hydrogen by pressurizing it up to 400-700 bar, increasing its density significantly. This allows for more compact storage volumes suitable for various applications. The tanks used in gaseous storage must be designed with optimized shapes and materials to withstand the high internal pressure without deformation. Typically, these tanks are constructed using highly resistant metal alloys or composites like fiberglass/aramid or carbon fiber with a metal matrix such as aluminum or steel.

Gaseous storage is particularly beneficial for stationary and road transport applications. However, when it comes to fuel cell-powered aerial vehicles with extended and irregular operation cycles, this storage method can lead to increased overall volume and weight of the storage system, presenting challenges depending on the specific usage scenario.

Hydrogen storage is a crucial component of the power system, as compressing the gas or using alternative methods is necessary to limit storage volume. Hydrogen is typically stored in tanks at either 350 or 700 bar, depending on weight and volume requirements. There are five different standards for compressed gas tanks:

- **Type I**: An all-metal cylinder.
- **Type II**: An load-bearing metal liner hoop wrapped with continuous filament.

These types are generally used for lower-pressure storage methods and, therefore, have higher volumes, making them unsuitable for vehicular applications.

- **Type III**: More advanced tanks that use metal liners.
- **Type IV**: Advanced tanks that do not use metal liners.
- **Type V**: All-composite storage tanks.

Liquid hydrogen storage systems have been developed due to the limitations of gaseous hydrogen, making them a key focus of the industry. The process involves liquefying hydrogen, which must be stored at extremely low temperatures of 32 K (-241 °C), resulting in a 700 times higher density compared to normal conditions. This reduces the storage volume by around 40 % when compared to gaseous storage. However, maintaining such low temperatures poses challenges in terms of energy requirements and materials, making these systems suitable only for specialized applications where volume reduction is crucial for feasibility.

In addition, ongoing research in this area aims to enhance current storage technologies and explore materials-based hydrogen storage. By dissociating hydrogen into atomic form within a metal lattice structure, it becomes possible to store hydrogen at low pressure and normal temperature with high volumetric density. This innovative approach shows promise for more efficient and practical hydrogen storage solutions in the future.

2.3.3 Potential and limitations

Hydrogen presents several advantages when used as a fuel. One of the key environmental advantages is the absence of carbon emissions when utilizing a HFC. Moreover, hydrogen can be generated using different techniques, and its high lower heating value enables its use in various applications, such as aerospace. Fuel cells demonstrate comparable or enhanced performance in terms of durability when compared to electric batteries, showcasing great flexibility in installation and operation. Nevertheless, it is important to highlight that fuel cells generally have lower efficiency levels than batteries.

Unlike batteries, hydrogen storage offers the advantage of creating long-term energy reserves that can be utilized for generating thermal or electrical energy. This quality makes hydrogen a versatile and strategic choice for energy storage solutions.

Nevertheless, hydrogen-based systems come with their own set of challenges. While fuel cells are not a new technology, their commercial applications have only recently been developed. Reliability data suggests that fuel cells may experience premature degradation under specific temperature and humidity conditions when compared to traditional engines.

Furthermore, the entire hydrogen life-cycle, spanning from production to consumption, encounters various obstacles that must be overcome for widespread adoption. Currently, the most cost-effective method of hydrogen production, methane gas steam reforming, is more environmentally harmful than conventional hydrocarbon usage. Alternative methods like electrolysis, although cleaner, are around seven times more expensive in the short term than fossil fuels. Moreover, electrolysis relies on electricity, which may not always be sourced from eco-friendly means.

The existing infrastructure for hydrogen production, storage, and distribution is inadequate to facilitate extensive implementation. While costs are decreasing, the necessary investments to propel this technology forward remain uncertain. Nowadays, there is a dilemma involving the current market. For producing Fuel Cell Vehicles (FCVs), a development of the infrastructure is necessary. Nevertheless, a significant number of FCVs must prove its worthiness to make the investment in infrastructure be done.

Despite the obstacles, there are grounds for hope concerning the future growth of hydrogen infrastructure. The market is being influenced by two main trends: the declining costs of renewable energy and the rising need for electricity. As renewable energy sources gain a larger portion of the energy production market, the supply chain may face increased short-term and long-term variability, as is common with wind and solar energy production. Hydrogen production has the potential to mitigate these fluctuations by storing excess energy during periods of high production and supplying power during times of low renewable energy production but high energy demand.

Research, like the examples shown in *Figure 2.10*, has proven that increased levels of renewable energy generation could result in substantial surplus energy that could potentially be transformed into hydrogen. This capability has prompted entities such as the European Union to view hydrogen derived from sustainable sources (often known as green hydrogen) as a feasible option for upcoming energy provision, notwithstanding the technical and financial obstacles that may arise.

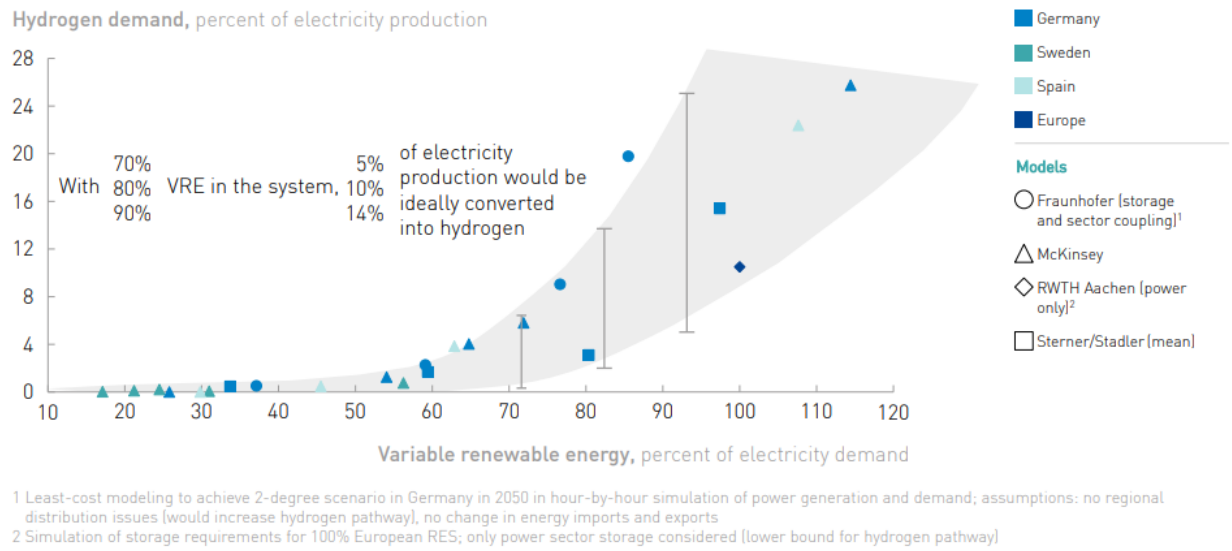

Figure 2.9: Analysis of the outcomes of power system simulations as the share of variable renewable energy increases [28].

By addressing these challenges through ongoing research and development, hydrogen has the potential to become a cornerstone of a sustainable and resilient energy system.

2.3.4 Selection of the propulsion system concept

Prior to determining the size, it is essential to identify the type of propulsion system for the UAV. It is important to highlight that the propulsion system under consideration in this research is a hybrid HFC-battery system, as shown in *Figure 2.10*.

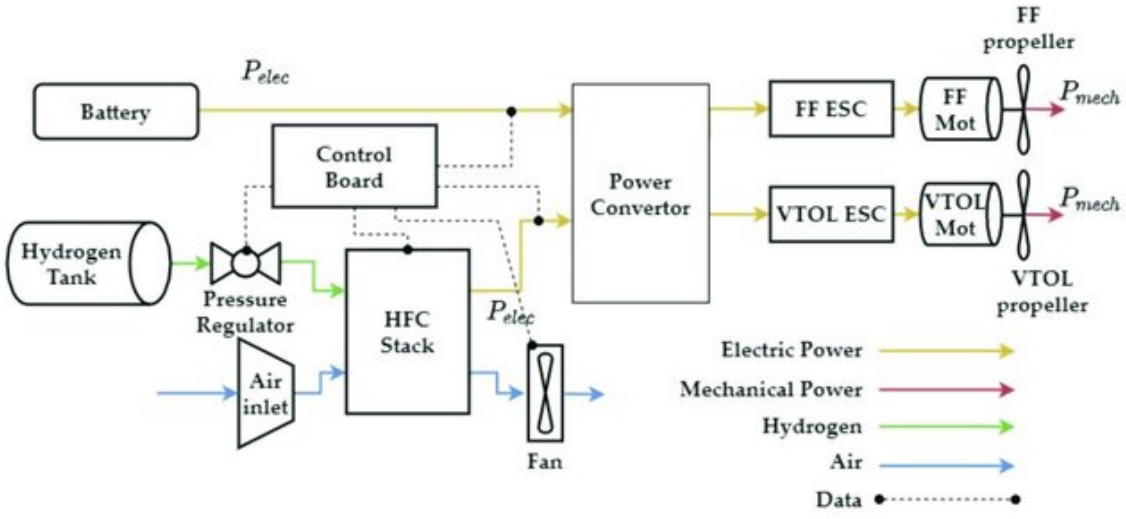

Figure 2.10: Propulsion system concept for a multi-mode HFC eVTOL UAV [14].

The HFC system comprises the primary HFC and the BoP, along with a hydrogen tank, an HFC stack for electricity generation, a regulator for fuel flow control, a control board for system monitoring using sensor data, an air inlet, and a fan for temperature regulation. The battery functions independently from the HFC system to provide power. Additionally, the multi-mode UAV operates separately from the FW and VTOL electric branch, which includes the motor,

Electronic Speed Controller (ESC), and propeller.

A selection of each component constituting the propulsion system, among the various types of them which have different characteristics, is done. Then, a suitable type is searched for applying to the UAV.

Initially, the PEMFC has been selected as the HFC due to its advanced technological development and ability to operate at a cool temperature range of 30-100 °C, which is well-suited for UAV use. In order to regulate the temperature of the PEMFC, an air cooling technique is employed, specifically designed for UAVs with a power output of less than 5 kW. A Type III tank is selected for the hydrogen storage among gaseous hydrogen tanks due to the wide range of these on the market. Although liquid hydrogen has higher energy density and is 800 times less in volume than gaseous hydrogen, it requires extremely low temperatures for storage. The chosen battery is a Li-polymer (Li-po) battery due to its lightweight, high energy density, and common usage in similar UAVs. The propulsion system details are summarized in *Table 2.5*.

Table 2.5: Configuration of the propulsion system for the HFC eVTOL UAV [14].

Components	**Type**
Hydrogen Fuel Cell	PEMFC
Cooling method	Air cooling
Hydrogen tank type	Type III tank
Hydrogen tank pressure	300 bars
Hydrogen storage method	Gaseous hydrogen
Battery	HFC
Motor	Brushless Direct Current (BLDC) motor

Chapter 3

UAV sizing methodology

3.1 Sizing Procedure

Intending to meet performance and mission requirements, several methods of estimating the size, mass, and power of aircraft are developed, resulting of great importance for aircraft design. There are several well-known sizing methodologies for FW aircraft [29–33].

Raymer has introduced the initial weight estimation method based on mission profile and a set of empirical equations [30]. The method is valid for a wide range of aircraft which are powered by Internal Combustion Engines (ICE). However, there is no sense to consider it for electric and multi-mode type propulsion systems. Significant effort was addressed to the sizing of electric FW UAVs by Gundlach [34]. The methodology presents an efficient way of calculating the battery mass fraction required for FW cruising flight as well as suggestions for UAV mass breakdown. Also, Riboldi and Gualdoni have proposed an integrated approach for the sizing of manned electric FW aircraft [35]. Keith and Hall [36] have proposed a sizing methodology for heavy ICE powered VTOL aircraft with MTOW of up to 27.5 tonnes.

This thesis presents a methodology for sizing of FW-VTOL electric UAVs selected from a mix of existing research which propose a similar procedure [13, 14, 37].

The methodology employed in this thesis is illustrated in *Figure 3.1*. Sizing is carried out by analyzing the requirements, mission profile, and making assumptions to predict the power, the geometry, and the weight of the UAV. An error margin of 15 % is considered acceptable to meet the specified requirements.

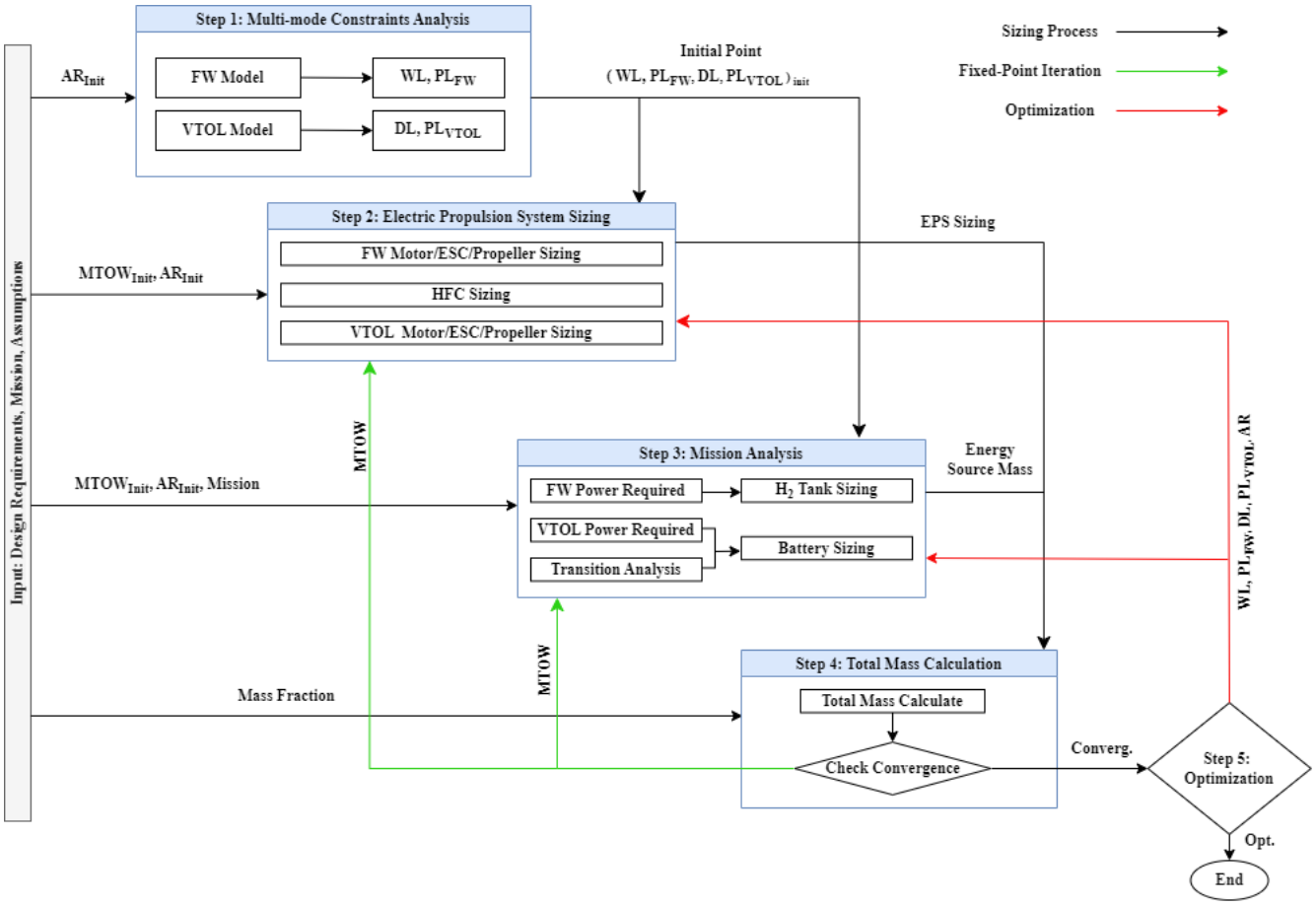

Figure 3.1: Sizing procedure applied.

The method takes into account the design requirement analysis and the mission profile data, which consists of the duration of each mission segment, the speed, the altitude, and the assumptions made for sizing, among other factors. The sizing of the multi-mode UAV is carried out in the sequence outlined in [14]:

- **Step 1. Multi-Mode Constraints Analysis (MCA)**: The MCA involves defining the design area and initial point using sizing parameters like Wing Loading (WL), Power Loading (PL), and Disk Loading (DL), as well as the initial Aspect Ratio (AR) based on performance constraints for the multi-mode operation of the UAV, encompassing both FW and VTOL modes.

- **Step 2. Electric Propulsion System (EPS) Sizing**: When sizing the EPS, it is important to consider the motor, ESC, propeller, and HFC. This process involves estimating the weight of the EPS, as well as the diameter of the propeller and the efficiency of the HFC.

- **Step 3. Mission Analysis**: This stage involves determining the necessary power for every mission segment carried out by the UAV, as well as estimating the weight of the battery and hydrogen tank accordingly. It also encompasses an evaluation of the transition segment.

- **Step 4. Total Mass Calculation**: This stage involves determining the Maximum Take-Off Weight (MTOW) of the UAV by combining the weight and mass fraction of UAV components obtained from the EPS sizing and mission analysis. The purpose of this stage is to confirm the accuracy of the calculated MTOW by iteratively performing EPS sizing and mission analysis until the MTOW converges using fixed point iteration.

- **Step 5. Optimization**: The design point is being optimized to ensure that the sizing result meets the design requirements. The objective function of the optimization is to minimize the MTOW, with design variables including WL, PL, DL, and AR.

3.2 Multi-Mode Constraints Analysis (MCA)

The constraints analysis is used to asses the design space of an eVTOL UAV with its significance. The WL and Thrust-to-Weight ratio (TW) parameters define the feasibility of the performance constraints by being expressed as $T/W = f(W/S)$. This evaluation is a key characteristic of the system. Working with a eVTOL UAV makes the performance constraints to be expressed in PL terms, as shown in *Equation 3.1*.

$$P/W = \frac{(T/W)V}{\eta_{prop}} \tag{3.1}$$

where V is the speed in the aircraft direction and η_{prop} is the efficiency of the propeller.

The EPS does not need to be adjusted for sea level conditions like ICEs do, as the performance of the motor is not impacted by variations in air density. There could be a battery capacity correction due to low temperature in some especial cases.

The criteria DL is included as a VTOL sizing parameter, and PL_{FW} and PL_{VTOL} must be defined. The most critical performance requirements for both FW and VTOL modes must be considered, which are displayed in *Table 3.1*.

Table 3.1: Constraints on performance for analyzing multi-modes constraints [14].

Flight Mode	Constraints
FW	Maximum speed level flight, maximum rate of climb, and stall speed
VTOL	Hovering, maximum speed take-off, and service ceiling

3.2.1 Forward Flight Mode

PL for Maximum Cruise Speed

The following *Equation 3.2* is an expression defining the PL constraints required when the UAV performs steady level flight [31, 38].

$$(\text{PL})^{\text{FW}}_{\text{cruise}} = \eta_{\text{prop}}/(V_{\max} \cdot q \cdot C_{D_0} \frac{1}{\text{WL}} + k \frac{V_{\max}}{q} \text{WL}) \tag{3.2}$$

$$q = \frac{1}{2}\rho V^2 \tag{3.3}$$

In this context, q represents the dynamic pressure as defined in *Equation 3.3* for a specific airspeed and altitude. The parameter C_{D_0} denotes the minimum drag coefficient, typically estimated during the initial design phase by comparing with similar UAV models. According to Raymer [30] and Roskam [33], a value of 0.03 is recommended for propeller aircraft, while Gudmundsson [31] suggests a range of 0.028–0.035 for fixed gear aviation aircraft. For multi-mode configurations with various propeller types, a higher value of 0.035 can serve as a starting point. The symbol ρ stands for air density, specifically ρ_0 at sea level with a value of 1.225 kg/m^3, and e represents Oswald's efficiency factor, which can be determined using *Equation 3.5* based on the aspect ratio AR.

$$e = 1.78\ (1 - 0.045 \cdot AR^{0.68}) - 0.64 \quad \text{Straight-wing aircraft} \tag{3.4}$$

$$e = 4.61\ (1 - 0.045 \cdot AR^{0.68})\ (\cos \Lambda_{\text{LE}})^{0.15} - 3.1 \quad \text{Swept-wing aircraft} \tag{3.5}$$

For the second equation, $\Lambda_{\text{LE}} > 30°$. In case the sweep angle is between 0 and 30, linearly interpolate between the results from the two equations [30]. On the other hand, Gundlach suggests the use, for e, of values between 0.65-0.72 for initial sizing purposes. Then, the value will be calculated and after that, it will be verified to be inside (or around) the range from Gundlach.

PL for Maximum Rate of Climb

For the maximum Rate of Climb (RoC) in the FW mode, the PL is calculated in the *Equation 3.6* [31, 38].

$$(\text{PL})^{\text{FW}}_{\text{climb}} = \eta_{\text{prop}} / (V_{\text{RoC}} \cdot q \cdot C_{D_0} \frac{1}{\text{WL}} + k \frac{V_{\text{RoC}}}{q} \text{WL}) \tag{3.6}$$

V_{RoC} is calculated as the airspeed in the direction of flight when climbing at maximum RoC as shown in *Equation 3.7*.

$$V_{\text{RoC}} = \sqrt{(\frac{2\ (\text{WL})}{\rho_0} \sqrt{\frac{k}{3C_{D_0}}})} \tag{3.7}$$

PL for Service Ceiling

The following equation can be used for calculating the service ceiling constraint. The service ceiling is the altitude where the maximum RoC is 0.508 m/s [31]. In order to account for the safety margin, it is necessary to utilize the ratio of air density. This ratio, which compares the air density at the service ceiling to the air density at sea level, can be determined using the formula provided in *Equation 3.8* and then substituted into the dynamic pressure.

$$\sigma_{\text{air}} = \frac{\rho_{\text{ceiling}}}{\rho_0} \tag{3.8}$$

Equation 3.9 represents the constraints function for level flight at stall speed.

$$(\text{PL})^{\text{FW}}_{\text{Service ceiling}} = \eta_{\text{prop}} / (V \frac{\text{RoC}}{V_{\text{RoC}}} + V \cdot q \cdot C_{D_0} \frac{1}{\text{WL}} + k \frac{V}{q} \text{WL}) \tag{3.9}$$

WL for Stall Speed

For the upper bound of the WL, the stall speed requirement is calculated through *Equation 3.10*:

$$(\text{WL})^{\text{FW}}_{\text{Stall Speed}} = 0.5 C_{L_{\max}} \rho_0 V^2_{\text{Stall}} \tag{3.10}$$

Where $C_{L_{\max}}$ refers to the maximum lift coefficient, starting with an initial value estimated for the initial sizing stage, but optimized afterwards. The V_{stall} is the stall speed.

3.2.2 VTOL mode

Hovering Flight

An FW-VTOL UAV uses multicopter type propulsion system for vertical take-off, landing, axial climb, descent and transition to forward flight. The force equilibrium equation in vertical flight can be written as in *Equation 3.11*.

$$T = W + D \tag{3.11}$$

Being T the thrust, W the weight and D the drag force.

The aircraft projection plane is perpendicular to the climb velocity vector. For this configuration of an aircraft, the flat plate drag assumption is valid. The flat plat drag coefficient is as in *Equation 3.12*.

$$C_D = 2sin^3\alpha \tag{3.12}$$

Then, C_D is equal to 2.0 in vertical motion (being the angle of attack, $\alpha = 90$ deg). The force equilibrium equation can be written in the form of the *Equation 3.13*.

$$(T)^{\text{VTOL}}_{\text{climb}} = W + \frac{1}{2}\rho \cdot \text{RoC}^2_{\text{hover}} S_{\text{ratio}} S_{\text{w}} C_{D_{\text{hover}}} \tag{3.13}$$

Where $\text{RoC}_{\text{hover}}$ is determined and $S_{\text{ratio}} = S_{\text{proj}}/S_{\text{w}}$ is introduce to account for the large portion of the drag, in vertical motion, produced by the tail and the fuselage, which cannot be neglected. It describes the ratio of total projected aircraft area to wing area. An initial guess can be assumed to be 1.3-1.4.

In the VTOL mode, the constraints function is established based on the axial momentum theory. Establishing the parameters for the profile power in the early design stage can be a challenging task. Following this, the total power needed is computed based on Figures of Merit (FoM), which indicates the relationship between the ideal induced power for a hovering rotor and the real power utilized by the rotor. The expression for FoM is illustrated in *Equation 3.14* [13].

$$\text{FoM} = 0.4742\ (T^{\text{VTOL}}_{\text{climb}})^{0.0793} \tag{3.14}$$

Equation 3.15 illustrates the power and weight constraints necessary for the UAV to maintain a hover at its maximum altitude [14].

$$(\text{PL})^{\text{VTOL}}_{\text{hover}} = \text{FoM}/\sqrt{\frac{(\text{DL})}{2\rho_0}} \tag{3.15}$$

Vertical Climb Flight

In order for the UAV to perform a vertical take-off, it needs to have climb power and parasite power along with induced power and profile power. The power limitations necessary for achieving maximum speed during vertical takeoff are outlined in *Equation 3.16*.

$$(\text{PL})^{\text{VTOL}}_{\text{take-off}} = \frac{1}{\frac{V_{\text{take-off}}}{2} + \frac{1}{2}\sqrt{V^2_{\text{take-off}} + \frac{2\text{DL}}{\rho_0}} + \frac{\rho_0 V^3_{\text{tip}} \sigma C_{D_{\text{blade}}}}{8\text{DL}} + \frac{rho_0 V^3_{\text{take-off}}}{\text{DL}} + \frac{\rho_0 V^3_{\text{take-off}}}{S_{\text{ratio}}\text{WL}}} \tag{3.16}$$

Here, $V_{\text{take-off}}$ is the vertical take-off speed.

$C_{D_{\text{blade}}}$ is the average value of the profile drag from the cross section of the propeller for the VTOL mode of the UAV, with a common value in the UAV [14]. σ represents the solidity, which expression is shown in *Equation 3.17*.

$$\sigma = \frac{n_{blade} \cdot c}{\pi R} \tag{3.17}$$

where n_{blade} is the number of blades, c and R the chord and the radius of each one. Nevertheless, for the initial design stage,it is assumed a value of 0.077 with reference to the data of the existing T-motor VTOL UAV propellers [14].

The tip speed of the VTOL propeller, denoted as V_{tip}, is determined using *Equation 3.18*. The RPM value is obtained from the specific research method utilized, and the corresponding model can be found in *Equation 3.19* [14].

$$V_{\text{tip}} = \frac{\pi \cdot \text{RPM} \cdot D_{\text{VTOL}}}{60} \tag{3.18}$$

$$RPM = 2762.786 \cdot D_{\text{VTOL}}^{-0.932} \tag{3.19}$$

3.2.3 Constraint Diagram

Though the previous constraint functions and selected data for the parameters defined, it is displayed a multi-mode constraint diagram for visualising the design region and design point.

For the x-axis, the PL is shown, with both the FW and VTOL modes sharing the y-axis in the graph but considering WL and DL, respectively. The area below the intersection between Maximum FW RoC and Stall Speed represents the design region for the FW mode. On the other hand, the area below the intersection between Transition and Maximum VTOL Speed curves is the VTOL mode design region. In this way, the points inside the design region are feasible points, selecting the initial points in this way.

Gudmundsson suggests that the selected points should minimized the wing area and the required power [31]. For this thesis, the initial point for sizing was selected for minimizing the wingspan and the FW/VTOL power. The *Figure 3.2* shows the constraint diagram mentioned.

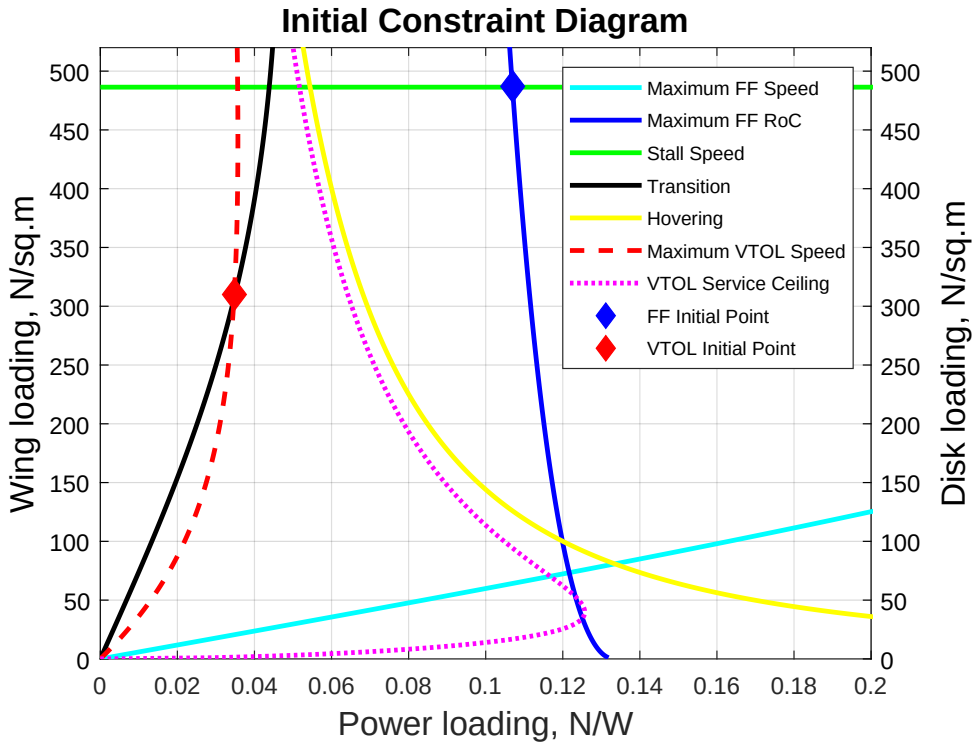

Figure 3.2: Multi-mode constraint diagram [13, 14, 37].

3.3 Electric Power System (EPS) Sizing

The motor, ESC, propeller and HFC are included in EPS. For this section, the regression models from the sizing method used are implemented [14].

3.3.1 Motor Sizing

The characteristics for the FW and the VTOL motors are different. The input for the following motor sizing, through the regression models, is the PL defined in MCA, verifying the correct operation of the motor in all mission segments. *Equation 3.20* and *Equation 3.21* are the regression models for sizing the FW and VTOL motors, respectively.

$$M_{\text{mot.FW}} = 0.19610^{-5}\, P^2_{\text{max.FW}} + 0.201\, P_{\text{max.FW}} + 5.772 \tag{3.20}$$

$$M_{\text{mot.VTOL}} = -0.92210^{-5}\, P^2_{\text{max.VTOL}} + 0.196\, P_{\text{max.VTOL}} + 23.342 \tag{3.21}$$

$P_{\text{max.FW}}$ and $P_{\text{max.VTOL}}$ are the maximum electrical power of each mode. Obtaining them through the calculated mechanical power obtained from PL and the efficiency of the motor which is approximately 90-95 %. The first value is the chosen one as it is the most restrictive.

3.3.2 ESC Sizing

The ESC is chosen to meet the peak current needs of the motor. A regression model [14] is employed to determine the maximum electric power divided by the rated voltage of the battery (U_{rated}) as the input. Considering that the maximum electric power is the maximum VTOL and

FW power needed, the *Equation 3.22* and *Equation 3.23* shows the expression for sizing the ESC for both the VTOL and FW modes, respectively.

$$M_{\text{ESC.VTOL}} = 0.324 \cdot 10^{-2} \left(\frac{P_{\text{max.VTOL}}}{U_{\text{rated}}}\right)^2 + 0.847 \left(\frac{P_{\text{max.VTOL}}}{U_{\text{rated}}}\right) + 1.532 \tag{3.22}$$

$$M_{\text{ESC.FW}} = 0.324 \cdot 10^{-2} \left(\frac{P_{\text{max.FW}}}{U_{\text{rated}}}\right)^2 + 0.847 \left(\frac{P_{\text{max.FW}}}{U_{\text{rated}}}\right) + 1.532 \tag{3.23}$$

3.3.3 Propeller Sizing

The VTOL disk's area is determined using *Equation 3.24* with the DL from the initial point in the MCA section. The combined area of the disk equals the sum of the complete disk area, and the diameter of the VTOL propeller can be determined by dividing this combined area by the quantity of VTOL propellers.

$$A_{\text{VTOL}} = \frac{W}{\text{DL}} \tag{3.24}$$

When determining the diameter of the FW propeller, various factors need to be taken into account. The performance of the FW propeller is influenced by factors such as its diameter, pitch angle, forward speed, and RPM. This complexity can make it challenging to navigate during the initial sizing phase. As a result, a regression model based on the chosen sizing method is employed [14]. The RPM per 1 volt (Kv) and the motor power are the most crucial factors in determining the diameter of the propeller. Kv is calculated based on the maximum power in *Equation 3.25*, and this value is then utilized as an input in *Equation 3.26* to compute the diameter.

$$kv = -0.228 \cdot 10^{-7} \cdot P_{\text{max.FW}}^3 + 0.0003 \cdot P_{\text{max.FW}}^2 - 1.101 \cdot P_{\text{max.FW}} + 1685.676 \tag{3.25}$$

$$D_{\text{FW}} = 4.735 \cdot \text{kv}^{-0.405} \tag{3.26}$$

Due to the different operating characteristics of the VTOL and FW modes, the propellers for each mode have different pitch angles and structure. Then, the mass of each propeller type is obtained separately through the regression models of the sizing method used [14].

In function of the propeller diameter for each mode, the mass of the own propeller is calculated in *Equation 3.27* and *Equation 3.28*;

$$M_{\text{prop.FW}} = 670.644 \cdot D_{\text{FW}}^{2.784} \tag{3.27}$$

$$M_{\text{prop.VTOL}} = 7.281 \cdot e^{3.389 \cdot D_{\text{VTOL}}} - 3.232 \tag{3.28}$$

3.3.4 Electric Branch Mass Calculation

The mass for the electric branch is calculated once the motor, ESC, and propeller sizing is done. The *Equation 3.29* and *Equation 3.30* show the way of calculating this mass for FW and VTOL mode, respectively.

$$M_{\text{propulsion.FW}} = f_{\text{install}} \left(n_{\text{mot.FW}} + (M_{\text{mot.FW}} + M_{\text{ESC.FW}} + M_{\text{prop.FW}})\right) \tag{3.29}$$

$$M_{\text{propulsion.VTOL}} = f_{\text{install}} \left(n_{\text{mot.VTOL}} + (M_{\text{mot.VTOL}} + M_{\text{ESC.VTOL}} + M_{\text{prop.VTOL}})\right) \tag{3.30}$$

3.3.5 HFC Sizing

A regression model from the sizing method [14] is used. In this way, the mass can be predicted accurately in function of the data from the currently HFC used in similar UAV. From the *Table 3.2* of the method research selected, and adding some HFC more from the market, it is shown the rated power, system weight, specific power. Also, the HFC configuration is the same for all the HFC pre-selected in order validate the use of the regression model, being the configuration of Stack, Control, Case, Fan, and Li-Po battery .

Table 3.2: HFC data from current market.

HFC	**Rated Power (W)**	**Weight (kg)**	**Specific Power (kW/kg)**
HES Aerostak A-250 [39]	250	0.72	0.35
HES Aerostak A-500 [39]	500	1.3	0.38
HES Aerostak A-1000v1 [39]	1000	2.06	0.49
HES Aerostak A-1000v2 [39]	1000	1.8	0.56
HES Aerostak A-2000 [39]	2000	4	0.50
Intelligent Energy IE-Soar 650 [40]	650	1.19	0.55
Intelligent Energy IE-Soar 800 [40]	800	1.28	0.63
Intelligent Energy IE-Soar 2.4kW [40]	2400	5.62	0.43
Doosan DM/DP15 Powerpack [16]	1250	2.9	0.43
H^3 Dynamics A-300 [41]	300	0.72	0.486
H^3 Dynamics A-800-G2 [41]	800	1.45	0.645
H^3 Dynamics A-1200 LV [41]	1200	2.15	0.560
H^3 Dynamics A-1200 HV [41]	1200	2.1	0.570
H^3 Dynamics A-2000 [41]	2000	3.00	0.667

The regression model for the HFC applied to the UAV can be seen in *Equation 3.31* using the provided data.

$$M_{\text{HFC}} = 0.423 \cdot 10^{-3} \cdot P_{\text{max.FW}}^2 + 1.08 \cdot P_{\text{max.FW}} + 451.651 \tag{3.31}$$

With this, the weight for the HFC system is predicted in conformance with the current technology level.

Chapter 4

Mission Analysis

The mission to perform is set down for the use of a LiDAR sensor as stated in previous chapters. The selected mission is to measure a forest near Valencia, called “Altos del Ragudo” with an area of 623.10 hectares (ha). And it is carried out in accordance with some of the requirements from the PNOA [8].

The code of the forest is cs3020 and it can be found in the “Conselleria de Medio Ambiente, Infraestructuras y Territorio” which is the Regional Ministry for the Environment, Infrastructures and Territory for the comunity of Valencia [42]. In addition, the limited area of the selected forest and an example of the mapping with the LiDAR sensor are presented in *Figure 4.1a* and *Figure 4.1b*.

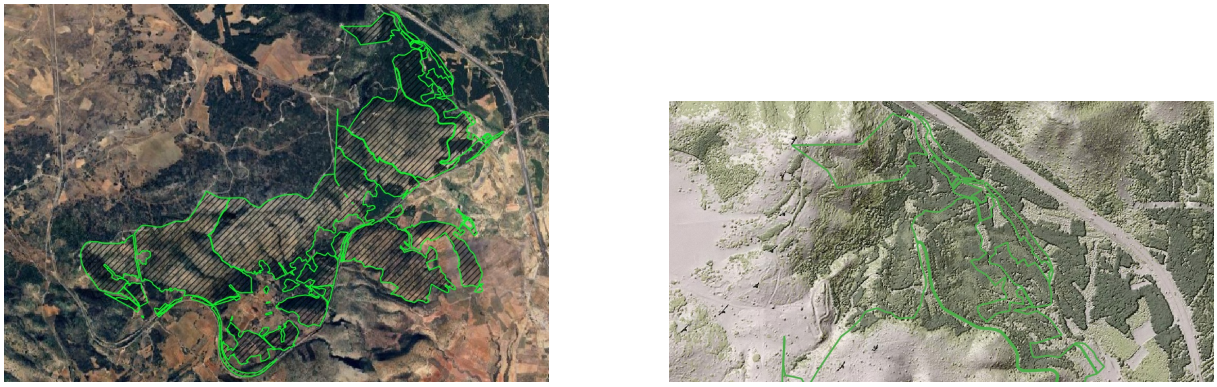

(a) (b)

Figure 4.1: Captures of the mission: (a) Area of the forest with a vector limitation. (b) Map of the forest obtained through the LiDAR sensor by the PNOA [7].

The *Figure 4.1a* is obtained by using QGIS, which is is an open source software [43]. It can handle raster and vector formats as well as databases.

Then, the different mission segments are particularised after being simplified.

Starting with a Vertical Flight for climbing until a certain altitude, continuing with a hovering flight after which, a climb in FW mode is performed. Then, the cruise segment starts with an estimated duration of 6 hours. To end with a descent in FW mode, hovering again and finally landing in VTOL mode.

4.1 Required Power Analysis

The goal of this section is to forecast the quantity and mass of fuel needed for the UAV to successfully execute the specified mission profile. This involves determining the power needed for every segment of the mission. This is achieved by converting the PL from the MCA section into a formula that determines the exact power based on WL and DL.

4.2 Transition Analysis

Transition analysis aims to calculate the power and time required for transition to decide on the appropriate battery or hydrogen tank size. The transition time for a multi-mode UAV is typically shorter and more fuel-efficient, making it less dependent on battery or tank size. Nevertheless, considering transition time and stability as crucial design factors, they must be taken into account early in the design process. While the transition mechanism for a multi-mode UAV is simpler than a tilting mechanism, a detailed analysis is necessary to determine the transition time and power requirements. Therefore, a few assumptions are made to simplify the sizing process.

The assumptions need to be consistent and guarantee the stability of the UAV during the transition process. Various strategies can be employed for the transition method, including maintaining altitude, accelerating through gliding at the start of the transition, or transitioning while climbing. This study focuses on the transition method of maintaining altitude, based on the specific mission characteristics. The assumptions for the transition analysis are outlined in [14]:

- **Assumption 1**: During the transition, the Flight Control Computer (FCC), automatically, handle all control of the UAV.
- **Assumption 2**: Throughout the transition phase, the Flight Control Computer (FCC) ensures that the altitude remains constant by balancing the forces, resulting in the lift from the wing being equal to the thrust from the VTOL propulsion system, which in turn equals the weight of the aircraft.
- **Assumption 3**: The UAV initiates the transition process once it has maintained a hovering state for a few seconds to ensure stability during the transition.
- **Assumption 4**: To ensure a stable transition, the UAV will end the transition once the FW speed reaches 1.2 times the stall speed. Additionally, the UAV will maintain the trim at the conclusion of the transition.
- **Assumption 5**: FCC offers a guide control for transition stability, allowing for a smooth switch of lift between the wing and VTOL thrust.
- **Assumption 6**: To ensure a stable transition, it is important to reduce the transition time by maintaining the FW throttle at 100 % until the FW speed reaches stall speed.

The provided assumptions make it possible to carry out a transition analysis using the parameters determined during the sizing stage, while also securing the stability of the transition. By leveraging these assumptions, the criteria for initiating and concluding the transition mode can be consolidated and presented in *Table 4.1*.

Table 4.1: Initial and final states of the transition mode for multi-mode UAVs [14].

Parameter	Initial Condition	Final Condition
V_∞	0 m/s	$1.2 \times V_{\text{stall}}$
L_w	0 N	W
T_{FW}	0 N	D
T_{VTOL}	W	0 N
Lift Sharing	100%	0%

Figure 4.2 illustrates the free body diagram of UAVs in transition mode, where force equilibrium must be achieved.

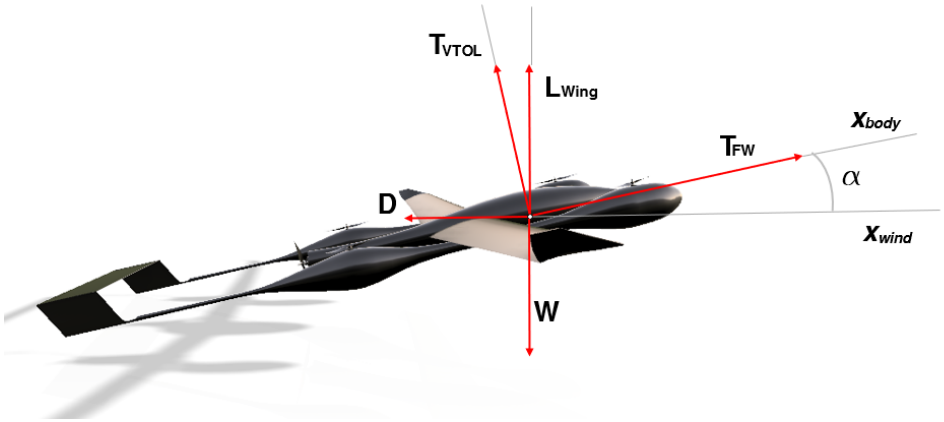

Figure 4.2: Body diagram in transition mode.

In this scenario, L_w represents the lift produced by the wing of the UAV, D denotes the drag force, W stands for the weight of the UAV, α indicates the angle of attack, T_{FW} symbolizes the thrust generated by the fixed wing propulsion system, and T_{VTOL} signifies the thrust produced by the VTOL propulsion system. Due to the low forward speed during transition and the angle of attack, it is possible to achieve adequate lift, the coefficient of which can be estimated using the lift curve of the airfoil. By applying the second assumption for transition analysis and examining the free body diagram, the force in the z-direction can be determined as shown in *Equation 4.1*.

$$\sum F_z = W - L_w - T_{FW}\sin(\alpha) - T_{VTOL}\cos(\alpha) = 0 \tag{4.1}$$

In addition, through the body coordinates selected, the x-direction force and forward acceleration are calculated as in *Equation 4.2*:

$$a_x = \frac{F_x}{m} = \frac{T_{FW}\cos(\alpha) - D - T_{VTOL}\sin(\alpha)}{m} \tag{4.2}$$

Using the fifth assumption, the lift from the wing is calculated through *Equation 4.1*. The lift sharing guide control can be characterized based on the operational parameters, and in this dissertation, it is represented by a basic sine curve as illustrated in *Equation 4.3*:

$$d = \left(\frac{W - L_w}{W} = \frac{W - q_\infty C_{L,\text{req}} S_w}{W}\right) = 0.5\left(\sin\left(\frac{\pi}{1.2V_{\text{stall}}}V_\infty - \frac{3\pi}{2}\right) + 1\right) \tag{4.3}$$

Here, d represents the lift sharing as a percentage of W, while CL_{req} stands for the necessary lift coefficient at that moment. Due to the low forward speed at the initial stage of the transition, a lift coefficient greater than the one at the stall angle of attack might be needed to produce the

lift required by the guide control. In such a scenario, CL_{req} can be substituted with $CL_{\max}$ at the stall angle of attack of the UAV, necessitating modifications to the guide control.

The sixth assumption in the transition analysis states that the forward flight thrust remains at its maximum level until the stall speed is reached. Then, the thrust gradually decreases to align with the drag force from the stall speed until the transition is completed.

Subsequently, calculations can be made for the forces of the UAV, speed variation, and transition duration in the transition phase. These calculations are essential for determining the required power, which is critical for battery capacity planning. Additionally, the process of transitioning back from FW mode to VTOL mode can be evaluated by reversing the initial and final conditions according to the assumptions mentioned above.

4.3 Li-po Baterry Sizing

Li-po batteries for eVTOL UAVs are most sensitive to the capacity and rated voltage, which have a significant impact on the weight. As a result, accurately estimating the battery weight involves considering the capacity and rated voltage. The most commonly used batteries have a rated voltage of 6S–12S (22.2–44.4 V), with 3S (11.1 V), 4S (14.8 V), and 6S (22.2 V) battery products available on the market. Additionally, a higher rated voltage can be achieved through series connection. A regression model for battery sizing, based on the data of 3S, 4S, and 6S batteries, is utilized [14].

To provide the necessary energy for the mission, the capacity of the battery (mAh) must be determined. This involves calculating the required capacity of the battery using the power required for each mission segment, as defined by the presented method, and the mission time outlined in the mission profile, as shown in *Equation 4.4*.

$$C_{\text{req}} = \frac{(\sum_{i=1}^{n_{\text{seg}}} \frac{P_{\text{req.i}}}{\eta_{\text{mot}}}) \cdot t_{\text{i}}}{U_{\text{rated}}\ \eta_{\text{batt}}\ f_{\text{usable}}} \tag{4.4}$$

In this case, f_{usable} serves as a factor aimed at minimizing voltage drop during prolonged battery discharge, typically set at around 0.85, while U_{rated} represents the Li-po rated voltage of the battery. The essential energy can be calculated by including a buffer from the overall mission duration specified in the mission profile. After determining the necessary energy, the weight of the battery can be predicted using model regressions in *Equation 4.5* based on the particular battery variant employed.

$$\begin{cases} 3S(11.1V) : M_{\text{batt}} = 0.019 \times 10^{-4} C_{\text{req}}^2 + 0.08 C_{\text{req}} + 7.864 \\ 4S(14.8V) : M_{\text{batt}} = 0.83 \times 10^{-7} C_{\text{req}}^2 + 0.083 C_{\text{req}} + 45.352 \\ 6S(22.2V) : M_{\text{batt}} = 0.116 \times 10^{-5} C_{\text{req}}^2 + 0.147 C_{\text{req}} + 27.827 \end{cases} \tag{4.5}$$

4.4 Hydrogen Tank Sizing

Sizing hydrogen tanks begins by determining the necessary electrical power for each phase of a mission, following a similar process to sizing batteries. The key distinction lies in the efficiency of the fuel cell based on the power needed for each mission phase, which is factored

into the sizing calculations.

Currently, the PEMFC operates at an efficiency of around 40–50 %. In the absence of data on the polarization curve of a single cell, this range can be utilized for sizing purposes. Nevertheless, with the polarization curve established, the efficiency of the HFC can be determined using *Equation 4.6*.

$$\eta_{\mathrm{HFC}} = \frac{2F \cdot P_{\mathrm{req}}}{\Delta H \cdot i_{\mathrm{FC}}} \tag{4.6}$$

The Faraday constant, denoted as F, has a value of 96,485.4 C/mol, while the chemical reaction energy, represented by ΔH, is 284,000 J/mol. The electrical power required by the mission operated by the HFC is denoted as P_{req}, and it is noted that the efficiency of the HFC decreases as the required power increases [44].

For the initial stage, the value of the HFC efficiency is considered as 0.5. Therefore, in such a situation, no use is made of the restrictive value, but the use of an optimum efficiency according to current standards is considered.

Upon calculating the necessary power for each segment of the mission and determining the fuel cell efficiency, the hydrogen consumption (HC) can then be computed using the formula provided in *Equation 4.7*.

$$HC = \frac{P_{\mathrm{req}}}{LHV \cdot \eta_{\mathrm{HFC}}} \tag{4.7}$$

In this case, the unit for HC is g/h, representing the rate of hydrogen consumption, while LHV stands for the low heating value of hydrogen, which is 33.3 Wh/g. By computing the hydrogen consumption for every mission segment, the total amount of hydrogen needed for the entire mission can be determined using *Equation 4.8* based on the mission duration provided in the mission profile.

$$m_{H_2} = \sum_{i=1}^{n_{\mathrm{seg}}} HC_{\mathrm{i}} \cdot t_{\mathrm{i}} \tag{4.8}$$

A regression model has been developed to predict the weight and volume of a hydrogen tank by analyzing the necessary amount of hydrogen [14]. This model was built using data from Type III and IV tanks, and can be represented by *Equation 4.9* and *Equation 4.10*.

$$M_{\mathrm{tank}} = 19.068 \cdot m_{H_2}^{0.8215} \tag{4.9}$$

$$V_{\mathrm{tank}} = 4.63 \cdot m_{H_2}^2 + 45.782 \cdot m_{H_2} + 0.102 \tag{4.10}$$

Chapter 5

Total Mass Calculation

The most critical parameter in the sizing procedure results is the MTOW of the UAV. It is determined by summing up the weights of the various components that make up the UAV, which are calculated throughout the sizing process. The total mass is computed using fixed point iteration, where the MTOW is iterated until it converges below a predefined tolerance level. The initial iteration starts with the MTOW specified in the design requirements. The actual values of the components that can be calculated are added to the total weight using the methods described above, while the remaining weight is considered as the mass fraction, which represents the ratio of the total weight [13].

The components for which the mass fraction needs to be assumed include the air frame, avionics, and subsystem. For the air frame weight, it is suggested to use a mass fraction of 25–35 % for Fixed Wing (FW) UAVs during the initial sizing estimation and 5 % for avionics [34]. The mass fraction of the subsystem varies based on the UAV's operational purpose, with 5–7 % for delivery drones and 15 % for advanced surveillance equipment [13]. The total weight of the multi-mode HFC eVTOL UAV is calculated according to *Equation 5.1*.

$$MTOW = \frac{M^{FW}_{\text{propulsion}} + M^{VTOL}_{\text{propulsion}} + M_{\text{HFC.sys}} + M_{\text{batt}} + M_{\text{payload}}}{1 - (MF_{\text{frame}} + MF_{\text{subsys}} + MF_{\text{avionics}})} \tag{5.1}$$

The weight of the complete hydrogen system, which includes the previously determined HFC, tank, regulator, and control board, is denoted as $M_{\text{HFC.sys}}$. The mass fractions are determined based on the most limiting value.

Next, the calculated maximum takeoff weight (MTOW) is utilized as a fixed-point iteration value in the multi-mode sizing loop. The loop is iterated repeatedly until the MTOW converges.

Chapter 6

Optimization

The MCA selected a design point within the design space to meet the performance constraints of the UAV, but it remains uncertain if it meets all design requirements. Previous methods, like carpet plots, were used to ensure design requirements were met, but finding the optimal point quantitatively and efficiently was challenging. This project introduced a method using a numerical optimization algorithm to define a design point that satisfies all requirements. The optimization objective is to minimize the UAV's MTOW, with constraints including performance requirements from the MCA. Key design variables like WL, FW/VTOL PL, DL, and AR were considered for multi-mode UAV sizing.

Table 6.1 is the optimization formulation considered for minimizing the MTOW.

It is ideal for addressing nonlinear optimization problems with constraints and for tackling sizing problems during the initial design phase due to its shorter computation time compared to alternative global optimization algorithms.

Table 6.1: Sizing optimization formulation [14].

Variable	**Value**
Maximum FW speed	≥ 30 m/s
Maximum RoC	≥ 6 m/s
Stall speed	≤ 18 m/s
VTOL ceiling	≥ 1000 m
Maximum take-off speed	≥ 10 m/s
Hydrogen fuel system mass	≤ 10 kg
Wingspan	≤ 4 m
FW propeller diameter	≤ 0.75 m
VTOL propeller diameter	≤ 0.75 m
Transition time	≤ 30 s

Now, the aim is to achieve the minimum MTOW through the maximum lift coefficient ($C_{L_{\max}}$) while minimizing the drag coefficient ($C_{D_{\min}}$) for obtaining the maximum aerodynamic efficiency ($AE_{\max}$), a high stall angle (α_{stall}), and the minimum momentum coefficient possible.

The airfoils described in the *Table 6.2* are the selected ones to be studied in order to achieve the aerodynamic optimization.

The airfoils are also arranged in *Figure 6.1*, being obtained through Airfoil Tools [45].

Table 6.2: Airfoil Profiles.

Airfoil Section	**$(t/c)_{max}$ %**	**$(t/c)_{max}$ % c**	**Max Camber %**	**Max Camber % c**
AH-34	9.30	31.33	5.18	48.35
AH-79 B	10.04	31.13	6.42	50.45
NACA 3408	8	29.03	3.00	39.54
NACA 4412	12	29.03	4	39.54
NACA 6414	14	29.03	6	39.54
NACA 44AH	10.22	31.63	6.18	50.95
NACA 0006	6	29.03	0	0

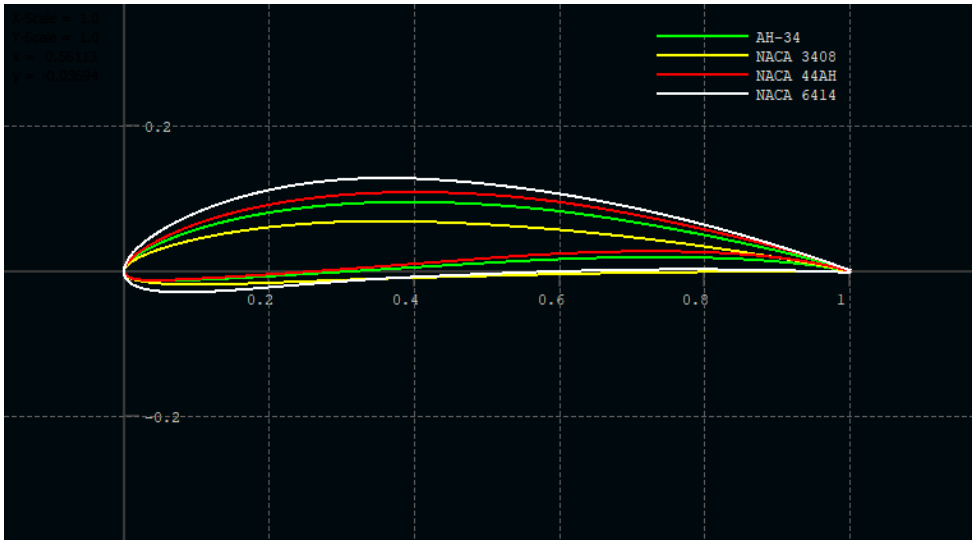

Figure 6.1: Some of the profiles pre-selected.

The performance of the pre-selected airfoils is analysed using the software xflr5 [46], obtaining the lift and drag polars for the airfoils at a range of Reynolds number between 50,000 and 990,000 for providing preliminary estimations of $C_{L_{\max}}$ and C_L/C_D. In Figure **??**, an airfoil comparison is done for a Reynolds number of 140,000.

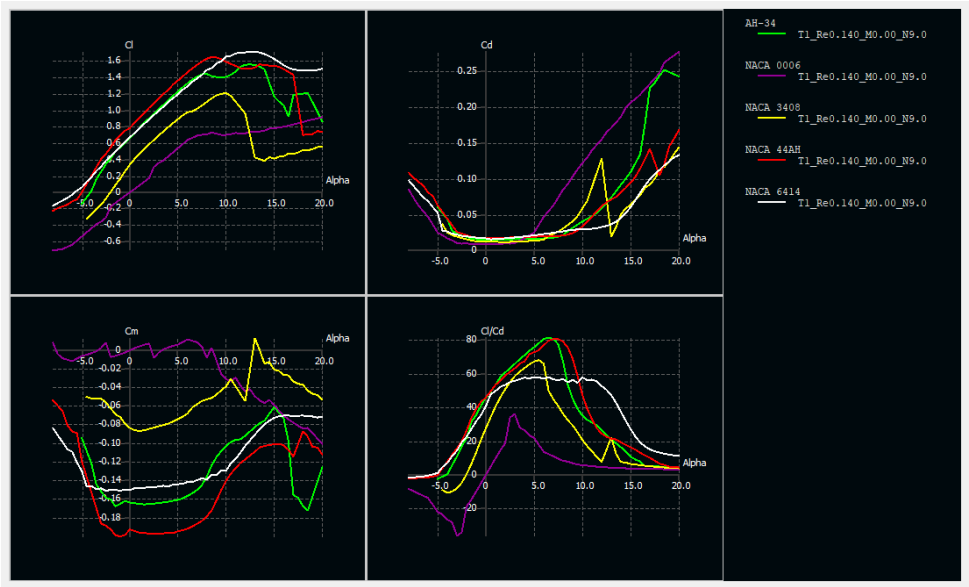

Figure 6.2: Comparison of some of the profiles pre-selected through xflr5 [45].

The NACA 0006 is added to be used in the tail section. Moreover, even if the NACA 6412 seems to have a considerable high $C_{L_{\max}}$, with a late stall entry, it is just selected for the tip section and an aerodynamic twist is applied. This is due to the fact that the interpolated airfoil NACA 44AH, obtained from the interpolation of NACA 4412 and AH-79 B, presents better conditions for the proposed mission, having higher values of C_L in for lower angles of attack and a better AE; so, it is selected as a root section airfoil.

Aerodynamic twist means that, with different airfoils along the wing, the zero lift angle varies for the different airfoils. Ultimately, it must ensure that the inner sections reach the stall angle first. It is important to note that the twist should be progressive along the entire semi-span from root to marginal. The the value of $C_{L_{\max}}$ at the tip increases.

There exist also the geometric twist, which is achieved by changing the angle of attack of the airfoil along the wing.

In both cases, the aim is to improve the stall characteristics of an aircraft. For reasons related to the distribution of WL and lift along the wing, stall generally starts earlier at the tips and spreads towards the root in a different way depending on the wing plan.

Aerodynamic twist, compared to geometric twist, generally results in lower cruise drag for the outer sections. However, it could complicate the design and therefore the production process. In high performance aeroplanes this complication can become justified, and it is assumed in this thesis. Sometimes, in the case of very narrow wings, a combination of aerodynamic and geometric torsion could be used.

After the 2D analysis, the profiles selected are placed in the wing geometry configurations designated and based on the market overview.

The choice of a low-fidelity analysis approach is implemented as it allowed to initially and efficiently iterate the design at a low computational cost for both aerodynamic and stability parameters. The use of the Software xflr5 [45] allows to consider two viscous solutions: the vortex lattice method (VLM2) based on ring vortex analysis being a linear solution, and the non-linear lifting line theory (LLT) approach as it is able to indicatively predict stall conditions as the solution includes non-linear approximations. Both methods are implemented in parallel

to obtain an overall initial understanding of the aerodynamic performance, since both present limitations in the analysis.

The VLM2 considers only the airfoil mean camber line for the analysis and assumes the small angle approach in the aerodynamic analysis, limiting the accuracy of the lift coefficient at extreme (outside the linear region of the lift curve, therefore near stall) low and high values of angles of attack, resulting in the trailing vortices being misaligned with respect to the free-stream velocity.

Oppositely, the non-linear LLT method has been primarily developed for high-aspect ratio and low-sweep wings, and therefore of limited application to the current design [47].

Some of the models studied, developed from the UAV market overview, are analysed. For the most of this models, the common factor is the wing span which goes from 3.9 to 4 meters, with a slightly positive dihedral for stability purposes. Considering a tapered wing where the airfoils used are the NACA 44AH for the root section and the NACA 6412 for the tip section. Also, a slightly negative offset is set.

The tail is the main difference between the models presented. A pusher propeller configuration is set to allow a wider field of view for sensors and cameras located in frontal part of the fuselage. Then, V-Tail, inverse V-tail or twin boom T-tail (also called Π-tail) configurations are common for UAVs with pusher propeller. Upper position of horizontal tail reduces the propeller slipstream effect on a tail. VTOL mode control is very sensitive to changes in moments of inertia, especially in yawing. Length of an aircraft should be minimized to reduce the moment of inertia around z-axis. Wing, tail, and propellers are arranged to minimize the overall dimensions of aircraft while leaving space for normal operation and adjustment of propellers.

Model 1 - Inverted V Tail

In *Figure 6.3*, the Model 1, with a inverted V tail form, is displayed. The parameters of the model are found in the *Table 6.3*.

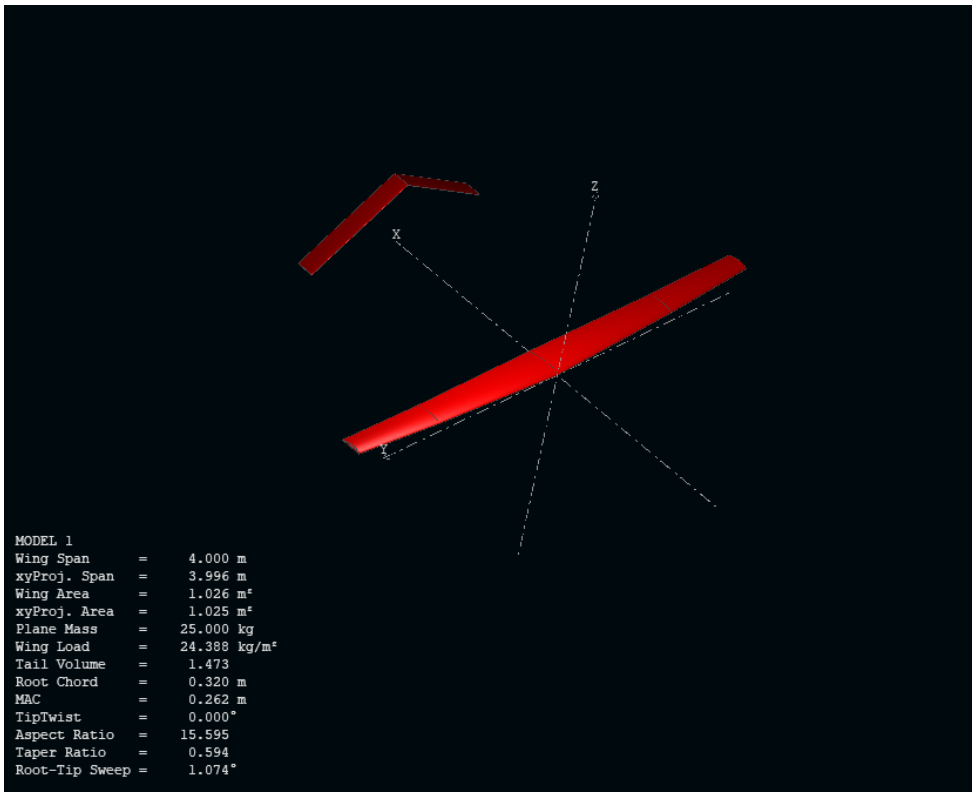

Figure 6.3: Preliminary design Model 1 in xflr5.

Table 6.3: Geometric data of Model 1.

Geometric Variable	**Value**
Wing Span (b_w)[m]	4.000
Wing Area (S_w)[m^2]	1.026
Tail Span (b_t)[m^2]	2.000
Tail distance (x-direction) [m]	1.800
Tail distance (z-direction) [m]	0.550
Tail Volume (V_t)[m^3]	1.473
Wing root chord ($c_{root.w}$)[m]	0.320
Wing mid chord ($c_{mid.w}$)[m]	0.245
Wing tip chord ($c_{tip.w}$)[m]	0.190
Tail chord (c_t)[m]	0.150
MAC [m]	0.262
AR [-]	15.595
Taper ratio [-]	0.594
Wing root Dihedral [°]	2.000
Wing tip Dihedral [°]	3.000
Tail Dihedral [°]	-30.000

Model 2 - V Tail

In *Figure 6.4*, the Model 2, with a V tail form, is displayed. The parameters of the model are found in the *Table 6.4*.

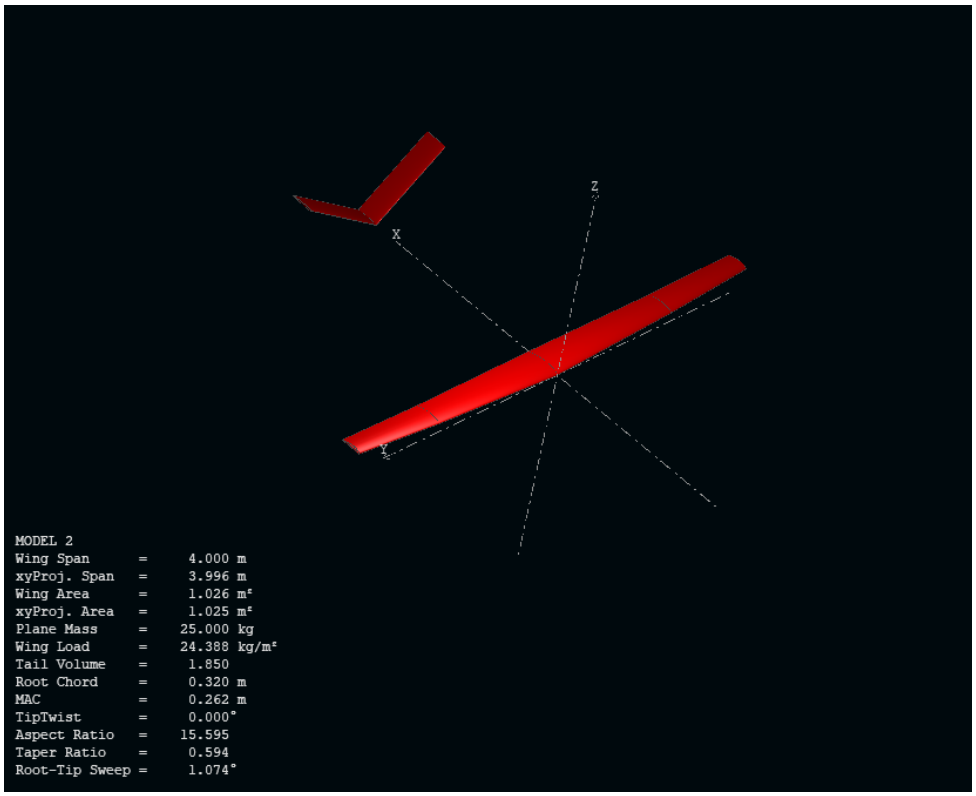

Figure 6.4: Preliminary design Model 2 in xflr5.

Table 6.4: Geometric data of Model 2.

Geometric Variable	**Value**
Wing Span (b_w)[m]	4.000
Wing Area (S_w)[m^2]	1.026
Tail Span (b_t)[m^2]	1.600
Tail distance (x-direction) [m]	2.100
Tail distance (z-direction) [m]	0.000
Tail Volume (V_t)[m^3]	1.850
Wing root chord ($c_{root.w}$)[m]	0.320
Wing mid chord ($c_{mid.w}$)[m]	0.245
Wing tip chord ($c_{tip.w}$)[m]	0.190
Tail chord (c_t)[m]	0.200
MAC [m]	0.262
AR [-]	15.595
Taper ratio [-]	0.594
Wing root Dihedral [°]	2.000
Wing tip Dihedral [°]	3.000
Tail Dihedral [°]	30.000

Model 3 - Π Tail with offset

In *Figure 6.5*, the Model 3, with a Π tail form with offset, is displayed. The parameters of the model are found in the *Table 6.5*.

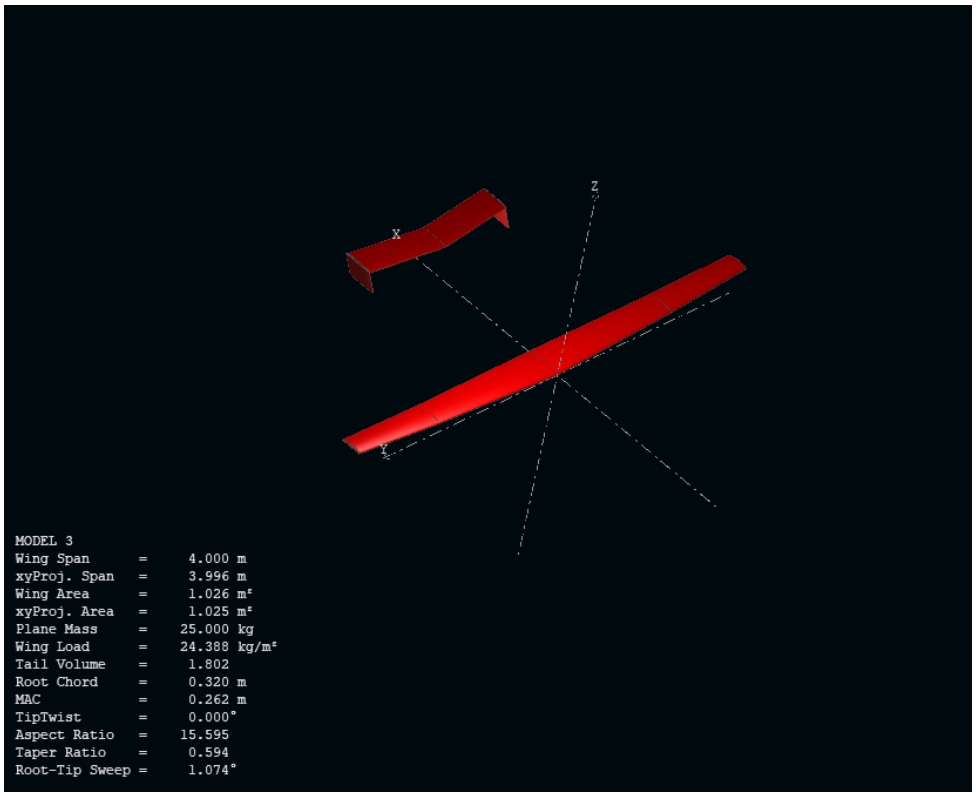

Figure 6.5: Preliminary design Model 3 in xflr5.

Table 6.5: Geometric data of Model 3.

Geometric Variable	**Value**
Wing Span (b_w)[m]	4.000
Wing Area (S_w)[m^2]	1.026
Tail Span (b_t)[m^2]	1.400
Tail distance (x-direction) [m]	1.400
Tail distance (z-direction) [m]	0.300
Tail Volume (V_t)[m^3]	1.802
Wing root chord ($c_{root.w}$)[m]	0.320
Wing mid chord ($c_{mid.w}$)[m]	0.245
Wing tip chord ($c_{tip.w}$)[m]	0.190
Tail chord (c_t)[m]	0.250
MAC [m]	0.262
AR [-]	15.595
Taper ratio [-]	0.594
Wing root Dihedral [°]	2.000
Wing tip Dihedral [°]	3.000
Tail Dihedral [°]	0.000

Model 4 - Π Tail without offset

In *Figure 6.6*, the Model 4, with a Π tail form without offset, is displayed. The parameters of the model are found in the Table **6.6**.

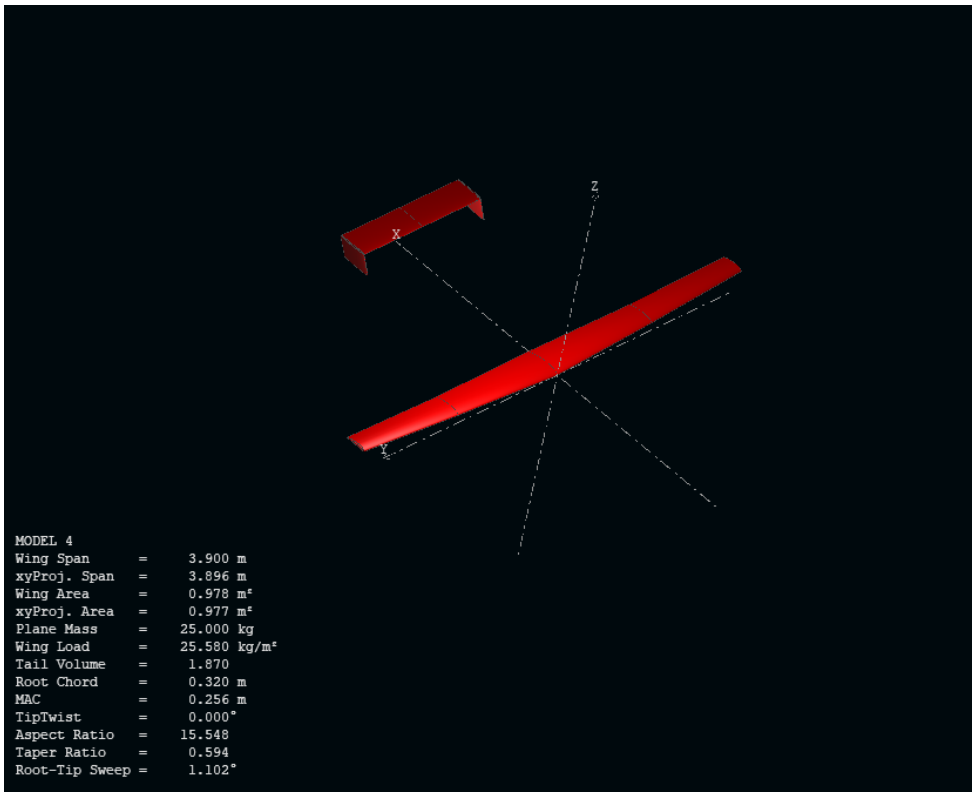

Figure 6.6: Preliminary design Model 4 in xflr5.

Table 6.6: Geometric data of Model 4.

Geometric Variable	**Value**
Wing Span (b_w)[m]	3.900
Wing Area (S_w)[m^2]	0.978
Tail Span (b_t)[m^2]	1.200
Tail distance (x-direction) [m]	1.580
Tail distance (z-direction) [m]	0.300
Tail Volume (V_t)[m^3]	1.870
Wing root chord ($c_{root.w}$)[m]	0.320
Wing mid chord ($c_{mid.w}$)[m]	0.245
Wing tip chord ($c_{tip.w}$)[m]	0.190
Tail chord (c_t)[m]	0.250
MAC [m]	0.256
AR [-]	15.548
Taper ratio [-]	0.594
Wing root Dihedral [°]	2.000
Wing tip Dihedral [°]	3.000
Tail Dihedral [°]	0.000

Analysis

The geometric wing configurations presented are now analysed by the Software xflr5 [46]. The VLM2 method is used in order to obtain preliminary values of the lift and drag coefficients. Also, through the momentum coefficient curve, the static stability criterion can be verified. The results for the curves obtain for the different models are shown in *Figure 6.7*.

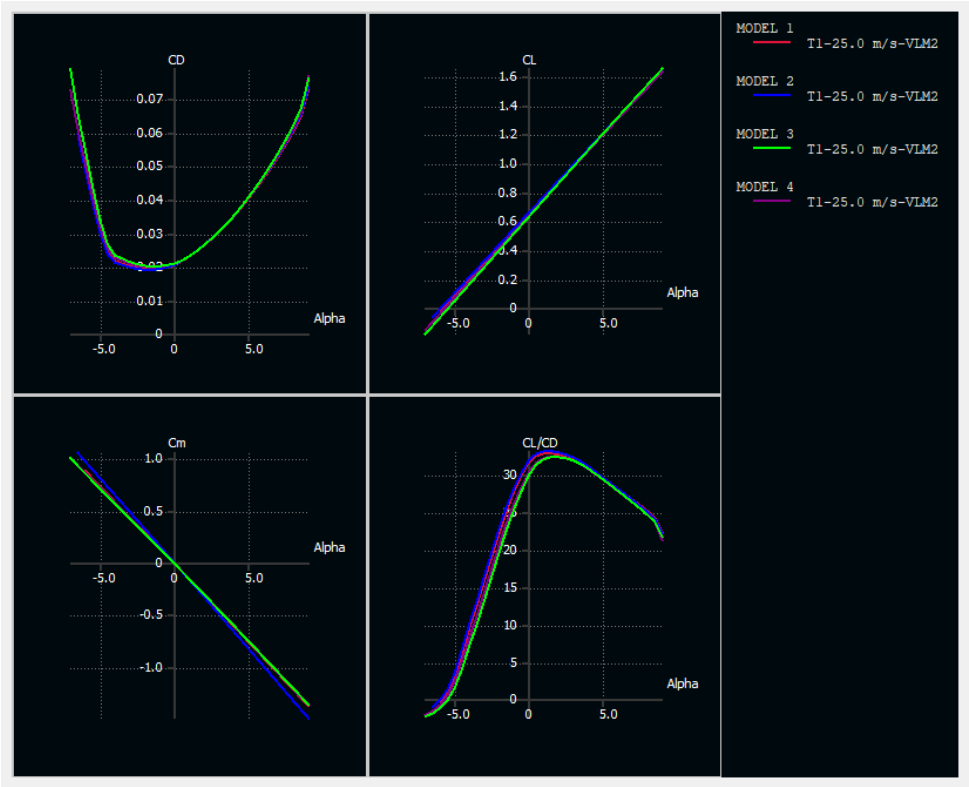

Figure 6.7: Results of the 3D VLM2 analysis in xflr5 for the models pre-selected.

After the iteration process through the Software xflr5, the results seem to be very similar. Even though the efficiency of the Model 1 and Model 2 could seem greater, the Model 4 is the selected for the conceptual design due to stability configurations and simplicity. As stated, the shorter the length of the aircraft, the lower moments of inertia are generated. Also, the results are similar to the other models despite the fact that its wing span is shorter.

Furthermore, winglets are added, which are optimized by a Computational Fluid Dynamics (CFD) study.

The fuselage is modelled with airfoil form in order to minimize the drag coefficient and to benefit the flow of the air around the body. In the same way, the structures for supporting the VTOL motors are design for increase efficiency. Its dimension is taken from similar UAVs but a deeper study should be done in future design stages.

Now, with the Software Fusion360 [48], a representative CAD 3D model of the Model 4 is done.

In *Figure 6.8a* and *Figure 6.8b*, the conceptual model obtained through an iteration process is shown.

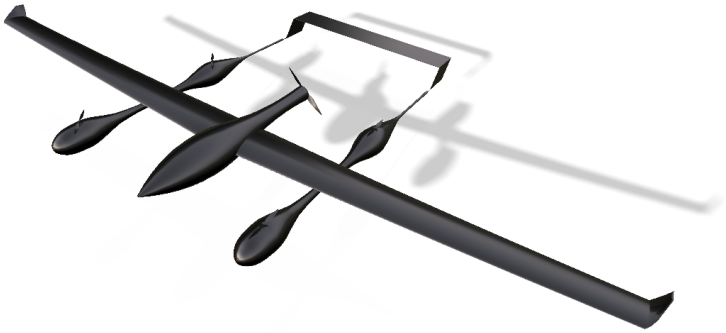

(a)

(b)

Figure 6.8: Model of the conceptual UAV: (a) Geometry of the final Model. (b) Rendering of the final Model obtained through Fusion360 [48].

Once the xflr5 study is done and the Model 4 is represented in the software Fusion360, the CFD simulations with the Software StarCCM+ [49] are started. The aim of obtaining the estimated values of the C_L, C_D and verify worthiness for the performance of the aircraft.

In addition, the observation of flow behaviour around the conceptual model could help to detect weak points in the configuration selected and, with the information obtained, be able to optimize the aerodynamic surfaces to successfully achieve an improvement of the properties of the UAV.

A Reynolds-Averaged Navier-Stokes (RANS) model has been applied. Two approaches have been used, the k-ω turbulence model equations in the SST formulation and the Spalart-Allmaras model. RANS k-ω SST model provides excellent approximation of pressure induced separation and the resulting viscous-inviscid interaction in comparison to other closures [50]. Specifically designed for aerospace applications involving wall-bounded flows, the Spalart–Allmaras model has been shown to give similarly good results for boundary layers subjected to adverse pressure gradients [51].

The first step is to define the domain dimensions. Following best practice cases for domain definition, a box-shaped domain is constructed. The objective is to set the boundaries far enough so they do not interfere with the aircraft. The inlet of the domain is placed in front at a distance

of five times the span of the aircraft, the outlet is seven times behind, and the lateral wall two times the wingspan. It can be seen in *Figure 6.9*.

In order to optimize computational time, only half of the geometry is simulated, with a symmetry plane imposed on the xz-plane along the axis of symmetry. Also, to resolve the boundary layer, an inflation of high aspect-ratio cells are designed in the near-wall region of the aircraft geometry, as shown in *Figure 6.9*.

Some control volumes are defined in order to refine the mesh size in the plane and in the critical parts such as wing and stabilizers where also a surface control is applied for adapting the curvature and dimensions of the leading edge and trailing edge, displaying all in *Figure 6.9*.

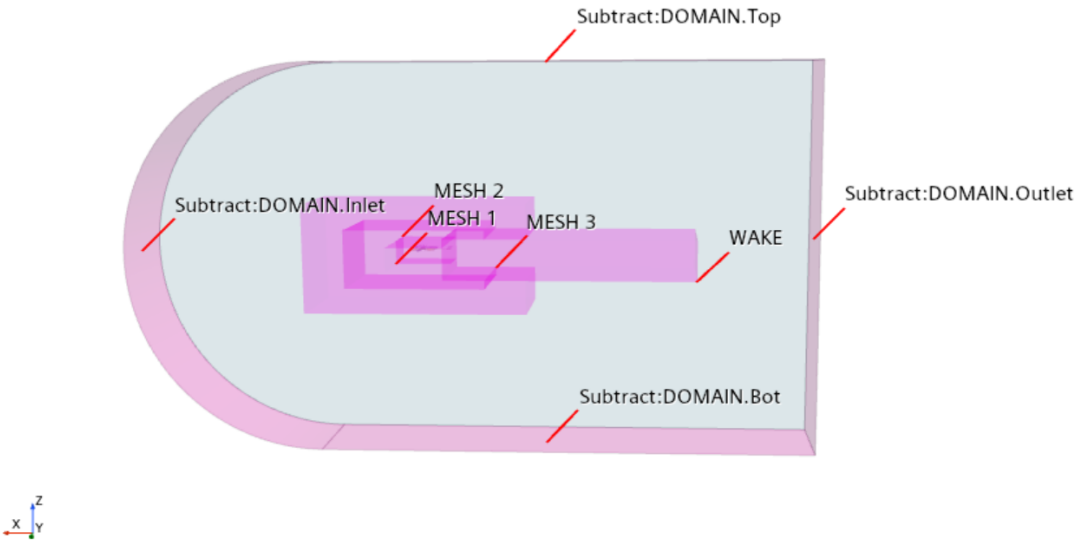

Figure 6.9: Domain for the simulation of the conceptual model.

The options selected for the meshing are the Polyhedral mesh, Prism layer mesh and Surface Re-mesh.

Taking all these elements into account, a fairly detailed mesh is produced with which the convergence of the simulation is achieved. So, some detailed views of the mesh are displayed in *Figure 6.10*.

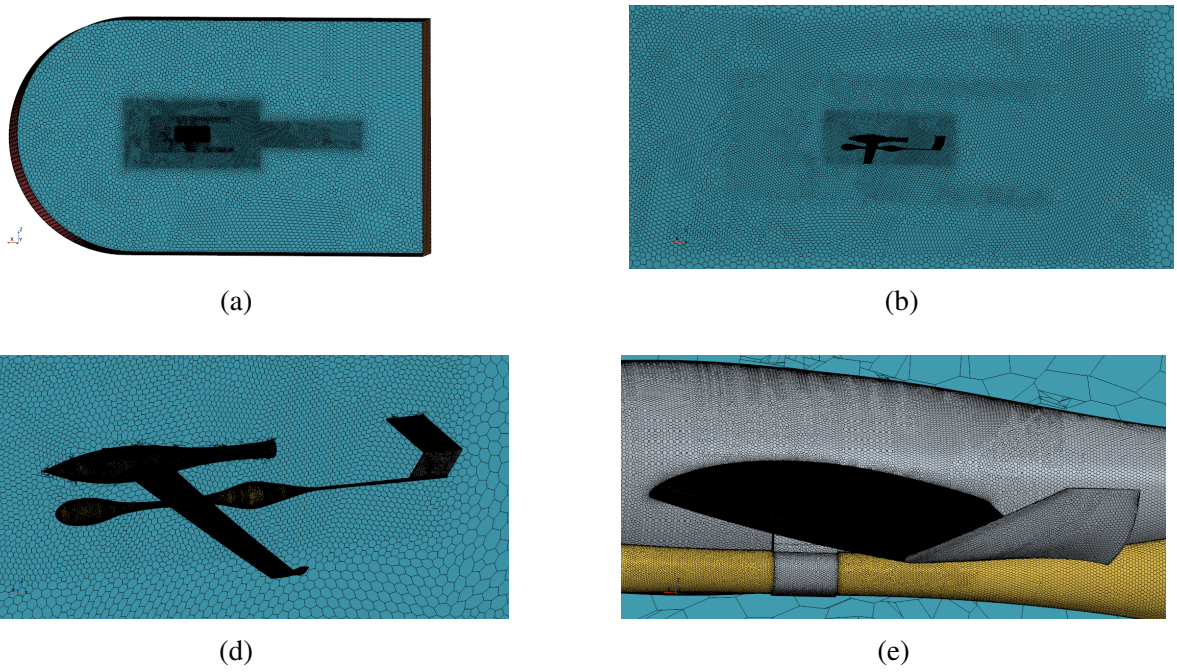

(a) (b)

(d) (e)

Figure 6.10: Different detailed views of the mesh for the conceptual model.

And the values selected for the mesh are shown in *Table 6.7*. Also, the Post Mesh Optimization options, which are Optimize Boundary Vertices and Optimize Cell Topology, are activated.

Table 6.7: Parameters of the mesh.

Parameter	**Value**
Base size [m]	0.4
Targeted Surface Size [m]	0.4
Minimum Surface Size [m]	0.04
Number of Prism Layer [-]	10
Prism Layer Stretching [-]	1.2
Prism Layer Total Thickness [m]	0.0025
Maximum Tet Size [m]	0.4

Then, for the surface control and volume control generated, the following parameter in *Table 6.8* and *Table 6.9*, respectively, are used.

Table 6.8: Surface control parameters.

Parameter	**Wing surface**	**Tail surface**
Target Surface Size [m]	0.003	0.004
Minimum Surface Size [m]	0.001	0.001
Surface Curvature [Points/circle]	60	60

Table 6.9: Volume control parameters.

Parameter	Mesh 1	Mesh 2 and Mesh 3	Wake
Custom size [m]	0.04	0.07	0.1
Number of Prism layer [-]	10	[-]	[-]
Prism Layer Total Thickness [m]	0.003	[-]	[-]

Then, the physical models are defined as the following:

- **Three dimensional**: Allows for a more accurate and detailed representation of the flow field, capturing phenomena like vortices and secondary flows.
- **Ideal Gas**: to determine the relationship between pressure, temperature, and density.
- **Coupled flow**: A coupled flow model solves the equations for momentum and energy (if heat transfer is involved) together in a single system. Often more stable and robust, especially for high-speed flows or flows with strong interactions between velocity and pressure fields. For segregated flow, the computational cost is lower but there are problems with the convergence of the simulation.
- **Constant density**: Eliminates the need to solve the energy equation for density variation, simplifying the governing equations.
- **Steady**: A steady-state simulation assumes that the flow properties at any given point do not change with time.
- **Turbulent**: This model accounts for the effects of turbulence in the flow.
- **RANS**: A method to solve the Navier-Stokes equations where the flow variables are decomposed into mean and fluctuating components, and the equations are averaged over time.
- **Spalart-Allmaras turbulance**: A one-equation turbulence model that solves a transport equation for a modified form of the turbulent viscosity. Relatively simple and less computationally demanding compared to two-equation models like k-ε or k-ω. Also, it is particularly well-suited for aerodynamic flows, especially in boundary layers with adverse pressure gradients.

Finally, for the different parts of the domain, the boundary conditions are defined as follows:

- **Wall**: for the surface of the conceptual model.
- **Velocity inlet**: for the inlet of the curve surface. The definition of the velocity is split into magnitude and direction. The flow direction is determined, in function of the axes which are found in *Figure 6.9*, by $[-\cos(\$Angle), 0.0, \sin(\$Angle)]$. The variable Angle is defined as the angle of attack. The velocity magnitude is set to be the cruise speed which is 25 m/s.
- **Pressure outlet**: for the outlet, selecting ambient pressure.
- **Symmetry**: used in the rest of the boundaries.

The reports for the lift and drag coefficients are set in the simulation analysis. From there, the objective is to obtain the values of the C_{D_0} and the $C_{L_{\max}}$.

In *Table 6.10*, a summary of the different values of the drag and lift coefficients is shown, considering the different methods for their derivation so far and thus being able to compare them.

Table 6.10: Comparison of aerodynamic parameters.

Parameter	VLM2	Non-Linear LLT	CFD
$C_{L_{\max}}$ [-]	1.634	1.590	1.100
$\alpha_{\max}$ [°]	9.000	12.000	13.000
C_{D_0} [-]	0.021	0.020	0.029

All the results are obtained for a speed of 25 m/s which is established as the cruise speed.

Stability and control

The centre of gravity is placed under the longitudinal static stability criterion so it always must be in advance with respect the neutral point (NP). The previous analysis in xflr5 shows that the neutral point is $x_{\text{NP}} = 0.334\ m$ respect the leading edge. Initially, the centre of gravity (CoG) is $x_{\text{CoG}} = 0.100\ m$, at a 39.06 % from the Mean Aerodynamic Chord (MAC). With the exposed data, the static marging (SM) is obtained through Equation **6.1**.

$$\text{SM} = \left| \frac{x_{\text{CoG}} - x_{\text{NP}}}{c_{\text{w}}} \right| = \left| \frac{0.100 - 0.334}{0.320} \right| = 73.13\% \tag{6.1}$$

Now, considering the static lateral and directional stability, the values for the lateral and directional derivatives, which describe the behaviour of the aircraft, are obtained through the xflr5. The coefficients are shown in *Table 6.11*.

Table 6.11: Aerodynamic derivatives.

	Model	Stability Criterion
C_{M_α}	-8.380	<0
$C_{\mathcal{L}_\beta}$	-0.042	<0
C_{N_β}	+0.028	>0

In this way, it is verified that the proposed configuration is enough in terms of longitudinal and lateral stability. Nevertheless, there are some values out of the range expected. The C_{M_α} is too small and refers to the pitch moment of the aircraft, or the $C_{\mathcal{L}_\beta}$ which refers to the vertical force and it is relatively small, what can lead to problems of misalignment with the flow in the longitudinal plane (yaw). These values serve to corroborate its feasibility.

A new stability study could be done by considering the control surface, measuring their efficiency by the aerodynamic derivatives related with them which appear in *Table 6.12*.

Table 6.12: Control aerodynamic derivatives.

	Definition	**Stability Criterion**
$C_{M_{\delta E}}$	Elevator	<0
$C_{\mathcal{L}_{\delta A}}$	Aileron efficiency	>0
$C_{N_{\delta A}}$	Induced yaw	
$C_{\mathcal{L}_{\delta R}}$	Induced roll	>0
$C_{N_{\delta R}}$	Rudder efficiency	<0

None of the coefficients are shown because the dimensions of the control surface are considered to be out of the scope of this thesis, which just a conceptual design is aimed to be presented.

Chapter 7

Case Study

The objective of this thesis is to create the conceptual blueprint for a hydrogen-powered UAV weighing 25 kg.

The defined objectives consist of achieving a maximum takeoff weight of 25 kg, endurance up to 3 hours, a hydrogen system mass under 10 kg (with a 40 % mass fraction), and continuous power of the HFC up to 2 kW. Prior to sizing, the design process involves requirements analysis and concept selection. The design requirements obtained from the requirements analysis are outlined in *Table 7.1*, and the operational concept for this UAV involves utilizing a LiDAR sensor for surveillance. The mission profile of the surveillance HFC UAV is illustrated in *Figure 7.1*.

Table 7.1: The 25 kg HFC UAV design requirements.

Requirements	**Value**	**Remarks**
MTOW	≤25 kg	Market analysis
Endurance	≥3 h	Market analysis
HFC system mass	≤10 kg	Similar research
Payload mass	≤3.5 kg	LiDAR sensor
HFC maximum continuous power	≥2 kW	Similar research
Wingspan	≤4 m	Market analysis
Cruise altitude	110 m (AGL)	European Union and sensor requirement
Maximum speed	≥30 m/s	Market analysis
Cruise speed	25 m/s	Market analysis
Stall speed	≤20 m/s	Market analysis
Maximum RoC	≥6 m/s	Market analysis
Maximum take-off speed	≥10 m/s	Market analysis
VTOL service ceiling	1000 m	Market analysis
FW propeller diameter	<0.8 m	Available size for regression
VTOL propeller diameter	<0.8 m	Available size for regression
Transition time	<30 s	Market analysis

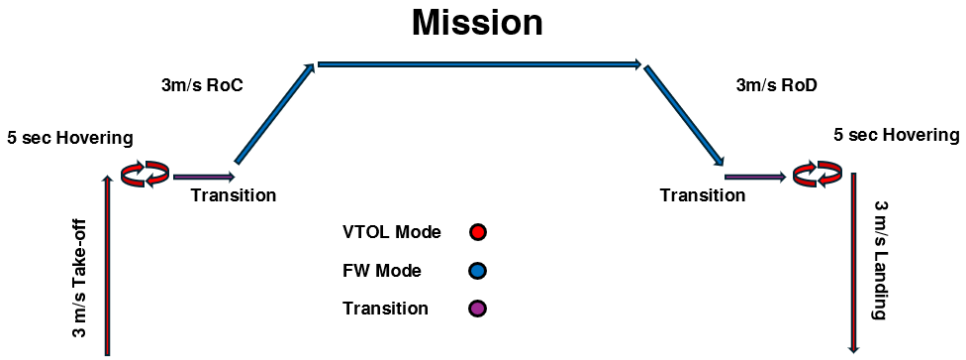

Figure 7.1: Mission profile for a multi-mode surveillance HFC UAV with a weight of 25 kg.

The sizing results are cross-referenced with the conceptual design outcomes of the UAV, derived from the sizing of individual components. A comprehensive analysis and configuration optimization of the UAV is conducted. Furthermore, high-fidelity aerodynamic analysis using CFD is taken into account. The HFC stack and BoP are meticulously designed, and the HFC sizing outcome is validated using data from the chosen product.

7.1 Optimum Sizing Result

The comparison between the initial point and the sizing result is illustrated in *Table 7.2*. The initial sizing denotes the result at the initial design point chosen by the designer prior to optimization, while the sizing result represents a design point that meets the design requirements after optimization.

Table 7.2: Comparison of starting point and sizing findings.

Parameter	Initial Point	Sizing Result
MTOW [kg]	48.702	24.852
WL [N/m^2]	355.000	250.000
PL_{FW} [N/W]	0.110	0.109
PL_{VTOL} [N/W]	0.034	0.029
DL [N/m^2]	338.538	252.000
AR [-]	15.000	15.548
S_w [m^2]	1.400	0.978
Payload [kg]	1.100	1.100
Endurance [h]	3.500	3.500
FW propeller diameter [m]	0.373	0.383
VTOL propeller diameter [m]	0.635	0.557
Airframe mass fraction [-]	0.300	0.300
HFC system mass [kg]	14.136	7.174
Battery mass [kg]	4.453	1.638
FW propulsion system mass [kg]	1.040	0.617
VTOL propulsion system mass [kg]	3.621	2.185
FW maximum power [W]	3509.126	2025.000
VTOL maximum power [W]	11,353.055	6306.429
Transition time [s]	20.000	20.000

Based on the information presented in *Table 7.2*, it is evident that the initial sizing result did not align with the design criteria. This discrepancy can be attributed to the fact that the starting point was situated in a design space that only satisfied the performance standards outlined by MCA. In contrast, the final sizing result successfully met all the design criteria. The initial point and the optimum point are illustrated in *Figure 7.2* and *Figure 7.3*.

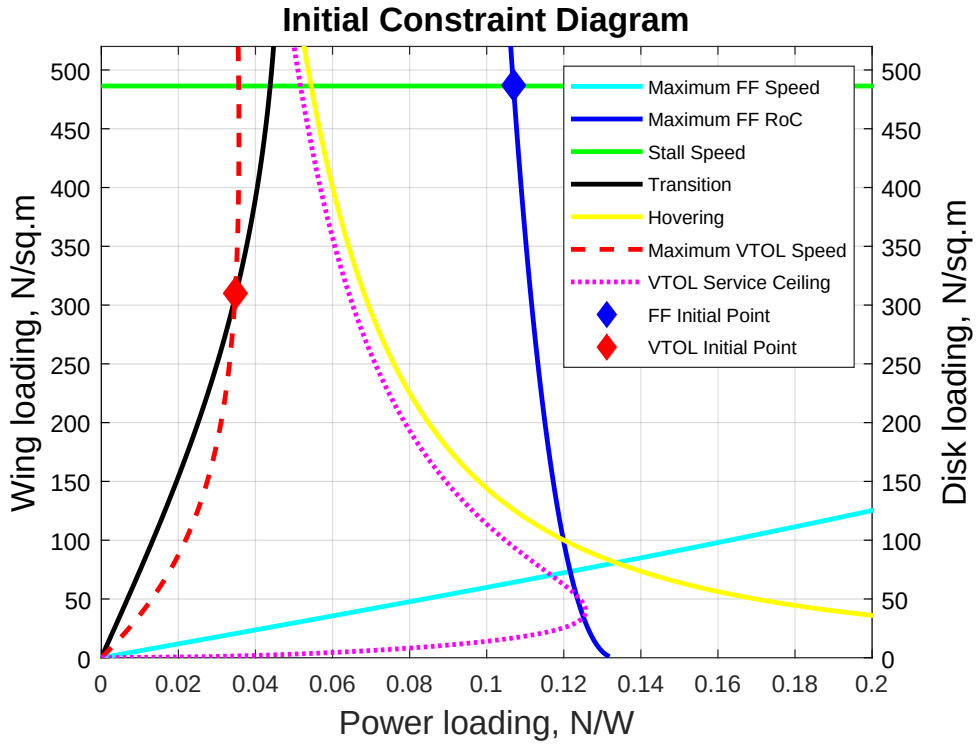

Figure 7.2: Initial point for minimizing the wing span and power needed for FW/VTOL operations.

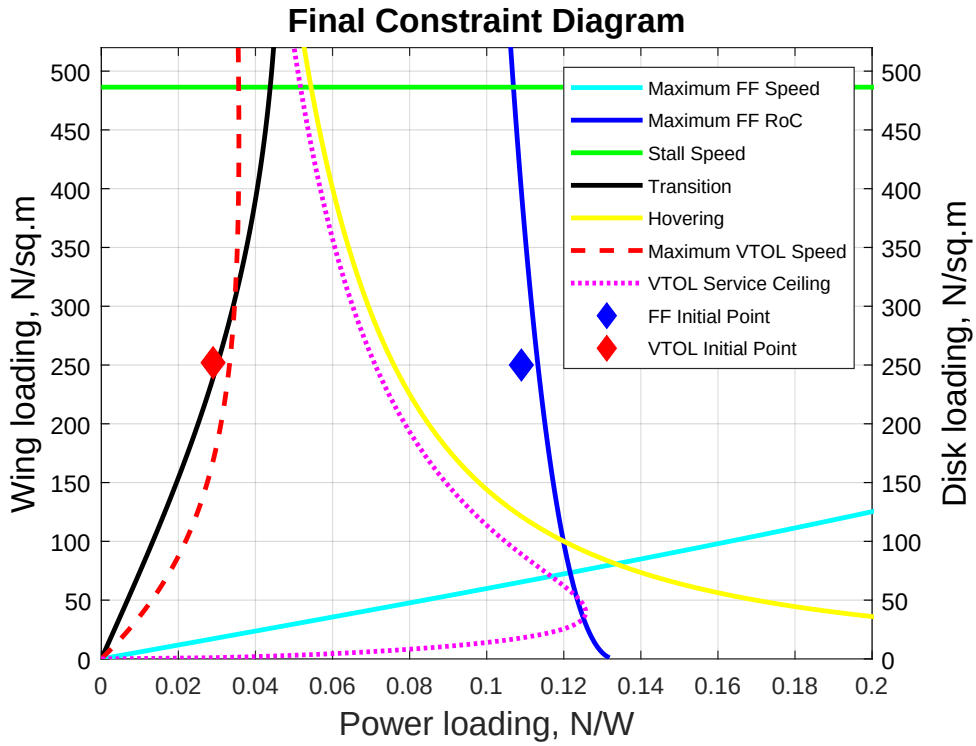

Figure 7.3: Optimal point for minimizing the MTOW of UAV, satisfying all the design requirements.

The ideal location has been adjusted to minimize the MTOW while still satisfying the design requirements within the design boundaries set by MCA throughout the optimization process.

7.2 Sizing Result and market selection

The EPS sizing results are evaluated for accuracy by comparing the mass of the motors, ESC, and propeller used on the real UAV with the HFC data. The comparison is presented in *Table 7.3*.

During the conceptual design phase, the FW motor is chosen based on the maximum power needed in FW mode, motor weight, and predicted Kv value from sizing. Similarly, the VTOL motor is selected based on the maximum power required in VTOL mode and motor weight [14].

Following motor selection, the appropriate ESC and propeller are chosen to match the motor specifications. The selection process ensures alignment with the Kv values, maximum power requirements for each flight mode, and motor weight calculated during sizing. While perfect alignment of all parameters is challenging, a margin of error is accepted. Nonetheless, the relative error for all components between the actual selection and sizing results should not exceed 15 %.

Also, the data and appearance of the HFC, selected from the market, is shown in *Figure 7.4*. Then, the comparison of the sizing result for the HFC with the actual data is placed in *Table 7.3*.

Table 7.3: Comparison of motor, ESC, propeller and HFC system from sizing result and actual data.

	Sizing Result	Actual Selection	Relative Error (%)	Remarks
FW motor [kg]	0.421	0.408	3.186	T-Motor AT4130 450W [52]
FW motor kv [-]	497.013	450	10.447	T-Motor AT4130 450W [52]
FW ESC [kg]	0.047	0.055	14.555	T-Motor Flame 70A 6S [53]
FW propeller [kg]	0.046	0.045	2.222	APC 15x10E [54]
VTOL motor [kg]	0.893	0.803	1.121	T-Motor U12 II [53]
VTOL ESC [kg]	0.187	0.180	3.889	Hobbywing FlyFun HV 110A V5 SBEC [52]
VTOL propeller [kg]	0.045	0.048	6.250	T-Motor V 22*7.4 [53]
HFC mass [kg]	4.373	4.800	8.900	IE-SOAR 2.4 [39]

Figure 7.4: (a) IE-SOAR 2.4, the HFC selected from the market options [39].

The relative error find at the comparison process is due to the fact of that the measures are so small. Also, the selected components are compared in different properties apart from the weight to ensure they are compatible with the conceptual UAV. Nevertheless, it is not the main objective to provide with an exact solution.

The comparison of the battery and hydrogen tank sizing results with the actual data is presented in *Table 7.4*.

Table 7.4: Comparison of battery and hydrogen tank sizing outcomes with actual data.

	Sizing Result	Actual Selection	Relative Error (%)	Remarks
Battery mass [kg]	0.819	0.802	2.120	Gens ACE G-Tech 6s 6000mAh 22.2V 45C Lipo Battery [52]
Battery capacity [mAh]	6056.648	6000.000	0.941	Gens ACE G-Tech 6s 6000mAh 22.2V 45C Lipo Battery [52]
Hydrogen tank mass [kg]	2.513	2.700	6.925	Cylinder L43F Type III [40]
Hydrogen mass [kg]	0.085	0.087	1.85	Cylinder L43F Type III [40]
Hydrogen tank volume [L]	4.020	4.200	4.478	Cylinder L43F Type III [40]

The comparison between the sizing result and the conceptual design result from the selected components is illustrated in *Table 7.5*. Following the optimization process, components that

were previously sized are chosen from the market, taking into account an acceptable error margin of 15 % in relation to the sizing results.

Table 7.5: Comparison of the results from sizing process and final conceptual design.

Parameter	**Sizing Result**	**Conceptual Design**	**Relative Error (%)**
MTOW [kg]	24.852	22.235	11.770
Payload [kg]	1.100	1.100	N/A
Endurance [h]	3.500	3.500	N/A
FW propeller diameter [m]	0.383	0.381	0.525
VTOL propeller diameter [m]	0.557	0.559	0.358
Airframe mass fraction [-]	0.300	0.300	N/A
HFC system mass [kg]	7.174	7.500	4.347
Battery mass [kg]	1.638	1.604	2.120
FW propulsion system mass [kg]	0.617	0.610	1.148
VTOL propulsion system mass [kg]	2.185	2.058	6.171
Transition time [s]	20.000	20.000	N/A

Only a comparison in terms of mass is made. However, errors may appear in the future in relation to other parameters of these components, even though they have been lightly monitored beforehand.

Chapter 8

Environmental impact

The chapter is focused on the potential long-term benefits of hydrogen propulsion, underscoring the need to evaluate the environmental impact of the new hydrogen-based models and their conventional counterparts. The primary aim of this chapter is to conduct a comprehensive analysis, with a specific focus on the total Greenhouse Gas (GHG) emissions of the UAV models. Moreover, the current status and future outlook of hydrogen as a viable aviation fuel are explored.

This analysis provides a holistic view of the environmental implications associated with the HFCs. The insights gained from this assessment is a crucial factor for understanding the true environmental footprint of hydrogen-powered aviation and its potential role in reducing aviation-related GHG emissions in the future.

8.1 Introduction

The rise of environmental issues worldwide and the growing worry about fossil fuels have propelled the shift towards renewable energies in recent years. Hydrogen is now being considered a top contender for being the primary fuel in the near future due to its abundance, sustainability, and eco-friendliness. Despite its carbon-neutral consumption, the production processes of hydrogen still pose certain drawbacks.

Figure 8.1 illustrates the global hydrogen production (2010-2022).

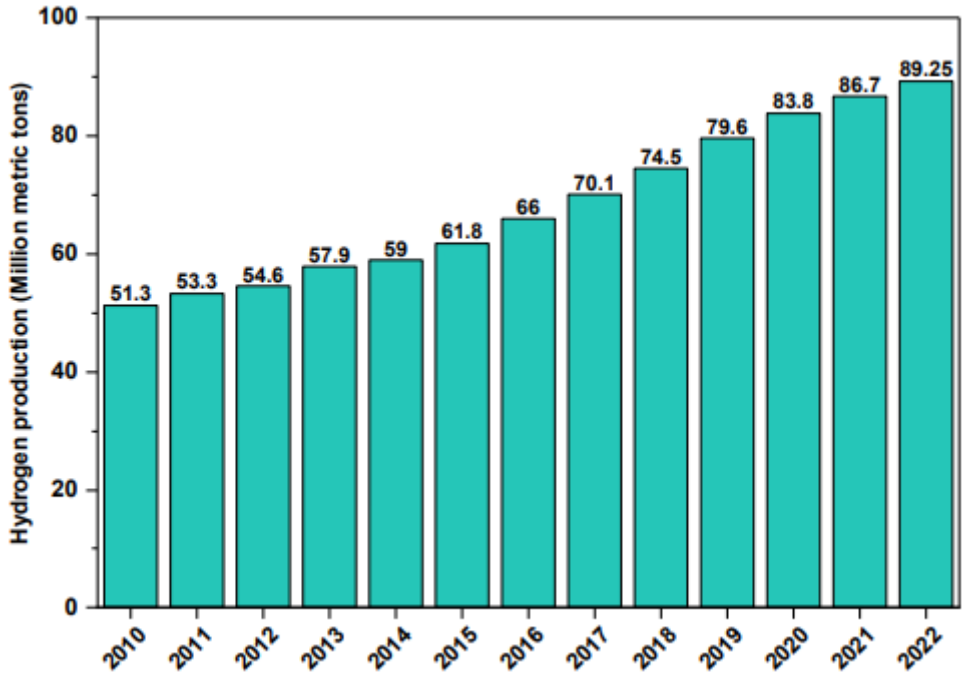

Figure 8.1: Global hydrogen production from 2010 to 2022 [55].

In general, there are two main methods for hydrogen production: natural gas reforming and electrolysis. Natural gas reforming involves extracting hydrogen from a hydrocarbon, typically methane, using processes like steam reforming and partial oxidation. This process produces carbon dioxide as a secondary product, creating grey hydrogen. To reduce the environmental impact, a carbon capture process can be added to create a more environmentally friendly fuel known as blue hydrogen.

On the other hand, hydrogen can be generated via electrolysis, a method that entails extracting hydrogen gas from water molecules without creating harmful byproducts. When the electricity needed for this procedure is derived from sustainable sources, the resulting hydrogen is referred to as green hydrogen. Nevertheless, due to the existing energy combination, electrolysis might not be as environmentally friendly as it seems, as the electricity utilized may still originate from non-renewable sources.

Addressing these production challenges is crucial for hydrogen to realize its full potential as a sustainable fuel source. Ongoing advancements in carbon capture technologies and the increasing integration of renewable energy sources into the grid are essential steps towards making hydrogen production truly environmentally friendly.

In *Figure 8.2*, a summary of the main types of hydrogen are displayed. The hydrogen types are in function of their production process and with a representation of their price per kg.

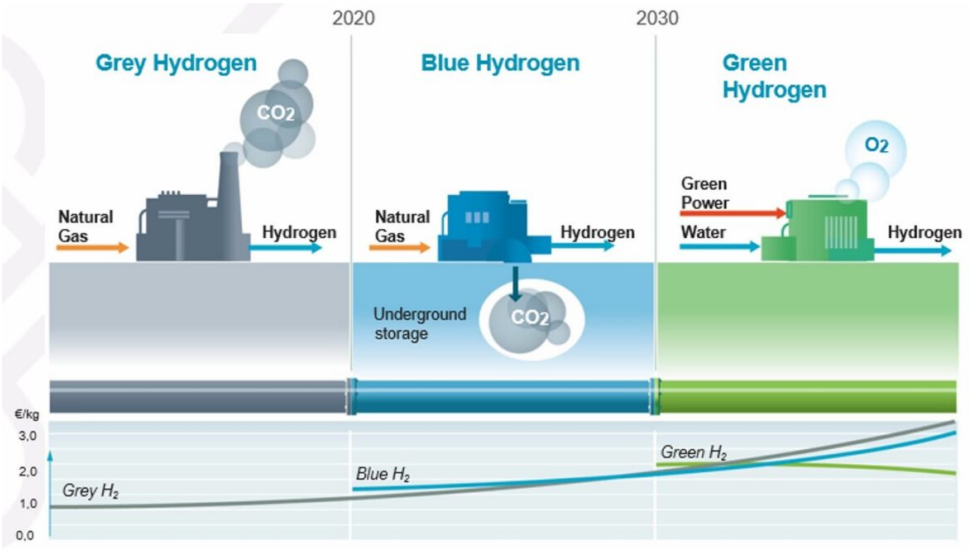

Figure 8.2: Three primary categories of hydrogen based on how they are produced [56].

Hydrogen energy is classified into various types depending on how it is produced, with the main categories including the following:

- **Gray hydrogen**: it is produced from fossil fuels like natural gas or coal using a method called Steam Methane Reforming (SMR). This process results in the emission of carbon dioxide (CO_2), which contributes to climate change.
- **Blue hydrogen**: it is derived from fossil fuels, but it undergoes an extra process known as Carbon Capture and Storage (CCS). This involves capturing the CO_2 released during hydrogen production and storing it underground to prevent it from being released into the atmosphere. The goal of blue hydrogen is to minimize the carbon footprint associated with hydrogen production.
- **Green hydrogen**: it is generated by utilizing sustainable energy sources like solar or wind power, utilizing electrolysis to split water (H_2O) into hydrogen (H_2) and oxygen (O_2) with the help of an electric current. Due to its dependence on renewable energy, the production of green hydrogen does not result in any direct carbon emissions, making it an environmentally friendly and viable choice.

Apart from production challenges, it is crucial to tackle transport and storage issues as well. The current leading suggestion for hydrogen production revolves around centralized plants, which require a distribution network. However, this network has shown inefficiency due to energy losses in pipelines and the environmental consequences of land transportation to refueling stations. Moreover, extra energy is needed to sustain low temperatures for liquid hydrogen storage once it reaches its commercial distribution point. These obstacles have sparked substantial criticism and skepticism towards hydrogen, with some going as far as branding it a failure because of the unrealistic expectations set for it.

8.2 Zero-Emission potential and discussion

Here, it is studied the use of hydrogen fuel as a power source. Hydrogen can either be burned in an ICE or be used to power a fuel cell to generate electricity for an electric propeller. There

are some limitations depending on the vehicle type, such as the impossibility to store it in a traditional wet wing, and hydrogen tanks must be housed in the fuselage or be supported by the wing.

But it must be highlighted an important aspect of the hydrogen use. A hydrogen aircraft using a fuel cell design are zero-emission in operation, whereas aircraft using hydrogen as a fuel for a jet engine, or an ICE are zero-emission for CO_2 but not for NOx (a local air pollutant). The burning of hydrogen in air leads to the production of NOx, O_2 reaction in a nitrogen-rich environment also causes the production of NOx. However, hydrogen combustion produces up to 90 % less nitrogen oxides than kerosene fuel, and it eliminates the formation of particle matter.

If hydrogen is available in quantity from low-carbon power such as wind or nuclear, its use in aircraft will produce fewer GHG than current aircraft: water vapor and a small amount of nitrogen oxide. Nevertheless, very little hydrogen is produced using low-carbon energy sources.

It is evident that, despite the benefits of hydrogen adaptation, there is still significant room for improvement as the majority of the carbon footprint of FCVs is attributed to hydrogen production. To further reduce GHG emissions, it is crucial to increase the utilization of renewable energies and electrolysis for H_2 production in the coming years. Although green hydrogen production is more costly in the short term, enhancing efficiency and lowering electrolysis costs should be a key objective to drive investment in renewable energy research and production. By making advancements in these areas, green hydrogen can become economically viable in the long run, especially when supported by inexpensive renewable energies on a large scale.

Fuel cell vehicles can play a crucial role in the transition towards zero-emission transportation and decreasing reliance on fossil fuels. Current situation led to the conclusion of the hydrogen cells to be a realistic and suitable option to reduce the contamination of aviation. The following aspects are some reasons for considering the hydrogen as the future renewable energy source:

- **Zero-emission transportation**: Fuel cell vehicles are an essential solution for combating air pollution and addressing climate change due to their zero tailpipe emissions. Unlike traditional ICE vehicles that release harmful GHGs and pollutants, fuel cell vehicles only produce water vapor as a byproduct of the electrochemical reaction in the fuel cells. This minimal environmental impact makes them a key player in reducing the negative effects of transportation on the environment.

- **Clean and efficient energy conversion**: Fuel cells provide a very effective way to convert chemical energy into electrical energy directly. The electrochemical reaction that takes place in the fuel cell allows for a more efficient use of fuel compared to the combustion process in internal combustion engines. This increased efficiency results in lower fuel consumption and reduced greenhouse gas emissions per kilometer traveled.

- **Reduced dependence on fossil fuels**: Hydrogen, the main fuel for fuel cell vehicles, can be generated from various sources, including renewable energy. Utilizing renewable energy sources like wind, solar, and hydroelectric power for hydrogen production via electrolysis can aid in decreasing reliance on fossil fuels for transportation. This contributes to improved energy security and encourages a more sustainable and varied energy blend.

- **Energy storage and grid integration**: Fuel cell vehicles have the potential to significantly impact energy storage and grid integration by utilizing excess electricity from renewable sources to produce hydrogen through electrolysis. The stored hydrogen can then be used in fuel cells, allowing for the efficient integration of intermittent renewable energy sources and helping to balance the electrical grid.

- **Renewable hydrogen production**: Utilizing renewable energy sources for hydrogen production ensures an environmentally friendly fuel cycle, making fuel cell vehicles a sustainable and zero-emission transportation option.

- **Decentralized energy generation**: Fuel cell vehicles, along with hydrogen refueling infrastructure, have the capability to provide decentralized energy generation. By producing hydrogen on-site from renewable sources, localized energy generation can be achieved, ultimately decreasing the reliance on long-distance energy transportation. This shift towards decentralized energy generation can improve energy resilience and minimize transmission losses.

Despite the fact that hydrogen has the potential to be the future green energy source, there are several challenges to overcame before this situation comes true. The main challenges are the following:

- **Infrastructure**: Building a comprehensive hydrogen infrastructure is a major obstacle for HFCVs due to the limited availability of hydrogen refueling stations. Unlike gasoline stations, which are plentiful in most areas, hydrogen refueling stations are few and far between, mainly concentrated in specific regions. Developing a widespread network of refueling stations, along with transportation and storage facilities, necessitates substantial investments.

- **Economic challenges**: At present, the expenses linked to the ownership and maintenance of hydrogen fuel cell vehicles (HFCVs) are significantly greater than those for a traditional internal combustion engine vehicle or a Battery Electric Vehicle (BEV). The elevated prices of vehicles, primarily caused by the expense of fuel cell systems, and the costly hydrogen fuel (stemming from high production, storage, and transportation costs) are key factors contributing to these financial obstacles.

- **Hydrogen production**: Hydrogen production for fuel cell vehicles presents challenges related to cost, energy efficiency, and environmental impact. The predominant method of hydrogen production involves SMR, which depends on natural gas as a raw material. Unfortunately, this process generates CO_2 emissions that counteract the environmental advantages of fuel cell vehicles. It is imperative to advance sustainable and low-carbon hydrogen production techniques, like electrolysis powered by renewable energy sources, despite the existing obstacles in terms of cost and scalability.

- **Energy efficiency**: Fuel cell vehicles exhibit higher energy efficiency compared to conventional internal combustion engine vehicles, yet fall short in efficiency when pitted against battery electric vehicles. The energy consumption involved in generating, transporting, and storing hydrogen, along with energy losses within the fuel cell system, contribute to an inferior overall energy efficiency in contrast to battery electric vehicles. Enhancing the energy efficiency of fuel cell systems and streamlining the entire hydrogen production and distribution process is imperative.

- **Safety concerns**: Hydrogen, as a highly flammable gas, poses safety risks in terms of storage, handling, and refueling. Despite the rigorous safety testing and multiple safety features in HFCVs, there are still concerns about potential leaks, hydrogen behavior in different accident scenarios, and the infrastructure's capability to handle emergencies. It is essential to enforce strict safety standards and regulations, as well as raise public awareness, in order to address these concerns effectively.

- **Limited vehicle models**: At present, there are only a few HFCVs available for purchase, making it difficult for consumers to find options that align with their needs. To encourage more widespread adoption, it is essential to increase the variety of models and make them more accessible in various locations.
- **Competition from battery electric vehicles**: HFCVs face a significant obstacle in the form of BEVs, which are currently leading the way in clean transportation. BEVs enjoy greater consumer awareness, a more established charging infrastructure, and continuously advancing battery technology, resulting in notable cost reductions and enhanced driving range.

HFCVs offer a promising solution for a sustainable and low-carbon future, boasting advantages such as zero tailpipe emissions, high energy efficiency, and fast refueling capabilities. Despite challenges such as high production costs and a lack of infrastructure, advancements in technology and R&D investments may help overcome these obstacles in the future. The involvement of stakeholders, including automakers and government policies, is crucial in promoting the widespread adoption of HFCVs and integrating them into broader energy and environmental strategies.

Chapter 9

Conclusion and future steps

It is crucial to review the objectives, methodology, and results of the project upon its completion, highlighting the key insights obtained and their importance, while recognizing the limitations of the study. Furthermore, given the subject matter, it is essential to delineate and place into context the subsequent actions needed for the practical application of the suggested model.

9.1 Conclusion

Throughout this dissertation, the procedures for conceptualizing the design of a multi-mode eVTOL UAV powered by a HFC and Li-po battery, equipped with a specific LiDAR function, are executed.

The primary goal of the project is to create an airplane that can tackle present-day transportation obstacles, especially those concerning environmental impact and the efficiency of propulsion systems. The importance of the study was first established by conducting a brief market analysis, which uncovered a rising market demand for this kind of aircraft, given their use in civil safety, emergency response, and agricultural operations, among other applications. Additionally, the interest in giving visibility to the LiDAR sensor corresponds to another of the main objectives, thus raising awareness of a device with a wide range of applications. LiDAR, together with UAVs, represent a great opportunity for the development of several and very important applications in everyday life, such as in the forestry field and more specifically in the dimensioning of forest plots and the creation of 3D maps of them. The addition of a hydrogen propulsion system would catapult the performance and complement the UAV, thus meeting the goal of the aerospace industry of achieving zero emissions and increasing the efficiency and therefore the performance of the aircraft.

The beginning of thesis starts with the introduction of the LiDAR sensor, it continues with the history of UAVs and their various applications in relation to LiDAR functionality, and end with a brief description of the current state of the art of hydrogen propulsion systems. Subsequently, the methodology of the study implemented is outlined. The proposed method entailed an iterative adjustment of the geometry of the aircraft and power components for a specific mission through statistical correlations and aerodynamic requirement calculations. MATLAB was utilized for this process, streamlining calculations and enabling the analysis of different configurations. This method enabled a thorough examination of potential applications and advantages, along with a more accurate identification of fuel-cell powered aircraft limitations.

In addition, an optimisation is carried out to improve the characteristics of the model. Through the dimensions obtained from the first iterations, different options for the UAV model are analysed through xflr5 and the final model is recreated with Fusion360. Subsequently, CFD simulations, with StarCCM+, are run and the selected model is refined. After the iterative process, the results are collected to compare them with the initial stage of the process and, above all, with the data of the components that are selected from the current market.

MTOW is decreased to meet the design criteria, but errors in the sizing result may still occur due to the propulsion system selecting the product with the closest performance based on calculated parameters during the conceptual design process.

The examination of different aircraft operations has resulted in the determination that they are not only currently viable but also demonstrate competitive advantages in terms of range and endurance when compared to similar aircraft. Moreover, they provide additional advantages over traditional ICE models, including a reduced environmental footprint. These environmental advantages were further investigated through a comparative environmental impact between UAV models powered by different energy sources, offering an opportunity to delve into the current status of the hydrogen economy.

It is essential to assess the constraints present in this project, beginning with the lack of specific references regarding light hydrogen-powered aircraft. This could have implications on the structural mass and aerodynamic performance calculations, as they were based on generic helicopter design models. Additionally, certain aerodynamic factors, such as the parasitic drag coefficient, were not thoroughly investigated and were estimated through statistical correlations and ultimately confirmed by a CFD simulation of a simplified model, potentially impacting the results. The approach involved making simplifying assumptions for model adaptation and environmental impact assessment to ensure consistency, which needs to be carefully reviewed before utilizing the findings. Given the academic nature of the project and the limited resources, it is important to acknowledge any other potential errors or criticisms related to the methodology.

The outcomes and implications of the project, while considering possible error sources, are considered noteworthy in the present aerospace sector. Showcasing a fuel-cell propelled UAV as a feasible choice for upcoming cargo delivery, land analysis tasks, and civil protection highlights the importance of this endeavor. The primary goals were effectively met, resulting in precise and unbiased conclusions via a clearly outlined approach. Including a safety buffer to allow for potential modifications in design and unexpected variables additionally bolsters the reliability of the outcomes.

Furthermore, the environmental impact of the project, through the one of the hydrogen as an energy source, is done. HFCVs offer a compelling solution for long-range and heavy-duty transportation needs where BEVs may not be as practical. Additionally, if hydrogen is produced from renewable sources, it can serve as a truly green fuel option, further aiding in climate change mitigation efforts. Despite facing challenges such as high production costs, lack of refueling infrastructure, and concerns about efficiency and environmental impact, advancements in technology, economies of scale, and substantial research and development investments are expected to help overcome these obstacles in the future.

The future of HFCVs is closely intertwined with the overall growth of the hydrogen economy as the world shifts towards renewable and sustainable energy solutions.

9.2 Future Steps

This is a complex iterative process in which there is a lot of dependence on different component values. The aim of this thesis is to give visibility to the conceptual design process of the UAV and to show how to incorporate the new technological advances, in relation to HFCs, to these aircraft.

The project focuses solely on evaluating the initial design elements of the vehicle, serving as a foundation for further detailed examination of its specific components. The range of potential studies to be conducted post-results is vast, with each playing a crucial role. Several key studies essential for advancing the design process include:

- Enhancing the level of detail in the initial 3D design by incorporating the suggestions outlined in this project based on the latest advancements in the field.
- Utilizing the previously discussed design to enhance the precision of estimating the weights of various elements and implementing stricter standards for material selection.
- Carrying out comprehensive aerodynamic assessments on different aircraft components, including fuselage drag, rotor efficiency, non-ideal effects, element interference, and blade profile design. This investigation is essential as some of the data used in this study is based on statistical correlations rather than direct research findings.
- Perform thorough structural evaluations focusing on the durability of the aircraft, performance, and vibration characteristics to improve safety, comfort, and overall efficiency, especially during critical flight operations such as landing and hovering. Special attention should be given to analyzing vibration properties to reduce noise levels and prevent potential safety hazards like ground resonance.
- Conducting simulations on the flight dynamics of an aircraft to anticipate and rectify any undesirable behaviors in the design stage. For UAVs, these findings can be utilized to create the necessary software for remote aircraft control or to enable an automatic pilot system to carry out designated missions.
- Designing effective control systems to facilitate smooth and enjoyable aircraft maneuvering, particularly with regard to its possible private usage.
- Customizing the interior space of the UAV to align with the mission and optimally organizing its various elements can provide insight into whether the aircraft needs to be resized overall.
- Perform a wind-tunnel analysis by scaling the prototype and compare aerodynamic results with the obtained ones through the CFD simulation.
- To develop a more comprehensive study on the impact of hydrogen as an energy source, through the development of a Life-Cycle Assessment (LCA) by using ISO 14040:2006 methodology [57].

As for hydrogen usage in aviation, numerous challenges are still on the horizon, waiting to be addressed and explored. The lack of infrastructure has been identified as the primary obstacle hindering the progress of hydrogen-powered vehicles. Therefore, it is crucial to push forward with various initiatives that cover all aspects of the hydrogen economy, ranging from

fuel generation to vehicle operation. There is ample room for enhancement in every sector, and future research endeavors should strive to build upon the momentum established over the past decade. Additionally, it is essential to formulate environmental policies that prioritize the expansion of renewable energy production and utilization. This will facilitate the transition of hydrogen production towards a market dominated by electrolysis, where the environmental advantages have been proven to be optimal.

Bibliography

[1] K. P. Valavanis and G. J. Vachtsevanos. *Handbook of Unmanned Aerial Vehicles*. First Edition. Vol. 5. Springer, 2014.

[2] Wikipedia contributors. *General Atomics MQ-9 Reaper*. Accessed: 2024. 2024. URL: https://es.wikipedia.org/wiki/General_Atomics_MQ-9_Reaper.

[3] Wikipedia contributors. *AeroVironment Helios Prototype*. Accessed: 2024. 2023. URL: https://en.wikipedia.org/wiki/AeroVironment_Helios_Prototype.

[4] Edwin Frank. "LiDAR Sensors: Technology and Applications Author". In: *ResearchGate* (May 2024). Accessed: 2024. URL: https://www.researchgate.net/publication/380269955.

[5] In: *LiDAR Principles, Processing and Applications in Forest Ecology*. Ed. by Qinghua Guo, Yanjun Su, and Tianyu Hu. Academic Press, 2023, p. iv. ISBN: 978-0-12-823894-3. DOI: https://doi.org/10.1016/B978-0-12-823894-3.12001-8. URL: https://www.sciencedirect.com/science/article/pii/B9780128238943120018.

[6] Rachel Shardlow. *Is UAV LiDAR the Next Big Thing for Surveying?* Accessed: 2024. 2017. URL: https://coptrz.com/blog/uav-lidar-next-big-thing-surveying/.

[7] Instituto Geográfico Nacional. *Plan Nacional de Ortofotografía Aérea (PNOA)*. Accessed: 2024. 2024. URL: https://pnoa.ign.es.

[8] Instituto Geográfico Nacional. *Especificaciones Técnicas Plan Nacional de Ortofotografía Aérea (PNOA)*. Accessed: 2024. 2024. URL: https://pnoa.ign.es/web/portal/pnoa-lidar/especificaciones-tecnicas.

[9] Teledyne. *Geospatial Optech Lidar*. Accessed: 2024. 2024. URL: https://www.teledyneoptech.com/en/products/airborne-survey/galaxy/.

[10] Heligràfics. *Technology airborne services*. Accessed: 2024. 2024. URL: https://www.heligrafics.net/fotogrametria-y-lidar/.

[11] YellowScan. *YellowScan Product Page*. Accessed: 2024. 2024. URL: https://www.yellowscan.com/es/products/.

[12] Jouav. *JoLiDAR-LR22*. Accessed: 2024. 2024. URL: https://www.jouav.com/products/jolidar-lr.html.

[13] Maxim Tyan et al. "Comprehensive preliminary sizing/resizing method for a fixed wing – VTOL electric UAV". In: *Aerospace Science and Technology* 71 (2017), pp. 30–41. ISSN: 1270-9638. DOI: https://doi.org/10.1016/j.ast.2017.09.008. URL: https://www.sciencedirect.com/science/article/pii/S1270963817300871.

[14] Jae-Hyun An et al. "Advanced Sizing Methodology for a Multi-Mode eVTOL UAV Powered by a Hydrogen Fuel Cell and Battery". In: *Aerospace* 9 (Jan. 2022), p. 71. DOI: 10.3390/aerospace9020071.

[15] YellowScan. *YellowScan Integrations Platform*. Accessed: 2024. 2024. URL: https://www.yellowscan.com/es/lidar-platform-integrations/.

[16] Doosan Mobility Innovation. *DM15*. Accessed: 2024. 2024. URL: https://www.doosanmobility.com/en/products/powerpack-dm15.

[17] JOUAV. *CW 25H hydrogen-powered VTOL fixed-wing UAV*. Accessed: 2024. 2024. URL: https://www.jouav.com/products/cw-25h.html.

[18] Sparkle Tech. *Sparkle Tech Fixed Wing Hybrid VTOL Eagle plus*. Accessed: 2024. 2024. URL: https://www.sparkleuav.com/drones-vtol/hybrid-vtol/fixed-wing-hybrid-vtol.html.

[19] JOUAV. *CW 25E long endurance electric fixed-wing VTOL drone*. Accessed: 2024. 2024. URL: https://www.jouav.com/products/cw-25e.html.

[20] Carbonix. *Carbonix Volanti*. Accessed: 2024. 2024. URL: https://carbonix.com.au/volanti/.

[21] Germandrones. *Germandrones Songbird*. Accessed: 2024. 2024. URL: https://www.germandrones.com/en/songbird.

[22] StriekAir. *StriekAir CarryAir*. Accessed: 2024. 2024. URL: https://www.striekair.com/.

[23] H^3 Dynamics. *H^3 Dynamics page*. Accessed: 2024. 2024. URL: https://www.h3dynamics.com/.

[24] María Escudero-Escribano. "Electrocatalysis and surface nanostructuring : atomic ensemble effects and non-covalent interactions". PhD thesis. Nov. 2011.

[25] Mykhaylo LOTOTSKYY et al. "The use of metal hydrides in fuel cell applications". In: *Progress in Natural Science* 27 (Feb. 2017), pp. 3–20. DOI: 10.1016/j.pnsc.2017.01.008.

[26] J.Hoogendoorn. "Fuel Cell and Battery Hybrid System Optimization". MA thesis. Delft University of Technology, 2018.

[27] José Desantes et al. "Feasibility Study for a Fuel Cell-Powered Unmanned Aerial Vehicle with a 75 Kg Payload". In: *Transactions on Aerospace Research* 2022 (June 2022), pp. 13–30. DOI: 10.2478/tar-2022-0008.

[28] Publications Office of the European Union. *A sustainable pathway for the European energy transition: the hydrogen roadmap*. 2019. DOI: 10.2843/249013.

[29] G.M. Hoffmann et al. "Quadrotor helicopter flight dynamics and control: theory and experiment". In: *Proc. of the AIAA Guidance, Navigation and Control Conference*. Vol. 2. 2007, p. 4.

[30] D.P. Raymer. *Aircraft Design: A Conceptual Approach*. 5th. Reston, VA: AIAA, 2012.

[31] S. Gudmundsson. *General Aviation Aircraft Design: Applied Methods and Procedures*. 1st. Oxford, Waltham, MA: Butterworth-Heinemann, 2013.

[32] L.K. Loftin. *Subsonic Aircraft: Evolution and the Matching of Size to Performance*. RP1060. NASA.

[33] J. Roskam. "Rapid sizing methods for airplanes". In: *Aircraft Design Systems and Operations Meeting*. Colorado Springs, CO, USA, 1985.

[34] Jay Gundlach. *Designing Unmanned Aircraft Systems: A Comprehensive Approach*. Reston, VA: American Institute of Aeronautics and Astronautics, 2011.

[35] C.E.D. Riboldi and F. Gualdoni. "An integrated approach to the preliminary weight sizing of small electric aircraft". In: *Aerospace Science and Technology* 58 (2016), pp. 134–149.

[36] J.D. Keith and D.W. Hall. "Rapid sizing methodologies for VTOL UAVs". In: *47th AIAA Aerospace Sciences Meeting including The New Horizons Forum and Aerospace Exposition*. 2009, p. 1617.

[37] A.M. Kamal and A. Ramirez-Serrano. "Design methodology for hybrid (VTOL + Fixed Wing) unmanned aerial vehicles". In: *Aeron Aero Open Access J.* 2.3 (2018), pp. 165–176. DOI: 10.15406/aaoaj.2018.02.00047.

[38] M.H. Sadraey. *Aircraft Design: A Systems Engineering Approach*. Aerospace Series. Chichester, UK: Wiley, 2013. ISBN: 978-1-119-95340-1.

[39] HES Energy Systems. *HES Energy Systems Fuel Cell Store*. https://www.fuelcellstore.com/hes-energy-systems. Accessed: 2024.

[40] Intelligent Energy. *Intelligent Energy*. https://www.intelligent-energy.com/. Accessed: 2024.

[41] H^3 Dynamics. *H^3 H2 Solutions for UAV*. https://www.h3dynamics.com/h2solutionsforuav. Accessed: 2024.

[42] Generalitat Valenciana. *Montes gestionados por la Generalitat*. Accessed: 2024. 2024. URL: https://mediambient.gva.es/es/web/medio-natural/montes-gestionados-por-la-generalitat.

[43] Quantum GIS. *QGIS Software*. https://qgis.org/download/. 2024.

[44] Teresa Donateo et al. "A new approach to calculating endurance in electric flight and comparing fuel cells and batteries". In: *Applied Energy* 187 (2017), pp. 807–819. ISSN: 0306-2619. DOI: https://doi.org/10.1016/j.apenergy.2016.11.100. URL: https://www.sciencedirect.com/science/article/pii/S0306261916317317.

[45] Airfoil Tools. *Airfoil Search*. Accessed: 2024. 2024. URL: http://www.airfoiltools.com/.

[46] xflr5. *xflr5: An Analysis Tool for Airfoils, Wings, and Planforms Operating at Low Reynolds Numbers*. https://www.xflr5.tech/. Version 6.61. 2024.

[47] S. Suewatanakul et al. "Conceptual Design of a Hybrid Hydrogen Fuel Cell/Battery Blended-Wing-Body Unmanned Aerial Vehicle—An Overview". In: *Aerospace* 9.5 (2022), p. 275. DOI: 10.3390/aerospace9050275. URL: https://doi.org/10.3390/aerospace9050275.

[48] Autocad. *Autocad Inc. Fusion360*. https://www.autodesk.com/products/fusion-360/overview. 2024.

[49] Siemens. *Siemens StarCCM+*. https://www.plm.automation.siemens.com/global/en/products/simcenter/STAR-CCM.html. 2024.

[50] F.R. Menter. "Two-equation eddy-viscosity turbulence models for engineering applications". In: *AIAA Journal* 32 (1994), pp. 1598–1605. DOI: 10.2514/3.12149.

[51] E.C. Douvy, I.A. Tsavalos, and P.D. Margaris. "Evaluation of the turbulence models for the simulation of the flow over a National Advisory Committee for Aeronautics (NACA) 0012 airfoil". In: *Journal of Mechanical Engineering Research* 4 (2012), pp. 100–111.

[52] RC Innovations.

[53] T-Motor. *Available online: https://uav-en.tmotor.com/*. 2024.

[54] APC Propellers. *Available online: https://www.apcprop.com/*. 2024.

[55] Quasay Hassan et al. "Hydrogen Fuel Cell Vehicles: Opportunities and Challenges". In: *MDPI Sustainability* 15 (15 2023). DOI: https://doi.org/10.3390/su151511501. URL: https://www.mdpi.com/2071-1050/15/15/11501.

[56] GREENZO ENERGY PVT.LTD. *Green hydrogen*. https://www.greenzoenergy.com/what-are-the-3-main-types-of-hydrogen/. 2024.

[57] International Standard Organization. *Environmental management – life cycle assessment – principles and framework*. International Standard. ISO 2006. 2006.

Part II

Specifications

Description of the works

The administrative, economic and technical specifications that have been taken into account for the study will be discussed below.

Work units

The works that have been carried out during this project are listed below:

- **Preparation and background research.**
- **Development of the sizing methodology.**
- **Analysis of the mission with its limitations.**
- **Optimization of the results.**
- **Particularization and discussion of the results.**

Preparation and background research

During this initial set of functional activities, the necessary data base is obtained in order to carry out a study with criteria either for the sizing method or for the analysis of the mission, the development of the results and their respective treatment and interpretation.

Development of the sizing methodology

The present group covers the development of the sizing method, from the description of the procedure to the analysis of the requirements necessary for each component of the system, together with the assumptions made during the process. The operations are therefore as follows:

- Establishment of the sizing procedure.
- Development of the Multi-Mode Constraints Analysis (MCA).
- Development of the Electric Power System (EPS) sizing.

Analysis of the mission with its limitations and requirements.

The different characteristics of the mission to be carried out are developed below, together with assumptions for the realisation of the mission. In addition, the power required is determined, thus sizing the energy sources used for this purpose. Among the activities included are:

- Description and objective of the mission.
- Power requirements.
- Sizing of the energy sources.

Optimization of the results.

In this subset of activities, the formulation for the optimisation of the designed model is determined. For this purpose, the following activities are given:

- Development of the geometry of the model.
- Aerodynamic analysis through CFD simulation.

Particularization and discussion of the results.

The activities collected in this subset give rise to the particularisation of the data according to the model sought. After data collection, they are analysed in order to validate the results by making physical sense of them and to draw final conclusions. Among other activities it concentrates on:

- Establishment of the aircraft design requirements.
- Collection of the optimum sizing results.
- Selection of the components from the current market.
- Discussion of the environmental impact.

General specifications

This section outlines a regulatory framework for the advancement of the pertinent activities concerning the various entities within the project, detailing both legislative components and the requirements for carrying out and completing the project.

Project contract

The contract establishing the margins of the present project should be incorporated in the contract:

- The current general specifications.
- The current general specifications.
- Technical specifications.
- The tender of the contractor accepted by the client.
- General project and detail blueprints.
- Others (work commencement report, service orders, agreements or proof of additional work, etc).

Optional general conditions

This subsection deals with the attributions of both parties to the contract with reference to their work.

- Actions of the developer/contractor.

  The contractor is committed to staying updated on the current regulations related to the project and ensuring compliance with health and safety standards in the workplace. Additionally, they will procure and supply necessary materials, equipment, and labor for the project, including the required software and 3D CAD tools for analysis, while ensuring the quality of materials used.

  The contractor will also create a detailed action plan, assign tasks to team members, and recruit necessary personnel. They will oversee the progress of the project, establish deadlines, maintain communication with the client, and conduct risk assessments.

  Furthermore, the contractor will provide after-sales services, including warranty and support, to address any potential issues after project completion.

- Actions of the chief project engineer.

  He/She is responsible for the planning, execution and monitoring of the activities that make up the business project, thus establishing a definition of the project objectives, development of the processes, coordination and procurement of resources together with the contractor as well as the decision making process in required moments.

  Additionally, he/she is responsible for the processing, management and understanding of the information as well as for the mediation of conflicts and/or identification of errors.

Performance specifications

Rhythms

The start of the works will be carried out as stipulated in these particular specifications, which set out a chronology of the activities carried out on the basis of pre-established periods for each of them. The contracted party therefore undertakes to comply with the stipulated times with the possibility of extension for reasons of force majeure if both contracting parties agree to do so.

Order of activities

The establishment of the successive activities will be at the absolute discretion of the contractor, with the exception of specific technical aspects in which the modification of the optional conditions of the current contract is deemed appropriate.

Stipulations for the development of activities

All work performed must adhere to the approved specifications and/or orders set forth by the entity (whether individual or institution) specified in a written report previously approved by the supervisor.

Project extension based on contingencies

Due to unforeseen circumstances, the contract can be extended with the same terms as outlined in the initial contract annex, if requested. Extending the project may involve creating new terms and/or adjusting project formulations with approval from the head engineer. This will require updating contractor assignments and revising budget allocations.

Particular specifications

Since only a sizing methodology is applied after a previous analysis of the critical requirements, not all the typical concepts of a traditional specification will be addressed, only aspects related to scope and scope, resources required, management, results and criteria will be discussed.

Scope and scope of application

The project will be carried out over a period of approximately three months. During this period, both the conceptual design of the UAV and the drafting of this document will be carried out.

With respect to the conceptual scope of the project, this is limited to the assumptions for the mission of the UAV for FW and VTOL modes conditions and its subsequent performance analysis. This therefore establishes the basis for the development and management of the project.

It should also be noted that the fact that arouses the interest in this project is the growing industrial development and the incorporation of this type of vehicle in a wide number of existing and/or future fields. As introducing the HFCS and LiDAR sensors as a disruptive change for many fields, being incorporated in UAVs.

The results obtained in this study may, with some modifications and a certain level of error, be extrapolated to other similar geometries. This increases the scope of application of the study, as it is not only limited to a specific geometry, but can be used in different sectors to establish approximate results of the behaviour of the vehicle in advance.

Resources required

The resources, related to the development of the project can be divided into: human, equipment, material and software resources.

- Human resources.
  - Author of the research project.
  - Associate tutor, in charge of supervising the development.
- Equipment resources.

  They are listed in the budget part as well, considering their specifications and cost.
  - HP 15-bs0xx computer.
  - Dell Inspiron 14 5420 computer.
  - HP Bluetooth mouse Z5000 wireless mouse.
- Material resource.

  Described in the market selection during the memory in case study chapter. Also, they are listed in the budget part for considering their costs.
- Software resources.

- Overlief open source software.
- xflr5 open source software
- qgis open source software.
- Matlab software.
- Microsoft 365 Personal.
- Autodesk Fusion 360 software.
- Star CCM+ software.

Working procedure

With reference to the organisational structure of the project, as mentioned above, the research team consists of 2 members. The tutor is in charge of the supervision, discussion and compilation of the results obtained.

On the other hand, there is the developer of the project itself, whose function is composed of the analysis of the mission requirements, the development of the sizing method process, the elaboration of conceptual design model from the limitations and assumptions stated, the selection of actual components and the final analysis of the optimum results reached.

Expected results

With respect to the sizing process, the results of the sizing process will be a set of feasible parameters that reliably reflect the geometrical dimensions and the power and consumption values, among others. These parameters will generate a database that will be used to understand the limitations and properties which defined the UAv behaviour, setting a process which can be span, by adapting it, to other UAVs with different geometrical parameters. Also, from the data mentioned, it will be carried out the selection of components for the current market.

Thus, since this is a research project, the final result will be a report specifying the trends of the basic characteristics of the UAV, delimited by the type of mission to be performed.

Assessment criteria

The evaluation of the project will be carried out on the basis of different aspects of the project. On the one hand, there is the evaluation of the sizing results. The criteria used to evaluate these results are based on an exposition and subsequent discussion of the results in the working group, which allows, based on the experience and knowledge of the tutors, to extract explanations and veracity of the same, justifying the possible errors that may appear. In addition, a process of experimentation independent of the project is proposed in order to ratify the validity of the results.

On the other hand, there are the evaluation criteria of the research and report, which are based on the verification of the fulfilment of the pre-established objectives in the same as well as the fulfilment of the schedule and compliance with the costs awarded to the project.

Sustainable Development Goals (SDGs)

Table 9.1: SDGs related to the thesis.

SDGs	*High*	*Medium*	*Low*	*Not applicable*
SDG 1. No poverty				**X**
SDG 2. Zero hunger				**X**
SDG 3. Good health and well-being				**X**
SDG 4. Quality education				**X**
SDG 5. Gender equality				**X**
SDG 6. Clean water and sanitation				**X**
SDG 7. Affordable and clean energy	**X**			
SDG 8. Decent work and economic growth				**X**
SDG 9. Industry, innovation and infrastructure		**X**		
SDG 10. Reduced inequalities				**X**
SDG 11. Sustainable cities and communities		**X**		
SDG 12. Responsible consumption and production	**X**			
SDG 13. Climate action	**X**			
SDG 14. Life below water			**X**	
SDG 15. Life on land	**X**			
SDG 16. Peace, justice and strong institutions				**X**
SDG 17. Partnerships for the goals				**X**

A sustainable transportation system should be inclusive, effective, eco-friendly, and have minimal carbon footprint. While transportation may not have specific sustainable development goals (SDGs) of its own, it plays a crucial role in advancing other SDGs. *Table 9.1* illustrates the SDGs that can be achieved through the use of HFCVs with the addition of the LiDAR sensor, directly or indirectly.

The relation with SDGs-7 is established by the environmental impact section, where the fact that hydrogen is a clean energy is addressed and discussed. The SDG-7 is primarily focused on ensuring that clean and modern energies are accessible to every household at affordable prices by 2030, while also aiming to double the global energy efficiency enhancement rate.

Similarly, SDG-9 and SDG-12 concentrate on promoting sustainable practices within the industrial and transport sectors. Green hydrogen European policy is designed to enhance infrastructure and upgrade industries to operate in a more sustainable manner by optimizing resources and encouraging more companies to adopt clean technologies and processes.

SDG-11 underscores the importance of providing safe and sustainable transport infrastructure for all, which aligns with European Union aspirations for a hydrogen economy. This target not only supports inclusive and sustainable urbanization efforts but also encourages sustainable human settlement planning.

Hydrogen fuel cell vehicles powered by green hydrogen can be a highly effective eco-friendly option when urgent action is needed to address climate change in line with SDG-13. The oceans, covering approximately three-quarters of the surface of the Earth, are a vital and prominent feature crucial to the biodiversity in the planet. Each year, numerous marine birds and endangered species such as bottleneck dolphins, spinner dolphins, melon-headed whales, and sperm whales are tragically killed due to oil spills. The adoption of green hydrogen for vehicles not only reduces the demand for oil production and imports by various nations but also contributes to a more sustainable future. The adoption of green hydrogen in vehicles will not only reduce the demand for oil production and imports by various nations but also open the door for the integration of green hydrogen in the shipping industry, indirectly supporting the goals of SDG-14.

The combination of the HFC system, equipped in the UAV, and the LiDAR sensor is highly related to the interests of the SDG-15. Safeguard, rejuvenate, and advocate for the responsible utilization of land-based ecosystems, effectively oversee forests, address desertification, prevent and undo land deterioration, and stop the decline of biodiversity.

Part III

Budget Breakdown

The budget allocated takes into consideration the costs of labor, materials resources, technical equipment and software used for the project with an additional 13 % for general expenses, a 6 % of industrial benefit and a 21 % of IVA.

Mention should be made of the fact that this is the estimated baseline budget for the development of the project.

Labor Cost

The collective bargaining agreement in the Spanish technical engineering companies, effective as of July 20, 2024, sets out the terms and conditions of employment, wages, and working hours. It establishes the general annual working hours at 1,792 hours and the entry annual salary at 22,224.26 € for the salary level II. These details can be found in "Disposición 6346 del Boe núm. 59 de 2023" and the updated salary table in "Disposición 5873 del Boe núm. 73 de 2024", serving both as a reference point for labor cost calculations, which are determined by multiplying the total project hours by the hourly salary rate of 12.40 €/h.

Additionally to the base salary, an hypothetical salary counting with the extra components is developed.

The summary of the labor cost is displayed in *Table 9.2*.

Table 9.2: Labor cost estimation.

Proffesor	**Cost**	**Student**	**Cost**
Work duration	0.50 h	*Work duration*	305.00 h
Base salary	22.90 €	Base salary	12.40 €
Common contingencies	23.60 %	Common contingencies	23.60 %
Intergenerational equity mechanism	0.58 %	Unemployment	5.50 %
Work accident and occupational disease	0.70 %	Professional training	0.60 %
		AT and EP	1.50 %
		FOGASA	0.20 %
		MEI	0.58 %
Total additional complements	24.88 %	*Total additional complements*	31.98 %
Labor cost per hour	28.60 €	Labor cost per hour	16.37 €
Total labor cost	14.30 €	**Total labor cost**	4,992.85 €

Equipment Cost

The estimated price of the technical equipment used for this project are the following ones:

- **HP 15-bs0xx**: one of the computers used to carry out the project, with an Intel(R) Core(TM) i5-7200U processor, 16 GB RAM and 446 GB SSD. A linear depreciation over a period of time of 8 years will be considered, so that its cost over the 3-month period of the project is found by dividing the original price of 1,000 €by 12.

- **Dell Inspiron 14 5420**: the other computer used to carry out the project, with an 12th Gen Intel(R) Core(TM) i7-1255U processor, 16 GB RAM and 933 GB SSD. A linear depreciation over a period of time of 2 years will be considered, so that its cost over the 3-month period of the project is found by dividing the original price of 1,200 €by 12.

- **HP Bluetooth mouse Z5000**: basic wireless mouse.

The summary of the equipment cost is displayed in *Table 9.3*.

Table 9.3: Equipment cost estimation.

Equipment	**Cost**
HP 15-bs0xx	125 €
Dell Inspiron 14 5420	150 €
HP Bluetooth mouse Z5000	40 €
Total equipment cost	315 €

Material resources Cost

The materials and components are selected from the current market in order to provide an estimate of the price linked to the material development of the conceptual UAV designed. Their characteristics are are listed in the case study section. Some of these materials are not mentioned in the project sections, so are not added to the initial budget, such as the structural material, servomotors, and wiring, among others. Also, some values such as the HFC and the hydrogen tank are estimated through the current market.

The summary of the material cost is displayed in *Table 9.4*.

Table 9.4: Material cost estimation.

Material	**Quantity**	**Total Cost**
T-Motor V22*7.4	4 units	587.16 €
APC 15x10E	1 unit	7.39 €
T-Motor Flame 70A 6S	1 unit	64.25 €
T-Motor U12 II	4 units	1,358.28 €
Hobbywing FlyFun HV 110A V5 SBEC	4 units	436.96 €
IES-SOAR 2.4	1 unit	9,180.10 €
Gens ACE G-Tech 6S 22.2V Li-po Battery	2 units	251.52 €
Cylinder L43F Type III	1 unit	1,836.02 €
Total material cost	18 components	13,721.68 €

Software licenses Cost

The expenses related to the software licenses are outlined as well, taking into account a depreciation period of 4 years for software packages with perpetual licenses, considering the academic journey period. Software packages like Overleaf, xflr5, or qgis, which were used for the project, are not listed as they are either open source or have a free version that met the requirements of the project.

The summary of the material cost is displayed in *Table 9.5*.

Table 9.5: Software cost estimation.

Software	**Type of license**	**Amortization Cost/3 months**	
Standard Matlab	perpetual (2,000.00€)	4 years	125.00 €
Microsoft 365 Personal	annual (1,234.05€)	1 year	308.51 €
Fusion 360 Personal	annual (484€)	1 year	121.00 €
StarCCM+	annual (30,000€)	1 year	7,500.00 €
Total software cost	[-]	[-]	8,054.51 €

Global budget

The preliminary global budget estimate is calculated by combining the total of individual costs with a portion of general expenses to account for unforeseen circumstances or additional expenses like utilities, the industrial profit, and IVA. This serves as an initial estimate that may undergo adjustments throughout the project implementation.

The global budget is found in *Table 9.6*.

Table 9.6: Summary of the global budget estimation.

Partial costs	**Total cost**
Labor cost	5,007.15 €
Equipment cost	315.00 €
Material cost	13,721.68 €
Software cost	8,054.51 €
Sum	27,098.34 €
Additional costs	
General expenses	13 %
Industrial profit	6 %
IVA	21 %
Global budget estimation	37,937.68 €

In summary, the initial budget estimation for the project is:
Thirty seven thousand nine hundred and thirty seven and sixty eight

Part IV

Blueprints

Now, in this part the different blueprints for the model definition are presented. The blueprints selected are the following ones:

- **3-View drawing.**
- **Isometric perspective.**
- **Section View**
- **Detailed View**

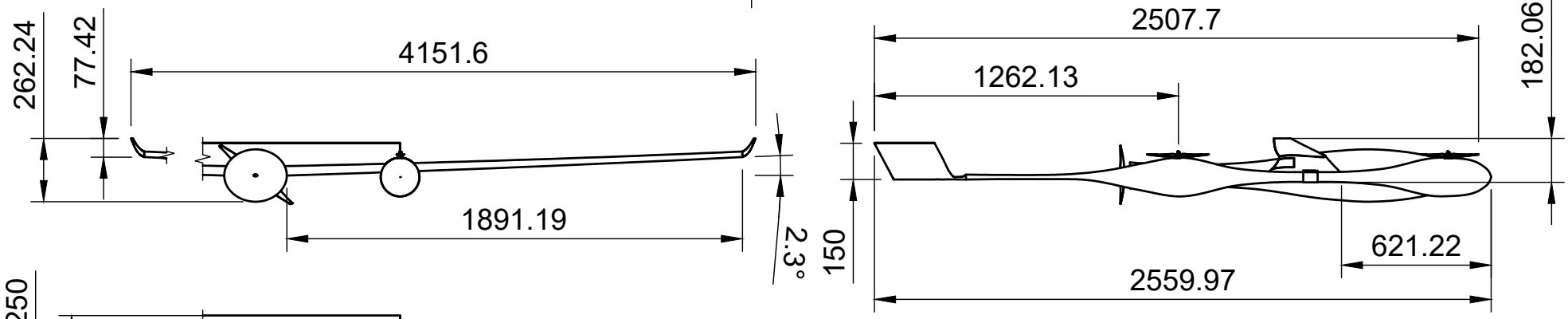

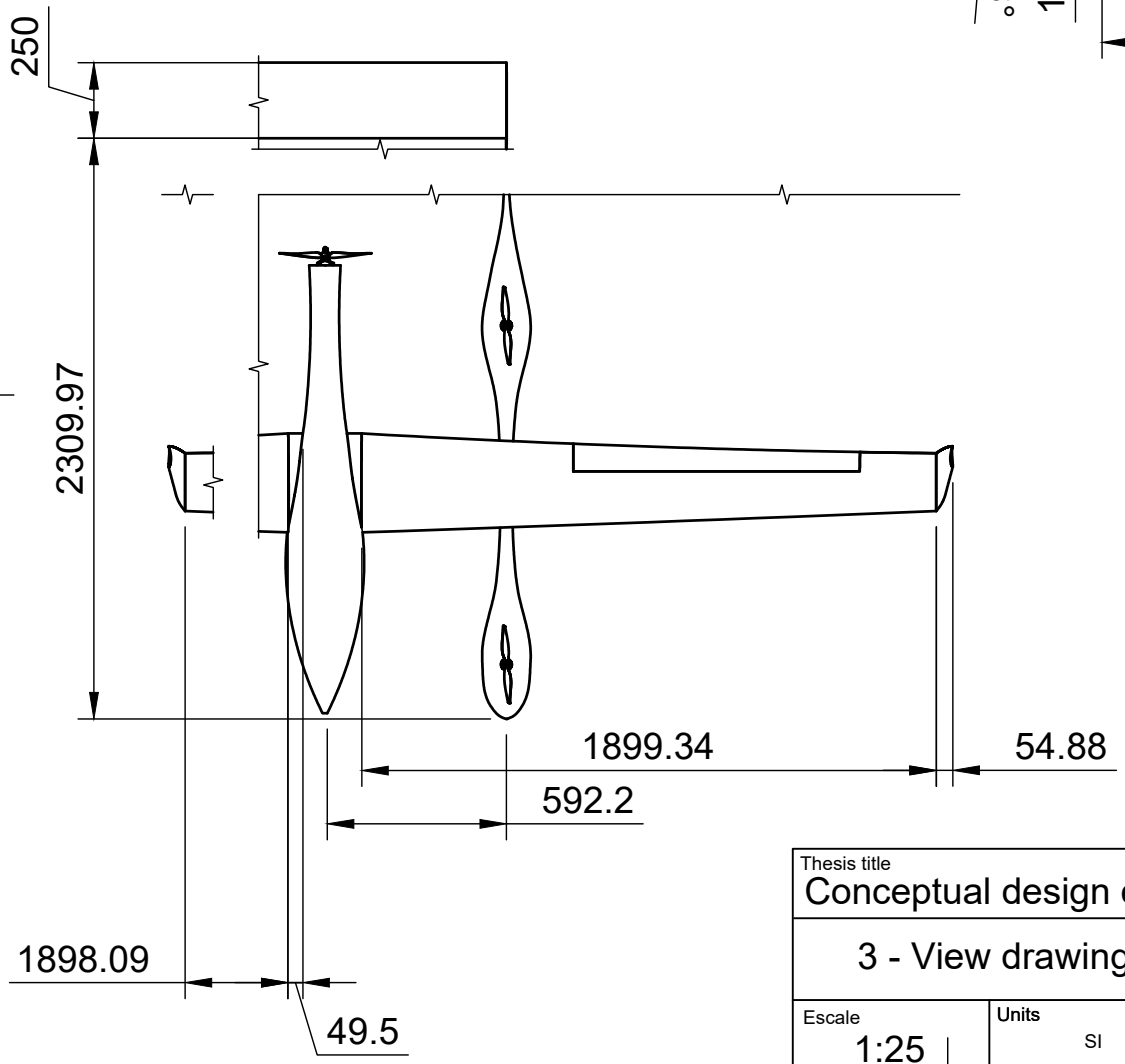

Dihedral	2.3	degrees
Wing Surface	0.978	m^2
Root Chord	320	mm
Mid Chord	245	mm
Tip Chord	190	mm
Wing Span	3900	mm
Length	2507.7	mm
Wing Airfoiil	NACA 44AH	[-]
Tail Airfoil	NACA 0006	[-]

Thesis title

Conceptual design of a hydrogen-powered UAV with LiDAR functionality

3 - View drawing

Created by

Jorge García Miñarro

Escale	Units	Date of issue	Sheet
1:25	SI Lineal longitudes in mm Flat angles in degrees	may 2024	1/4

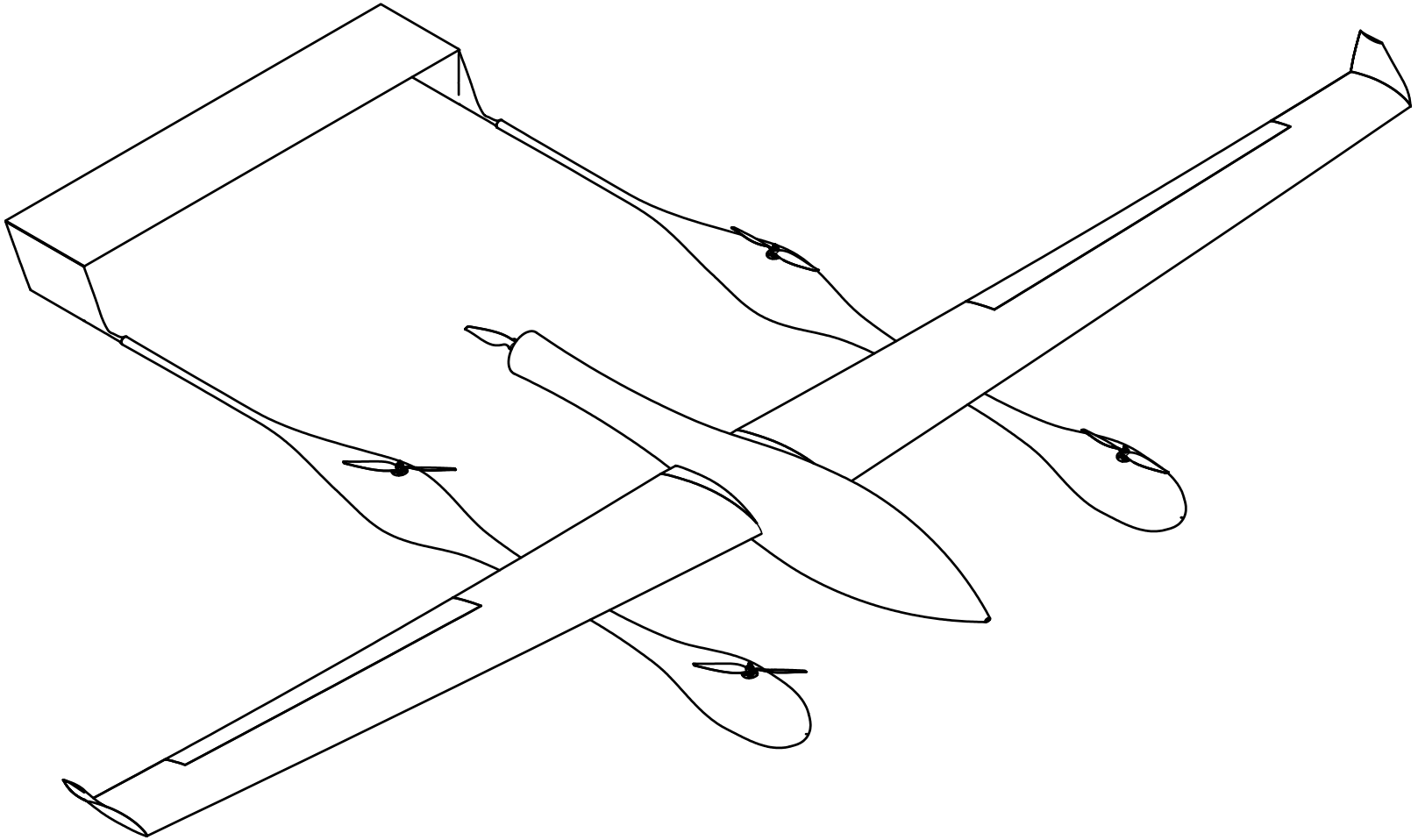

Thesis title: Conceptual design of a hydrogen-powered UAV with LiDAR functionality			
Isometric perspective		Created by: Jorge García Miñarro	
Escale: 1:15	Units: SI — Lineal longitudes in mm; Flat angles in degrees	Date of issue: may 2024	Sheet: 2/4

A-A (1:15)

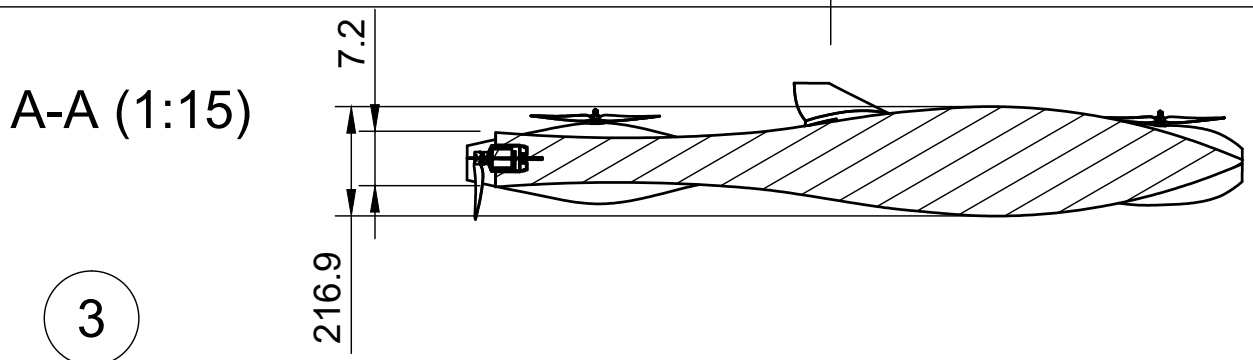

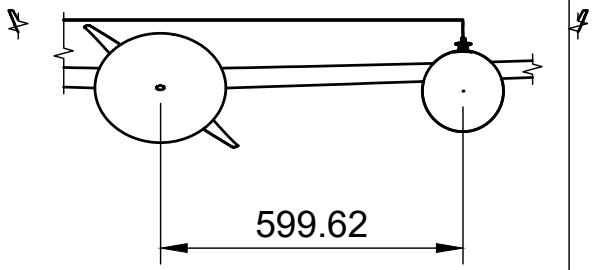

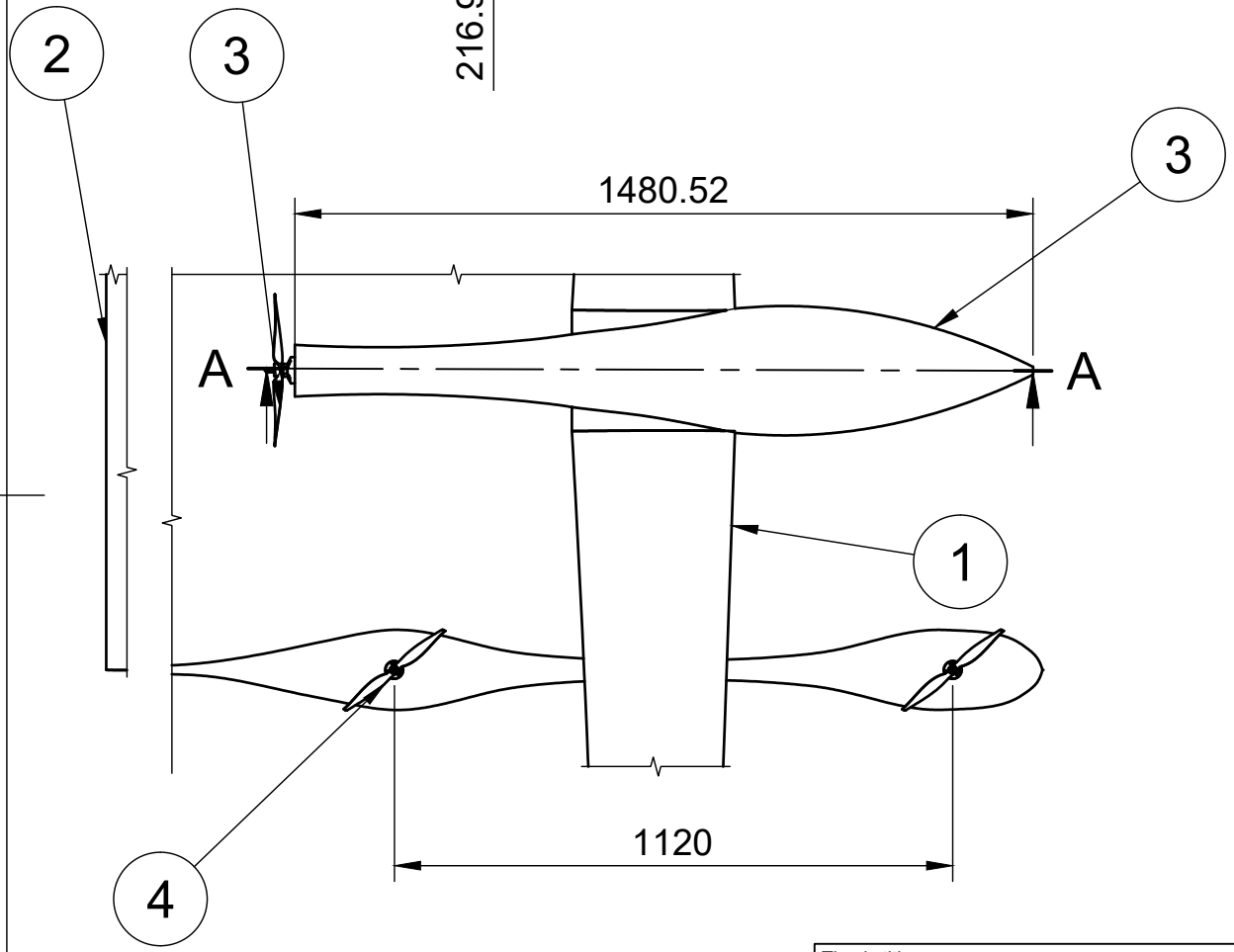

4	Motor VTOL Mode
3	Fuselage and Motor FW Mode
2	Tail
1	Wing
List of pieces	

Thesis title: Conceptual design of a hydrogen-powered UAV with LiDAR functionality			
Section View		Created by: Jorge García Miñarro	
Escale: 1:15	Units: SI — Lineal longitudes in mm; Flat angles in degrees	Date of issue: may 2024	Sheet: 3/4

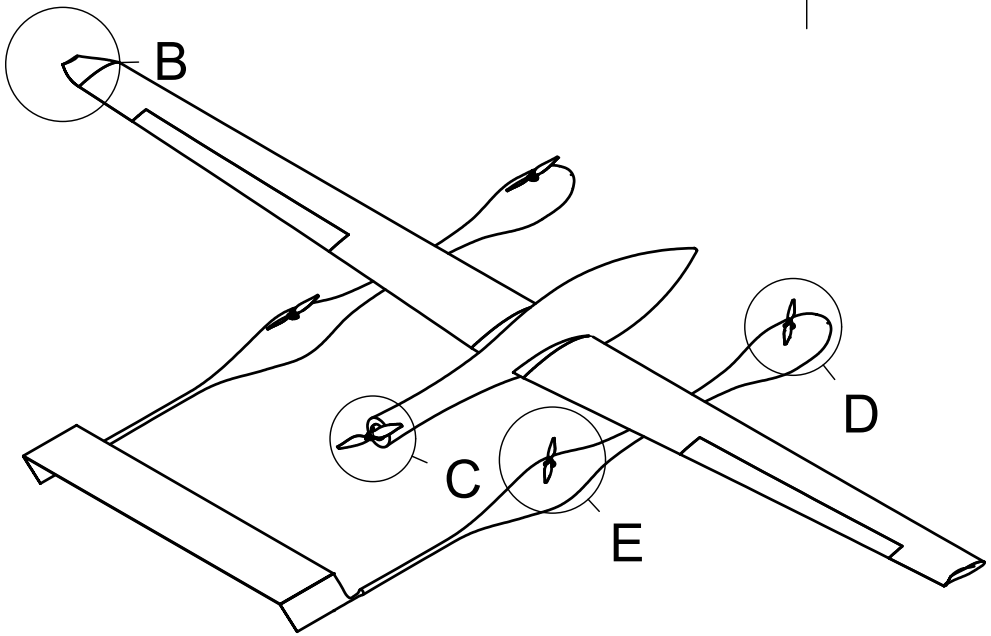

D (1:5)

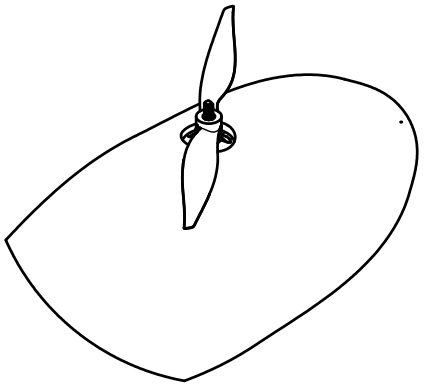

B (1:7)

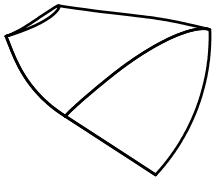

E (1:5)

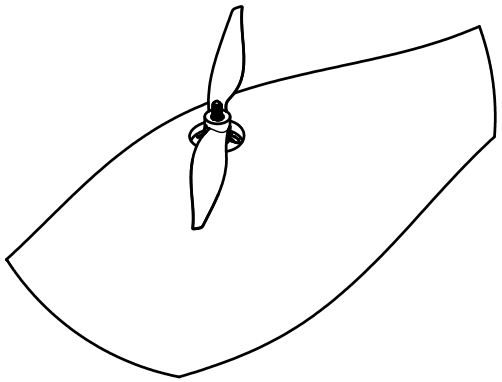

C (1:4)

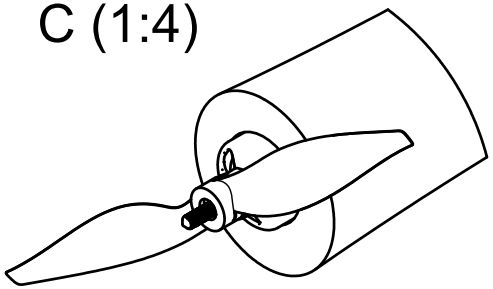

E	Back VTOL Motor
D	Front VTOL Motor
C	FW Motor
B	Winglet
Detailed View	

Thesis title: Conceptual design of a hydrogen-powered UAV with LiDAR functionality			
Detailed View		Created by: Jorge García Miñarro	
Escale: 1:15	Units: SI — Lineal longitudes in mm; Flat angles in degrees	Date of issue: may 2024	Sheet: 4/4